2012-08-01

Acquisition and Analysis of High Rate Pattern Electroretinograms

Jonathon A. Toft-Nielsen
University of Miami, jtoftnielsen@gmail.com

UNIVERSITY OF MIAMI

ACQUISITION AND ANALYSIS OF HIGH RATE PATTERN ELECTRORETINOGRAMS

By

Jonathon A. Toft-Nielsen

A DISSERTATION

Submitted to the Faculty
of the University of Miami
in partial fulfillment of the requirements for
the degree of Doctor of Philosophy

Coral Gables, Florida

August 2012

UNIVERSITY OF MIAMI

A dissertation submitted in partial fulfillment of
the requirements for the degree of
Doctor of Philosophy

ACQUISITION AND ANALYSIS OF HIGH RATE PATTERN ELECTRORETINOGRAMS

Jonathon A. Toft-Nielsen

Approved:

_____ Özcan Özdamar, Ph.D. Professor of Biomedical Engineering	_____ M. Brian Blake, Ph.D. Dean of the Graduate School
_____ Jorge Bohorquez, Ph.D. Assistant Professor of Professional Practice of Biomedical Engineering	_____ Fabrice Manns, Ph.D. Associate Professor of Biomedical Engineering
_____ Vittorio Porciatti, Ph.D. Research Professor of Ophthalmology	_____ Justin C. Sanchez, Ph.D. Associate Professor of Biomedical Engineering

TOFT-NIELSEN, JONATHON A. (Ph.D., Biomedical Engineering)

Acquisition and Analysis of High Rate Pattern Electoretinograms. (August 2012)

Abstract of a dissertation at the University of Miami.

Dissertation supervised by Dr. Özcan Özdamar.
No. of pages in text. (117)

The first investigations into the electrophysiology of the retina were published over 80 years ago (Kahn and Löwenstien, 1924). In the decades since, electroretinography (ERG) has become a widely used tool in ophthalmology for monitoring the health of the visual system. Different variations of the ERG, such as flash ERG (FERG) and pattern ERG (PERG) can be used to isolate the response of the various cellular generators, giving an overall view of retinal health.

Currently, there are a number of visual display units (VDUs) available for eliciting the wide array of ERG responses. These VDUs range from conventional CRT and LCD displays, to digital micro-mirror devices, to laser interferometer based systems. Unfortunately, many of the VDUs available are limited in the way they display visual stimuli, particularly when it comes to precise timing control.

In order to perform advanced signal analysis techniques, such as the recently developed Continuous Loop Averaging Deconvolution (CLAD) technique, on ERG responses it is crucial to ensure precise delivery of stimuli with sub-millisecond accuracy. CLAD is capable of extracting additional information from ERG responses, which has the potential of increasing the diagnostic value of the response, particularly at high

stimulation rates. Unfortunately, conventional VDUs are not able to take advantage of the technique.

For this dissertation, a number of high rate pattern reversal VDUs were designed and developed which would allow for the application of the CLAD technique to the PERG response. Using these specially designed displays in conjunction with CLAD, it was shown that individual waveform components, normally lost as stimulation rates exceed 6 reversals per second (Bach et al., 2012), could be retrieved regardless of the stimulation rate used. This study also investigated the rate based effects of the PERG response. It was shown that as stimulation rates are increased the conventional PERG response morphology changes to reveal new high rate waveform components.

The individual waveform components of the PERG response are used to diagnose and monitor a number of degenerative retinal disorders such as glaucoma. The ability to extract these components at higher rates can potentially improve the diagnostic value of the PERG by detecting dysfunction earlier. Additionally, the new, high rate waveform components might provide insight into the detection of other retinal maladies.

Table of Contents

List of Abbreviations

AEP – Audio Evoked Potentials

CLAD – Continuous Loop Averaging Convolution

CRT – Cathode Ray Tube

ECG – Electrocardiography/Electrocardiogram

ECochG – Electrocochleography/Electrocochleogram

EEG – Electroencephalography/Electroencephalogram

EP – Evoked Potentials

ERG – Electroretinography/Electroretinogram

FERG – Flash Electroretinography/Electroretinogram

FFT – Fast Fourier Transform

GUI – Graphic User Interface

IHS – Intelligent Hearing Systems

IRB – Institutional Review Board

ISCEV – International Society for Clinical Electrophysiology of Vision

ISI – Inter Stimulus Interval

LCD – Liquid Crystal Display

LED – Light Emitting Diode

LGN – Lateral Geniculate Nucleus

mfERG – Multifocal Electroretinography/Electroretinogram

NAF – Noise Amplification Factor

OP – Oscillatory Potentials

PERG – Pattern Electroretinography/Electroretinogram

$PERG_{ss}$ – Steady state Pattern Electroretinogram

$PERG_{tr}$ – Transient Pattern Electroretinogram

PWM – Pulse Width Modulation

qPERG$_{ss}$ – Quasi Steady State Pattern Electroretinogram

qPERG$_{tr}$ – Quasi Transient Pattern Electroretinogram

synPERG$_{ss}$ – Synthetic Steady State Pattern Electroretinogram

synPERG$_{ss(2rps)}$ – Synthetic Steady State Pattern Electroretinogram from 2 reversals per second transient

RGB – Red/Green/Blue

RGC – Retinal Ganglion Cells

RNFL – Retinal Nerve Fiber Layer

rps – Reversals per second

SNR – Signal to Noise Ratio

VEP – Visual Evoked Potentials

VDU – Visual Display Unit

Chapter 1 - Introduction

1.1 Electrophysiology and Neurosensory Systems

Many of the neural structures in the human body produce small amounts of electrical activity in the process of carrying out their normal functions. These biopotentials can be measured and studied to expand the understanding of the body and to provide clues as to how different pathologies affect it. Abnormal heart beats can be detected and diagnosed using the Electrocardiogram (ECG). The Electroencephalography (EEG) can help identify and localize seizure loci in epilepsy patients. Sensory organ and neural pathways produce evoked potentials (EP) that can be acquired using averaging techniques (Regan, 1968). Audio evoked potentials (AEP) and visual evoked potentials (VEP) are examples of such potentials that are commonly used clinically and in research. When an active electrode is placed near a sensory organ, the sensory peripheral organ can be tested in more detail. Electrocochleogram (ECochG) from the cochlea and the auditory nerve is such an example. ECochG can be used in intraoperative monitoring during surgery, as well as diagnostically for otherwise difficult to test patients such as infants (Ferraro, 2000). These are but a few of the ways studies of electrophysiology have helped improve diagnostic techniques and treatment paradigms.

One of the earliest discovered biopotentials was the Electroretinogram (ERG). Despite its early discovery, the ERG has taken decades of study to understand and develop clinically (De Rouck, 2006). This is in part due to the immense complexity of the response, and the generators involved. The retina is a stack of closely packed nerve cells which covers the posterior surface of the eye. While it resides in the eye, the retina

is widely considered an extension of the brain (Kolb, 2006), and is responsible not only for the detection of light, but a considerable amount of processing of the visual signals as well. This early image processing is carried out by the numerous cell types which populate the retinal layers and the interconnections between them. The inherent complexity of the ERG response is due to these various generators and the functions they carry out, and while it might seem that this complexity would discourage its use and diminish its diagnostic value, the opposite is actually true. Specific generators can be emphasized by altering the temporal, spatial, contrast, color and other parameters of the stimuli. Currently, in both clinical and research settings, the electrophysiology of the retina is being studied in order to better treat and diagnose a wide variety of degenerative retinal disorders.

One particular stimulus paradigm utilized in ERG is the pattern reversal stimulus. The pattern reversal stimulus consists of an isoluminant display of black and white segments which modulate with time (Bach et al., 2012). The pattern reversal stimulus elicits a response from the retina known as the pattern electroretinogram (PERG). The PERG response is believed to largely arise from the Retinal Ganglion Cells (RGC) in the retina and is considered to provide a measure of central retinal and RGC function (Frishman, 2006). As such the PERG is used in diagnosing and monitoring of conditions which affect these regions of the retina, most notably glaucoma (Porciatti and Ventura, 2004).

Currently, the analysis of the PERG response is separated into two categories, based upon the stimulation rate the response was obtained at. PERG acquired at rates < 6 reversal per second (rps) are referred to as transient PERG ($PERG_{tr}$) and settle before

subsequent stimuli are delivered. $PERG_{tr}$ are analyzed in the time domain, measuring the time to peaks and amplitudes of individual waveform components. At reversal rates >10 rps, subsequent responses overlap with one another, resulting in a vaguely sinusoidal response called the steady state PERG ($PERG_{ss}$). Because of the convolution of subsequent components, individual waveform components are obscured. Currently, the only avenue available to analyze $PERG_{ss}$ responses is frequency domain analysis.

While $PERG_{ss}$ is widely utilized in a number of research and clinical settings, the ability to extract the “per stimulus” response at higher reversal rates would allow access to individual waveform components regardless of the stimulation rate used and might add additional diagnostic value to the response.

The purpose of this dissertation is to develop and apply a method of extracting the "per stimulus” response from high-rate electroretinograms, allowing for the real time acquisition of the traditional steady-state response, as well as the high-rate transient response. It is the hope of the researchers involved that the unveiling of the high rate “per-stimulus” response will provide more specific information about the electrophysiology of the retina and lead to quick and better diagnosis and treatment of diseases of the eye.

Chapter 2 - Background

2.1 Anatomy and Physiology of the Visual System

The visual system is comprised of the eye and the neural pathways leading to the visual cortices, all of which interpret light in order to build a representation of the world around us. The following section will touch upon the various elements which comprise the visual pathway.

A. The Eye

The visual pathway begins with the eye (see Figure 2.1), a complex sensory organ which collects and focuses light, converts it into electrical signals and transmits along the rest of the pathway via the optic nerve. Light entering the eye is initially refracted by the cornea, the transparent front portion of the eye. It then passes through the pupil, an opening in the aperture like iris which controls the amount of light entering the eye. After passing through the iris, light enters the posterior chamber of the eye. At this point, light is further refracted by the crystalline lens. Unlike the cornea which causes a fixed refraction, the lens is capable of changing shape to alter its refraction, effectively altering the focal distance of the eye. This process is called accommodation, and allows the eye to focus on objects at different viewing distances. Together, the lens and cornea focus incoming light onto the next stage in the visual pathway, the retina.

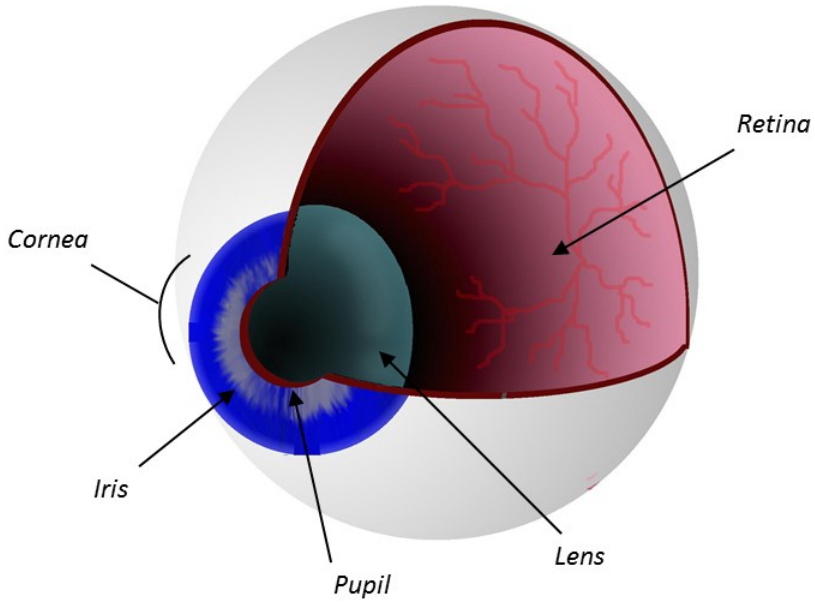

Figure 2.1 – Schematic of the eye. Section cut away to reveal some of the structures within. Labeled are the cornea, iris, pupil, lens and retina.

B. The Retina

Located on the inner posterior surface of the eye, the retina acts as the main transducer of the visual system, converting incoming light into electrical signals which are then transmitted along the rest of the visual pathway. The retina is comprised of millions of closely packed nerve cells, arranged in layers with synaptic neuropil between layers (see Figure 2.2). Each layer serves a different role in the detection and early processing of incoming light. The actual organization of the retinal layers is reverse to what one might intuitively expect. Photoreceptors, the actual sensory cells of the retina, sit at the back of the retinal stack, furthest away from incoming light. Light falling on the retina must travel through the various layers of the retina, and the length of the photoreceptors themselves before reaching the light sensitive pigment molecules (Kolb, 2006).

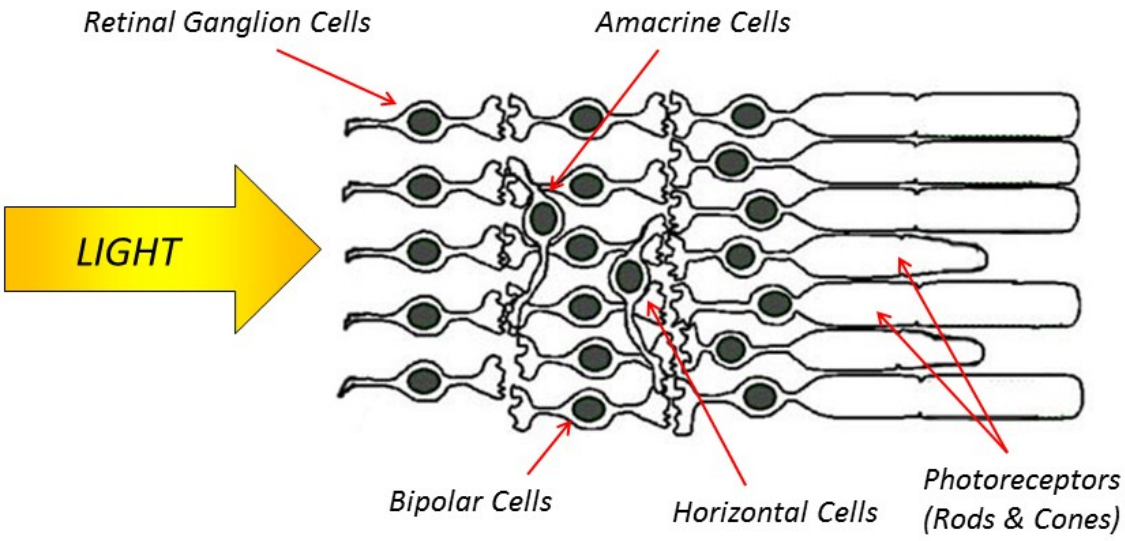

Figure 2.2 - The Retina: Cross section of a segment of the retina, showing various cells in the retinal layers. Light enters the eye, is focused by the earlier structures, and passes through the retinal layers, finally reaching the photoreceptors. Photoreceptors comprise of Rods and Cones. Cells in the middle layer include bipolar and horizontal cells. The inner most layer is comprised of amacrine cells and retinal ganglion cells. Retinal Ganglion cell axons exit they eye, forming the optic nerve. (modified from Kolb 2006)

Humans possess a duplex retina, one containing two classes of photoreceptors: Rods, responsible for dark adapted vision, and Cones, responsible for light adapted vision and color discrimination. In humans, there are three varieties of cone, each sensitive to a different spectral region of light (red sensitive, green sensitive and blue sensitive). Photoreceptors then synapse with the dendrites of cells in the next layer of the retina, bipolar and horizontal cells**.** These cells work together to give rise to the center/surround structure of the receptive field (Masland, 2001). Bipolar cells exhibit either excitatory (ON) or inhibitory (OFF) behavior which they convey to Retinal Ganglion Cells (RGC). Often ON and OFF bipolar cells work together providing separate but parallel paths to the RGCs (Kolb, 2006). This creates the center of the receptive field. This behavior is then further emphasized by the opponent surround of the receptive field, created by the horizontal cells (see Figure 2.3).

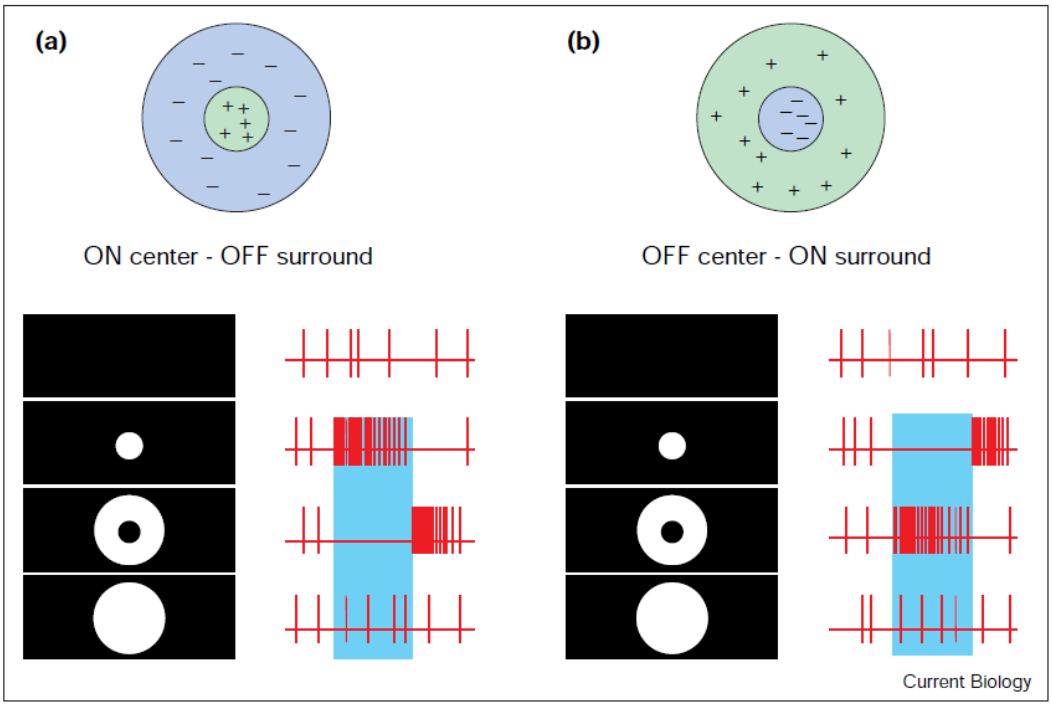

Figure 2.3 - On-Center and Off-Center Receptive fields: Graph illustrating how lateral inhibition from horizontal cells gives rise to receptive fields in the retina. Two types of receptive fields are shown (a) ON center – OFF surround and (b) OFF center – ON surround, as well as how different stimulus levels affect the firing rate of the associated retinal ganglion cell. (Neves and Lagnado, 1999)

The final cell layer of the retina is comprised of retinal ganglion cells and amacrine cells. Retinal ganglion cells make up the final stage of the retina, signal-wise, as their axons join to form the optic nerve, and send their responses to the lateral geniculate nucleus. Bipolar cells in the previous layer synapse with RGCs and transmit their center surround receptive field organization. RGC can also synapse with amacrine cells, which while not completely understood, are believed to further process the receptive fields established at the lower levels of the retina (Kolb, 2006). The various connections of the retinal cells help to encode and process visual information before it has even reached the brain.

C. Path to the Thalamus

RGC axons from the retina gather and exit the eye at the optic disc, forming the optic nerve. The optic nerves from both eyes meet at the optic chiasm. At the optic chiasm, axons from the nasal portions of each eye cross over, while axons from the temporal portions of each eye remain on the same side. Prior to the optic chiasm, nerve bundles are organized by eye (optic nerve). After the cross-over of fibers at the chiasm, nerve bundles are instead organized by visual field (optic tracts). Right and left visual field information is carried along the optic tracts to the lateral geniculate nucleus (LGN) in the thalamus. The LGN is arranged in six layers, which process information from different populations of RGC.

D. The Visual Cortex

The visual pathway continues out of the LGN via the optic radiation and terminates at the primary visual cortex. The visual cortex is located in the occipital lobe of the brain and is responsible for processing visual imagery. The organizational mapping of the retina to the LGN is preserved in the primary visual cortex, also referred to as V1. The V1 area of the visual cortex feeds into many different extrastriate layers. While the exact contributions of each of the extrastriate areas are under debate, it is currently believed that the visual pathway continues out of the V1 cortical layer in two streams. These streams are referred to as the dorsal stream, responsible primarily for visual motion, and the ventral stream, primarily involved in perception and recognition (Goodale & Milner, 1992).

2.2 Electrophysiology of Vision

The first published electrophysiological investigations of the retina date back as far the 1920s, with the work of Kahn and Löwenstein (Kahn and Löwenstein, 1924). At the time, they determined their method was too difficult to be used as part of clinical examination of the human eye. Today, electroretinography (ERG) is a widely used electrophysiological test in ophthalmology. ERG measures the electrical potentials generated in the retina. There are several different variations of the ERG, based mainly on the type of stimulus being used. All forms of ERG utilize some form of visual, light-based stimulus; however, there are specialized versions of the ERG which can be used to focus on particular structures in the retina. Two such specialized ERGs are the Flash Electretinogram (FERG) and the pattern electroretinogram (PERG).

2.3 The Flash Electroretinogram

In the FERG, a full field, flashing light is used as the stimulus. The International Society for Clinical Electrophysiology of Vision's (ISCEV) Standard ERG evaluation includes the following responses, each named according to conditions of adaptation and the stimulus, where flash strength in represented in $cd{\cdot}s{\cdot}m^{-2}$. (Marmor et al., 2009)

(1) Dark-adapted 0.01 ERG

(2) Dark-adapted 3.0 ERG

(3) Dark-adapted 3.0 oscillatory potentials

(4) Light-adapted 3.0 ERG

(5) Light-adapted 3.0 flicker ERG

These five stimulus scenarios make up the standard ERG evaluation (see Figure 2.4). Each scenario involves different stimulus parameters and subject adaptation. Adaptation involves allowing the subject to adjust to either light or dark setting before initiating the test. Varying the adaptation can help to selectively emphasize or inhibit the contribution of different generators, and thus is used as a method to isolate different retinal structures.

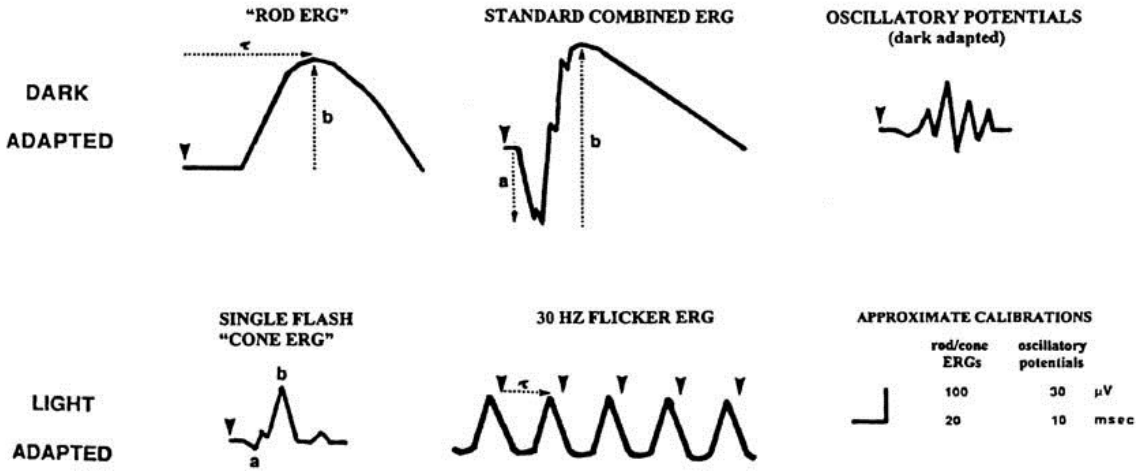

Figure 2.4 - Diagram of the five basic ERG responses as defined by the ISCEV. Nomenclature defines the adaptation of the subject, the flash intensity. Arrows indicate presentation of stimulus. As shown above, the morphology of the ERG response varies greatly depending on the stimulus parameters and subject adaptation level. These differences in the ERG waveform are glimpses of the different structures of the retina (Marmor et al., 2009).

The different paradigms of FERG are used to assess a number of retinal diseases including: retinitis pigmentosa, cone and/or rod dystrophy, retinal vascular diseases, and monitoring of toxicity levels (Larsson & Andreasson, 2001). ERG can also be used in conjunction with Visual Evoked Potentials (VEPs) recorded from the cortex in order to localize impairments of the visual pathway (Holder et al., 2010).

2.4 The Pattern Electroretinogram

The pattern electroretinogram (PERG) is considered a specialized type of ERG (Marmor et al., 2009). PERG is a retinal response evoked by viewing an isoluminant, temporally alternating pattern (either square-wave, or sinusoidally modulated), usually a black and white checkerboard or grating (Hess & Baker, 1984; Holder et al., 2007). PERG is unique in that it is a retinal response that is evoked in the absence of a net change of stimulus luminance. The pattern reversal stimulus causes cancellation of any linear luminance response as white and black portions of the pattern cause equal, but opposite responses, as seen in Figure 2.5. These local luminance responses cancel out over the entirety of the retina (Bach and Hoffman, 2006).

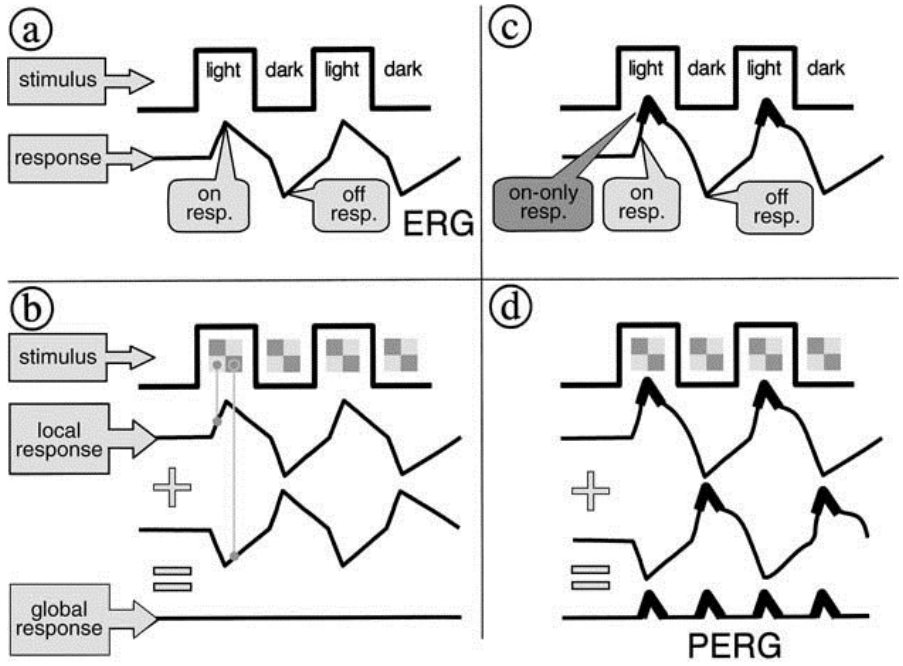

Figure 2.5 - Nonlinear PERG response. (a) When the entire retina is illuminated, there is an equal and opposite response to light onset and light offset. (b) In the case of Pattern stimuli, local luminance onset and offset responses will cancel out when averaged over the retina. (c) However, there exists a nonlinear on-only component. (d) Averaged over the retina, this response does not average out, resulting in the PERG (Baker & Hess, 1984; Brannan et al., 1992; Bach and Hoffman, 2006).

PERG is widely used in both clinical and research settings due to the reproducibly of the resulting waveforms, across individual subjects and across the population. Clinically, PERG can be used to differentiate between macular and optic nerve dysfunction, which can help improve the interpretation of cortically generated Visual Evoked Potentials (VEP) (Holder, 2001). Additionally, PERG is used as a diagnosis and monitoring tool for glaucoma (Porciatti and Ventura, 2004; Ventura et al., 2005; Bach et al., 2006).

A. **The Transient Pattern Electroretinogram**

At low temporal frequencies (< 6 rps; equivalent to <3 Hz) transient PERGs ($PERG_{tr}$) (Figure 2.6) are obtained (Holder et al., 2007). In these cases, the responses have time to settle by the time the next contrast reversal occurs. For $PERG_{tr}$, peak amplitudes, and the times between peaks are used to analyze these waveforms. The transient PERG waveform consists of three separately measurable components: a small negative component, N35, at 30-35 ms, a prominent positive component, P50, at approximately 50 ms, and a large negative component, N95, at 90-100 ms. To date, only the P50 and N95 components have demonstrated clinical value (Holder et al., 2007).

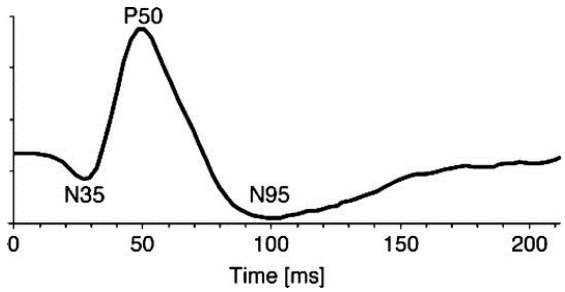

Figure 2.6 - A normal transient PERG response. The PERG waveform is composed of three waveform components: N35, P50, and N95. The amplitude of P50 in a normal subject is usually between 2 and 6 μV. (Bach et al., 2012)

B. **The Steady-State Pattern Electroretinogram**

In instances where the inter-stimulus interval (ISI) drops below the duration of the PERG response, (above 10 rps or 5 Hz), the acquired signal becomes the "steady-state" PERG response (for flash ERG responses this is often referred to as the flicker ERG rather than 'steady state' (Marmor et al., 2009; Wu and Burns, 1996.)). This will be designated as the $PERG_{ss}$ in this study. One explanation for the steady state response is that it is arises from the convolution of subsequent event related transients. This superposition hypothesis has been tested in several studies (Capilla et al., 2011; Toft-Nielsen et al., 2012). The convolution of responses yields a periodic waveform (see Figure. 2.7). Because of this overlapping of subsequent responses, the analysis techniques used on transient responses, i.e. individual component analysis, can no longer be applied. As a result, steady-state responses are typically analyzed in the frequency domain. Typically, the standards suggest analyzing the amplitude and phase of the "second harmonic" of the response. This is because the convention for PERG is to define the stimulation rate as the period for the stimulus, i.e. when the pattern returns to its initial state. A stimulation frequency of 1 Hz is actually 2 rps, one reversal to change the pattern state, and then another reversal to return the pattern to its initial condition. As stated before (Figure 2.5), a PERG response actually is periodic to the stimulus ***reversal rate***.

While it is generally believed that individual component analysis is of greater diagnostic value, and ISCEV standards for pattern ERG (Bach et al., 2012) only refer to transient waveforms, steady-state PERGs are still desirable and utilized in clinical and

research settings (Maffei & Fiorentini, 1990; Porciatti and Ventura, 2004, Ventura et al., 2005, Ben-Shlomo et al., 2007).

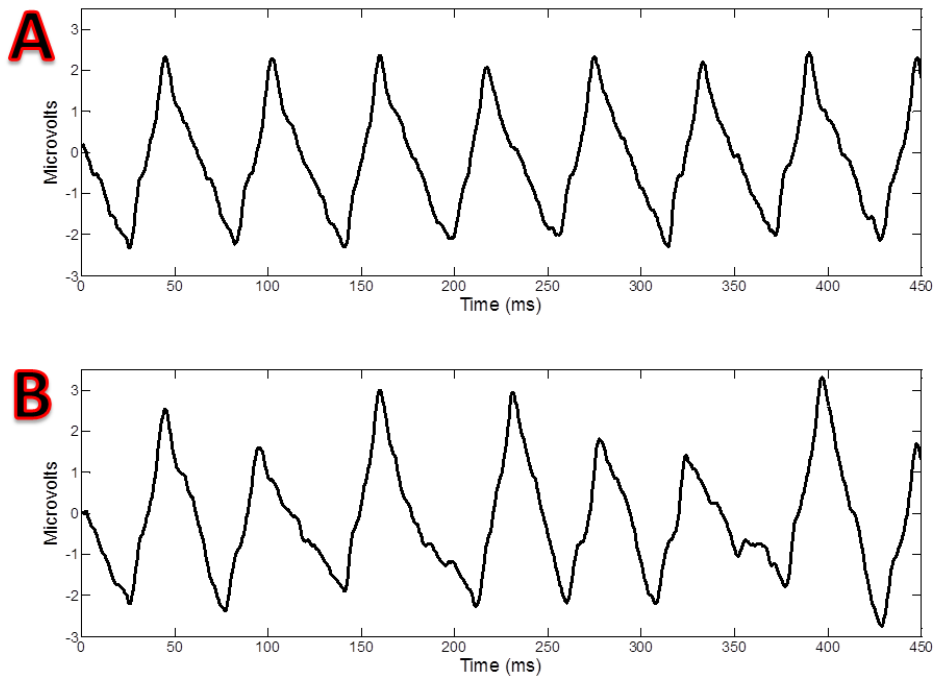

Figure 2.7 - $PERG_{ss}$ and Quasi Steady State PERG ($qPERG_{ss}$) – (A) $PERG_{ss}$ acquired at 17.4 rps. The convolution of subsequent responses at higher rates leads to periodic response shown above. Individual waveform components are obscured. (B) qPERGss acquired at a mean reversal rate of 17.4 rps. By introducing slight advances or delays to the stimulus onset (jitter) the quasi $PERG_{ss}$ can be acquired. The $qPERG_{ss}$ response will be discussed in depth in later chapters.

2.5 Isolation of the Various Generators of ERG

As previously stated, the retina consists of several layers of different cells. When acquiring ERG responses from a distance, i.e. the recording electrodes placed on the cornea or on the lower eyelid (Porciatti and Ventura, 2004), waveforms are comprised of the contributions of cells from the various layers. Factors which effect the contributions

of the various cell types to the ERG include: stimulus energy, stimulus wavelength, background illumination, duration and spatial extent of the stimulus and location of the stimulus within the visual field (Frishman, 2006). The outer most cell layer of the retina consists of photoreceptors (rods and cones) which respond to light entering the eye. The response of the photoreceptors is the primary component in dark and light adapted FERG waveforms. The photoreceptors send signals to the next layer, which is made up of bipolar and amacrine cells. These cells primarily are responsible for lateral inhibition, and their response can be observed in Oscillatory Potentials (OP) (Figure 2.8). The inner most cell layer of the retina contains the Retinal Ganglion Cells (RGC). Photoreceptors are much more abundant than RGCs, outnumbering them by a factor of about 100:1 (Drasdo, 1989; Curcio and Allen, 1990; and Sjöstrand et al., 1999). Because of this, the retina is segmented into regions called "receptive fields". Each visual field consists of a single RGC which may have many photoreceptors, bipolar cells and amacrine cells feeding into it. RGCs compile the responses of all of cells within their receptive field, altering their firing activity based on a large number of inputs from previous layers of the retina, encoding visual information and sending it to the optic nerve via the retinal nerve fiber layer (RNFL). As described in Figure 2.5, the use of pattern stimuli can exploit the structure of the retina, resulting in the accentuation of the RGC response specifically (Bach et al., 2012). Due to this antagonistic 'center-surround' organization of the retina, PERG stimulation results in a response which is primarily due to the contribution of the RGC (see Figure 2.9).

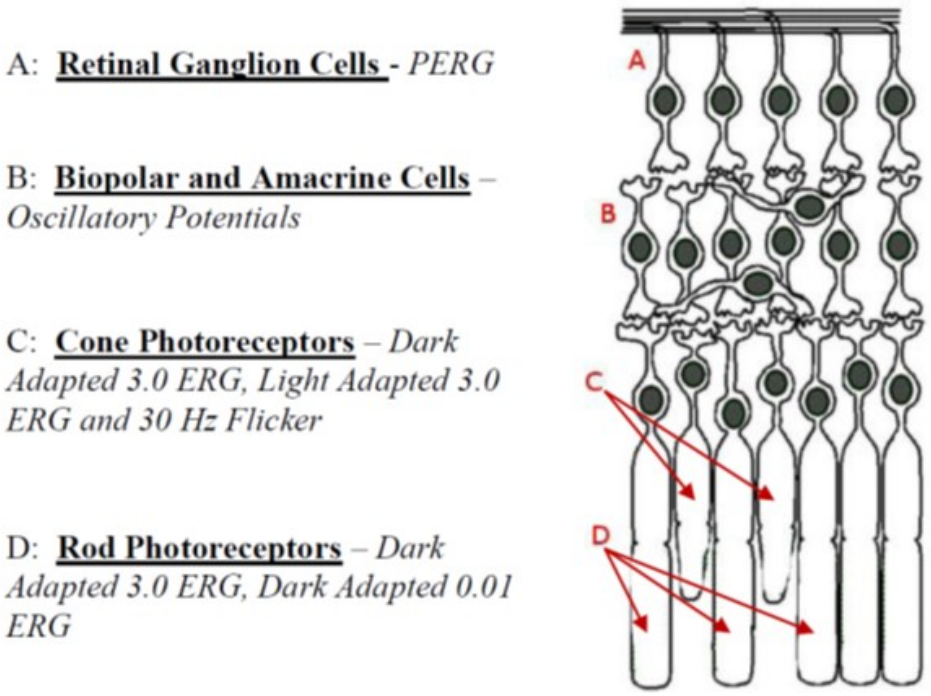

Figure 2.8 - Diagram of Retinal Layers. Cell types are labels A-D along with the corresponding ERG recording to isolate the response of each cell type. (Modified from Kobb, 2006)

For clinical evaluation this is desirable because RGCs are susceptible to a wide range of degenerative retinal disorders, such as glaucoma (Porciatti and Ventura, 2004; Bach et al., 2006). Because of this specific focus on RGC function, PERG recordings exhibit considerable changes to wave morphology in the presence of retinal dysfunction in the macula or ganglion cells (Fiorentini et al., 1981; Marmor et al., 1996; Holder et al., 2010).

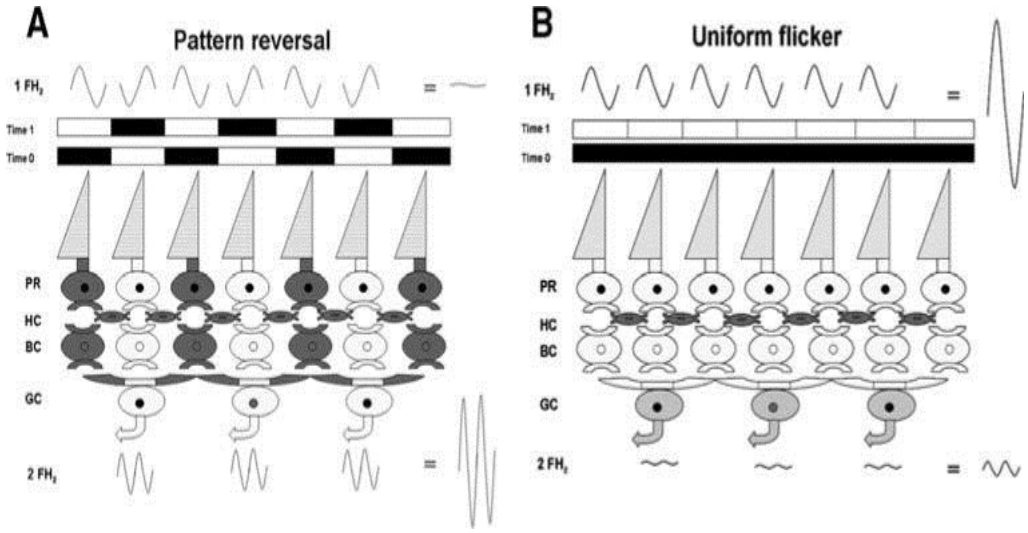

Figure 2.9 - Cross-section of the retina. Cells are arranged with RGCs on the bottom and Photoreceptors on the top. The figure illustrates how lateral inhibition leads to masking of photoreceptor response and accentuation of RGC response in PERG. Local luminance responses of the photoreceptors during pattern stimulation average out at the electrode site, while RGC fire in unison due to center-surround groups. The exact opposite is true in uniform flash stimuli; luminance is the same over the entire retina, so photoreceptor responses constructively interact, while RGC firing is limited by lateral inhibition (Porciatti, 2007).

As stated, PERG recordings are widely used in both clinical and research settings (Porciatti and Ventura, 2004; Ventura et al., 2005). Studies have shown that PERG amplitudes are dependent on both spatial and temporal frequency (Porciatti, et al., 1992). These 'optimal' frequencies are used in many clinical applications of PERG. The temporal frequencies which have been found to result in the maximum amplitude for PERG responses are in the steady state range. In other words, at these temporal frequencies, the inter-stimulus intervals are less than the response length. This results in the characteristic sinusoidal steady-state waveforms. While these steady state responses are analyzed in the frequency domain, it becomes difficult if not impossible to perform any temporal analysis of the responses, or to detect subtle changes in wave morphology when this high-rate convolution occurs. Ideally, we would like to choose rates which will

maximize response amplitude, while still able to extract individual components observed in the transient PERG waveform.

2.6 ERG Analysis Methods and Reporting

Currently, analyses of ERG waveforms are either performed in the time or frequency domain. For low rate responses where there is no evidence of waveform overlapping, peak based analysis is performed in the time domain. At higher rates, however, peak information is lost and analysis is done in the frequency domain.

A. Temporal Domain

Once ERG responses are acquired quantitative analysis in the time domain consists of peak amplitude and latency measurements. For the PERG waveform, there are three main components: N35, P50 and N95. The N35 component is measured from the baseline to the tip of the N35 trough. The P50 component is measured from the trough of N35 to the peak of P50. The N95 component is measured from the peak of the P50 component to the trough of the N95 component. Latencies are all measured from the stimulus onset to the corresponding peak (Holder et al., 2010). Typically, PERG reporting consists of P50 and N95 amplitudes and P50 latency (because of the broadness of the N95 component, N95 latency is sometimes omitted from reports) (Bach et al., 2012).

B. Spectral Domain

At higher stimulation rates, resulting in a steady state waveform, analysis is performed in the frequency domain. Convolution of successive waveforms obscures

individual waveform components. As a result, reporting of $PERG_{ss}$ responses consist of magnitude and phase of the responses at the second harmonic of the stimulation rate (the reversal rate) (Bach et al., 2012). Although phase and magnitude measurements obtained from $PERG_{ss}$ give some information on the latency and amplitude of the $PERG_{tr}$ making up that response, that information is approximate and cannot be directly associated with P50 and N95 components. Deconvolution analysis presented in section 2.8 provides a solution to this problem.

2.7 Visual Display Units

Conventional visual stimuli can be separated into two categories: unstructured, and spatially structured. Ganzfeld stimulators are a series of devices which deliver uniform light stimulus to the entire visual field and are among the most common option for delivering unstructured stimuli in general ERG studies (Gunkel et al., 1976). Spatially structured stimuli consist of patterns of light, typically black and white segments and are utilized in PERG and multifocal electroretinography (mfERG) studies (see Figure 2.10). There are a number of different visual display units (VDUs) used in electroretinography, each of which utilizes different technologies for presenting visual stimuli. These devices are used to obtain ERG responses, and monitor retinal health, in both clinical and research settings.

Figure 2.10 - Two commercial PERG stimulators. Note that in both models, the stimulus is presented on a CRT monitor. Because of the way CRT monitors display their image, these stimulators are limited in the available stimulus rates. As such they are incompatible with the CLAD algorithm. (Neurosoft, Neuro-ERG)

The 'gold standard' of clinical visual electroretinography has long been the cathode ray tube monitor (CRT). Many studies have explored the minutia of the CRT as a VDU (Nagy et al., 2011; Husain et al., 2009; Elze, 2010; Hogg, 2006). In recent years, as Liquid Crystal Displays (LCD) have, by and large, replaced CRT as the primary display technology for computer monitors, many LCD based VDUs have emerged. Each of the different VDU technologies used for electrophysiological studies possesses disadvantages which can limit the functionality of these displays. These limitations, particularly those involving display timing and stimulus presentation, can reduce the pool of available VDUs which can be used with the CLAD technique.

A. CRT Display and Limitations

The visual image on a CRT monitor is comprised of a discrete raster of pixels. Each pixel is excited to give off light, one at a time, by an electron beam. The beam traverses

the display in a set pattern defined as the raster, as seen in Figure 2.11. In most CRT displays the beam begins in the upper right corner and travels across the screen from left to right. Upon reaching the end of a horizontal row, the beam shuts off and moves to the leftmost pixel in the next row down. This period is referred to as a *horizontal blank*, and no pixels are excited during this time. The beam continues on this pattern until reaching the rightmost pixel in the final row, at which point the beam shuts off and returns to the leftmost pixel in the first row. This period is referred to as a *vertical blank*. The period between vertical blanks is called a frame. The refresh rate of a CRT is rate at which frame changes (Elze, 2010). The refresh rate effectively dictates how fast images can be changed on the display. Patterns displayed on a CRT VDU can only be changed at multiples of the frame rate. Most CRT displays have refresh rates of 60-75 Hz, with corresponding time between frames of 16.67 ms and 13.34 ms. There are specialty CRTs available which have refresh rates as high as 200 Hz (Elze, 2010).

The raster pattern of the CRT monitor means that the display is constantly changing. This can adversely affect responses acquired with CRTs by broadening the components of the response (Zele and Vingrys, 2005; Elze, 2010). Additionally, the phosphors luminance begins to decay immediately after the electron beam has moved off the pixel. Typically, CRT phosphors decay in around 2 ms (Elze, 2010). With a typical refresh rate between 10-17 ms, CRT pixels are off for between 8 and 15 ms of each frame.

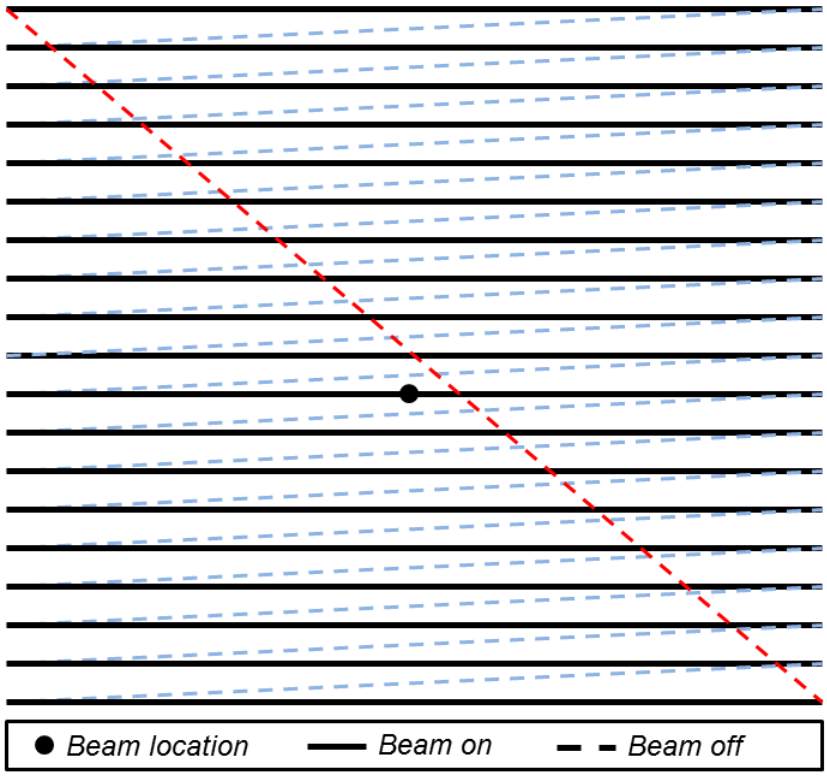

Figure 2.11 – Typical CRT raster pattern – Images are created on CRT displays by an electron beam moving in a raster pattern. The beam traverses the display from left to right across each row of pixels. Upon reaching the end of a row, the beam shuts off and moves to the next row. The solid lines represent when the beam is on, broken lines represent when the beam is off. Blue traces show horizontal blanks, while the red trace shows the vertical blank (Adapted from Hogg, 2006)

B. LCD Display and Limitations

Liquid crystal displays (LCD) are another type of VDU. LCD monitors produce images by varying the polarization state of a uniform backlight. The image of an LCD monitor is also composed of a number of pixels. Each pixel is composed of a layer of orthogonal molecules between two polarizing filters and two electrodes. The voltage across each pixel can be varied to change the alignment of the molecules in the LCD pixel. The alignment of the molecules alters the polarization of the light passing through

the pixel, effectively controlling the amount of light which pass through it. Using an array of RGB pixels, an image can be constructed by controlling the amount of light passing through each pixel, as seen in figure 2.12.

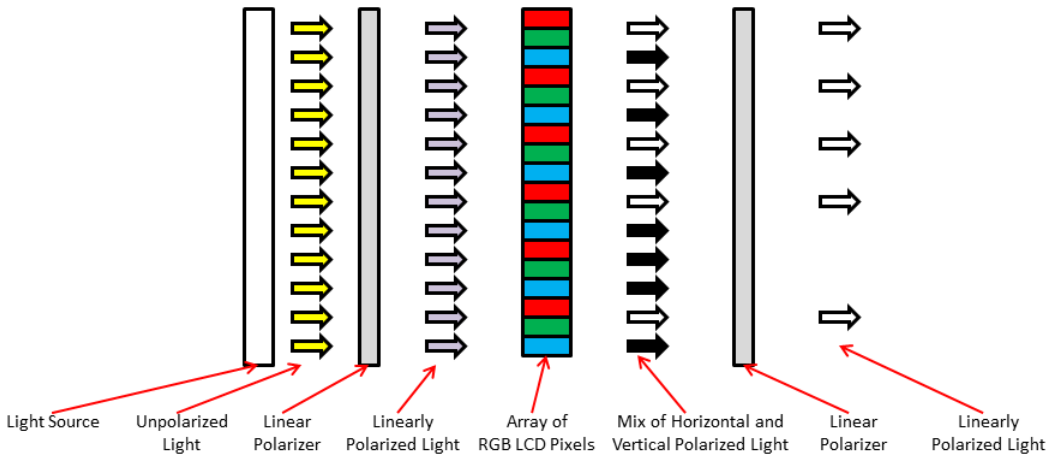

Figure 2.12 – General Layers of an LCD display – Images are created on LCD displays by varying the polarization state of linearly polarized light to form images. A uniform white backlight is passed through a linear polarizer layer. This results in a field of linearly polarized light. The polarized light passes through the array of LCD pixels. The alignment of the molecules in each pixel are arranged to selectively alter the polarization state of the light passing through the pixel to control how much light passes through the outer polarization layer. Once the mixed polarization light passes through the outer polarization layer, portions of the light are blocked and the light that passes through is in the form of the desired image.

Despite the fact that there is no raster in LCD displays, LCD are driven by the same monitor control protocols as CRT devices, and as such, are still refreshed at a set rate (Elze, 2010). Additionally, LCD display characteristics are further complicated by pixel response times. In most visual electrophysiological experiments the display will present dynamic stimuli. With LCD displays, when there is a required change in luminance, the voltage must be changed on the particular pixels. The molecules in each pixel must then realign to voltage. This lag between signal input and stimulus output is known as response time (see Figure 2.13). Additionally, LCD displays typically control their

backlight illumination with pulse width modulation (PWM). PWM can introduce a high frequency flicker artifact into ERG responses, (although typically, this artifact is much higher than the interested frequencies).

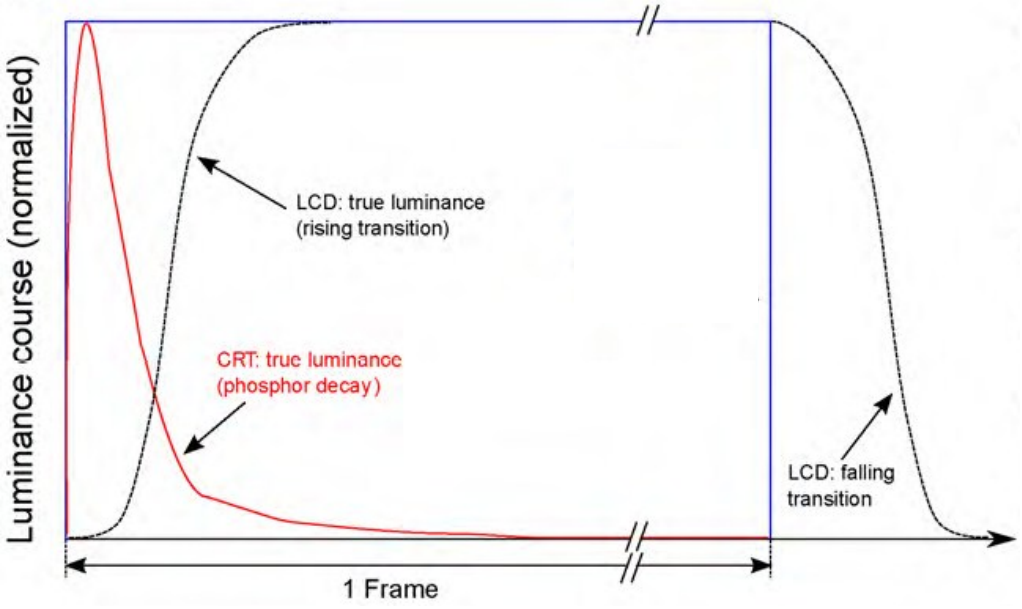

Figure 2.13 – Effect of phosphor decay and LCD response time on display frame luminance – The blue trace above shows the ideal luminance course for a VDU. CRT visual displays units illuminate pixels (red trace) by exciting a phosphor with an electron beam. The initial response of the phosphor is very fast, but the phosphor immediately begins to decay, typically with a time constant of around 2ms. For this reason, CRT pixels do not remain illuminated for the entirety of a frame. LCD pixels (black trace) change luminance by altering the state of molecules within the pixel to allow for more or less light to pass. There is no phosphor decay with LCD pixels, but it takes time for the LCD pixel to change states. Typical LCD response times range from 8 – 16ms. If there is no luminance change, LCDs (unlike CRT) are capable of maintaining a constant luminance. Unfortunately, during a luminance change, the longer response times of LCD can cause 'ghosting' of images, with LCD transitions lagging into the following frame. (Modified from Elze, 2010)

2.8 Continuous Loop Averaging Deconvolution (CLAD)

The Continuous Loop Averaging Deconvolution (CLAD) algorithm was developed in time domain by Delgado and Ozdamar (Delgado and Ozdamar, 2004), and later expanded to the frequency domain by Ozdamar and Bohorquez (Bohorquez and Ozdamar, 2006). The primary application is the extraction of unitary responses from high rate evoked potentials. By introducing jitter to the normally isochronic stimulus rate, it becomes possible to deconvolve a steady state signal and acquire the "per stimulus" response (or unitary response) at high stimulation rates.

CLAD makes the assumptions that during the recording period the unitary response does not change, and that each stimulus evokes the same response. If this is the case, the response measured will be the superposition of all the evoked elementary responses. In the time domain, the measured response can be thought of as the convolution of the elementary response with the stimulation sequence. Transforming to the frequency domain via the Fourier transform changes convolution to multiplication, and now the elementary response can be isolated by dividing by the stimulation sequence. In instances where the transfer function of the stimulation sequence contains zeros (such as normal, isochronic sequences), this operation will result in a division by zero, and cannot be performed. CLAD stimulation sequences are designed specifically to contain no zero values, allowing for the above operation, and the isolation of the unitary response.

CLAD algorithm in the frequency domain is explained in Figure 2.14. Any convolved response $v(t)$ is the result of the convolution of the sequence, $s(t)$, and the

unitary response, or the response due to a single stimuli, $a(t)$. Taking the Fast Fourier Transform (FFT) of the described equation gives $V(f) = A(f)S(f)$, since the frequency domain version of convolution is multiplication. Now the unitary response $A(f)$ can be isolated merely by dividing by $S(f)$, provided the transfer function of the sequence used contains no zeroes.

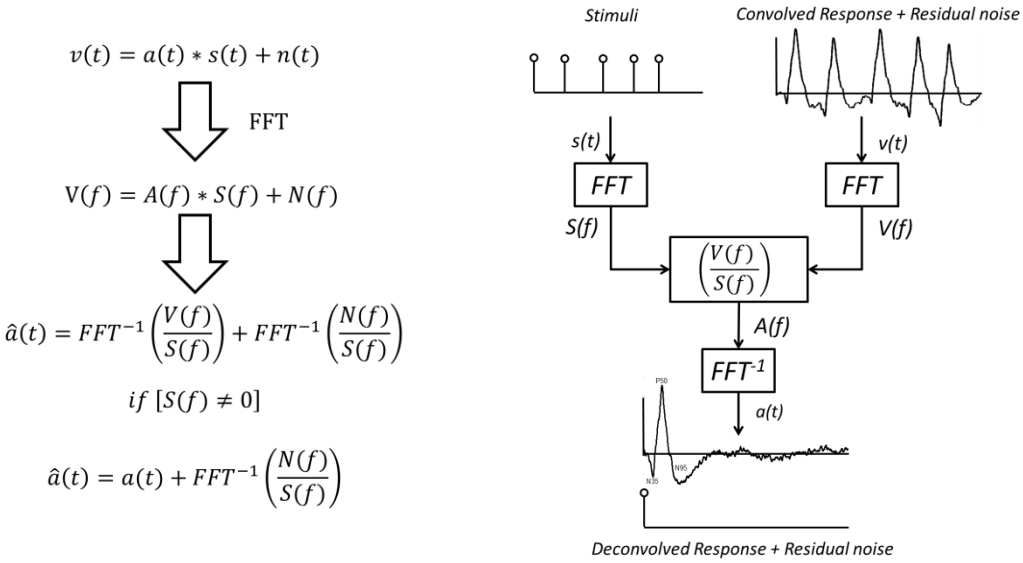

Figure 2.14 - Frequency domain analysis of the deconvolution method. The recorded response v(t) is equivalent to the convolution of the unitary response and the stimulus. In the frequency domain, convolution is equivalent to multiplication. By dividing by the Fourier transformed stimulus, S(f), we can isolate A(f). This is of course contingent that the transfer function of the stimulus contains only non-zero values. Finally, performing the inverse Fourier yields the time domain transient response a(t). However, any noise recorded in the original signal, n(t) will be effected by the division of the sequence s(t) in the frequency domain. Depending on the sequence, this can amplify noise, destroying the signal, or attenuate noise, improving signal to noise ratio(SNR) (Ozdamar and Bohorquez,2006)

Special care must be taken in generating these CLAD sequences. A consequence in generating these non-zero stimulation sequences is the potential addition of noise and a resulting reduction in the signal to noise ratio (SNR) (Ozdamar and Bohorquez, 2006). Any residual noise recorded with v(t) will be affected by the frequency domain division

by the sequence S(f). This noise shaping property of CLAD sequences can be detrimental or beneficial to the SNR depending on the sequence. In a well-designed sequence, however, this factor can actually improve the SNR, but care must be given to ensure it does not increase noise and degrade the acquired signal. The noise shaping properties of CLAD sequences are quantified by a noise amplification factor (NAF). The NAF of the sequence is a measure of the inverse of the transfer function of the jittered sequence, $\frac{1}{s(f)}$. In order for CLAD to work, the S(f) must contain no zero values. However, due to the noise shaping properties of the CLAD sequences (Figure 2.14), NAF values > 1 will amplify noise, while NAF values < 1 will attenuate noise. This is another consideration when designing CLAD sequences. Ideally, the NAF would completely contain values close to zero. This is often not possible given the constraints placed on the jitter. Typically sequences are designed to have a NAF below 1 for all values, and a value as close to zero as possible at the mean stimulation rate.

Another consideration/constraint on the design of CLAD sequences is the amount of jitter introduced. Before deconvolution, responses acquired using CLAD sequences are referred to as “quasi-steady-state”(qss). The attached “quasi” is there because the jitter introduced delays or advances the onset of stimuli in the sequence from a pure steady-state sequence. This is done, as previously stated, to achieve a non-zero transfer function. The balance that must be attained is between introducing enough jitter to achieve a non-zero transfer function, while still keeping the jitter narrow enough that the attained response still approximates a true steady-state response. The tradeoff is that the closer to the true steady-state, the higher the noise amplification factor (NAF). For further on CLAD sequences, see Figure 2.15.

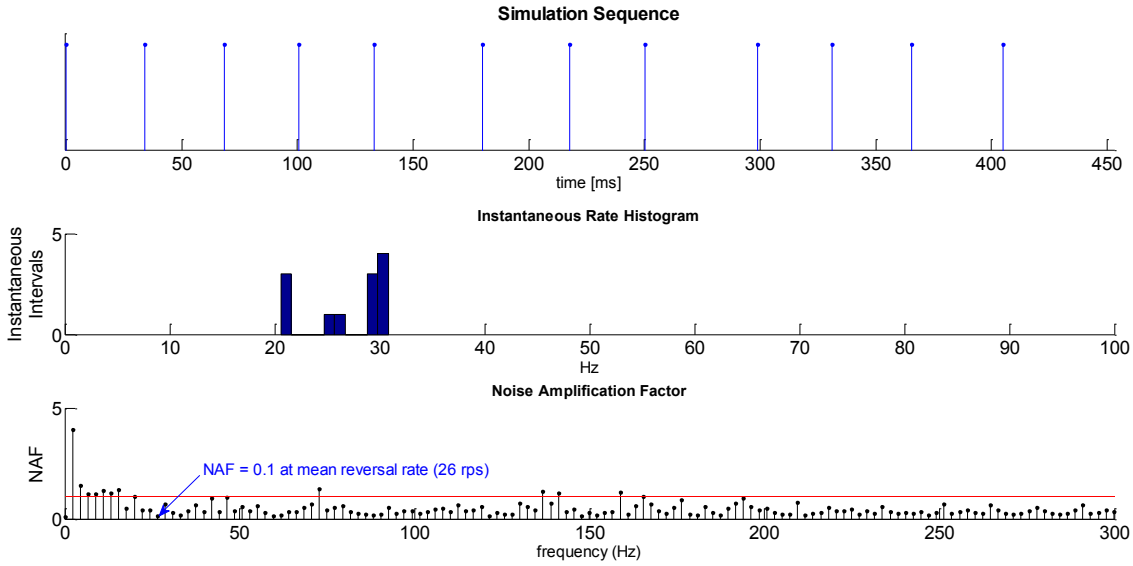

Figure 2.15 - Sample CLAD sequence: The above figure shows some of the parameters of a CLAD sequence. The top shows the onsets of each of the stimuli (a reversal or a flash for ERG). Note that the inter-stimulus intervals vary for each interval. The middle graph is a histogram showing how far the jittered intervals stray from the center frequency (in this case, the mean reversal rate is 26 rps). The bottom graph illustrates the noise shaping parameters of the sequence, the noise amplification factor. Ideally, the entirety of the frequency response would be below one, with the harmonics of the center frequencies as close to zero as possible. The tradeoff however is that the closer the histogram is to the center frequency, the worse the noise amplification.

Once optimal sequences for the desired stimulation rates have been generated, it is possible to obtain the traditional steady-state response and extract the per stimulus contribution to the response (extracted transient response) simultaneously and in the same acquisition time as using a conventional steady-state stimulation sequence.

A. **Applying CLAD to the Electroretinogram**

As previously stated in this proposal, the analysis of ERG recordings differs depending on whether the responses are transient (stimulation rate <3 Hz/6 rps) or steady-state (stimulation rate >5 Hz/ 10 rps). In transient ERG analysis, analysis is peak-based, looking at the amplitudes and phases of named peaks. With steady-state responses,

peak based analysis is impossible, as peaks are obscured by overlapping responses. Because of this, steady-state analysis is typically done in the frequency domain, looking at magnitude and phase of the responses. The most immediate potential benefit of applying CLAD to ERG responses is a unification of analysis techniques. CLAD can theoretically be used to extract the response from a single reversal from a $PERG_{ss}$ response (see Figure 2.16). By unwrapping higher rate, steady-state responses and attaining the obscured unitary response it is possible to apply peak-based analysis to higher rate responses. This could lead to a uniform analysis paradigm that could be applied to all PERG signals, regardless of the stimulation rate.

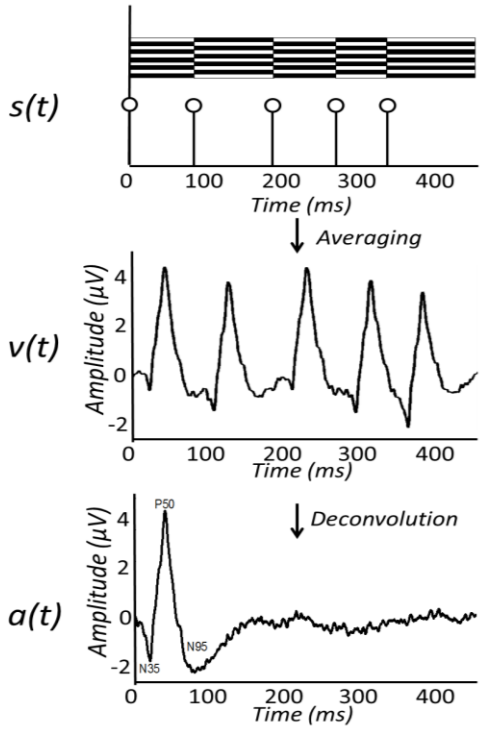

Figure 2.16 - Deconvolution of $qPERG_{ss}$: h(t) above shows the CLAD sequence. Each stem represents a trigger sent to the stimulus. This trigger will result in a reversal of the pattern stimulus. v(t) shows the resultant convolved $qPERG_{ss}$ which will be acquired from the subject. After passing v(t) through the Deconvolution algorithm, we will extract a(t), the response due to each individual reversal.

Prior to designing any CLAD sequences for this study, it was important to determine the sweep length to be used for the PERG recordings. The absolute minimum sweep length recommended for PERG recordings is 150 ms (Holder et al., 2007), however more recent updates to PERG standards suggest sweep lengths of 250 ms (Bach et al., 2012). At higher stimulation rates, waveform components can begin to lag in latency. In order to allow for the potential shifting of peaks at higher stimulation rates, a sweep length of 450 ms was chosen. This sweep length would ensure that regardless of the stimulation rate, and any rate based adaptation, deconvolved responses would have sufficient time to settle. Additionally, a sweep length of 450 ms would allow the same sequences to be used for the acquisition of VEPs as well (Odom et al., 2010), or even the simultaneous recording of PERG and VEP (despite that the acquisition of cortical potentials is outside the scope of the studies herein).

The current CLAD sequence generation technique utilizes a 10-bit buffer to create jittered stimulation sequences. Utilizing a 450 ms sweep length, the increment of jitter will be:

$$Jitter\ Increment = \frac{Sweep\ Length}{2^N} = \frac{450ms}{2^{10}} = \mathbf{439\ \mu s}$$

This means that the PERG stimulus onsets will need to be able to be advanced or delayed in increments of 0.44 ms when designing CLAD sequences for PERG.

B. VDU Implications for CLAD compatibility

Refresh rates for the aforementioned displays not only limit the maximum possible stimulation rate, but also limit intermediate rates to integer multiples of this refresh rate. This becomes especially problematic when trying to introduce jitter to an isochronic sequence. These limitations add even more constraints on the already non-trivial process of generating CLAD sequences, essentially rendering the displays incompatible with CLAD as depicted in Figure 2.17. The above limitations demonstrate the necessity to develop a display which would have the freedom of stimulus rate required for the CLAD algorithm.

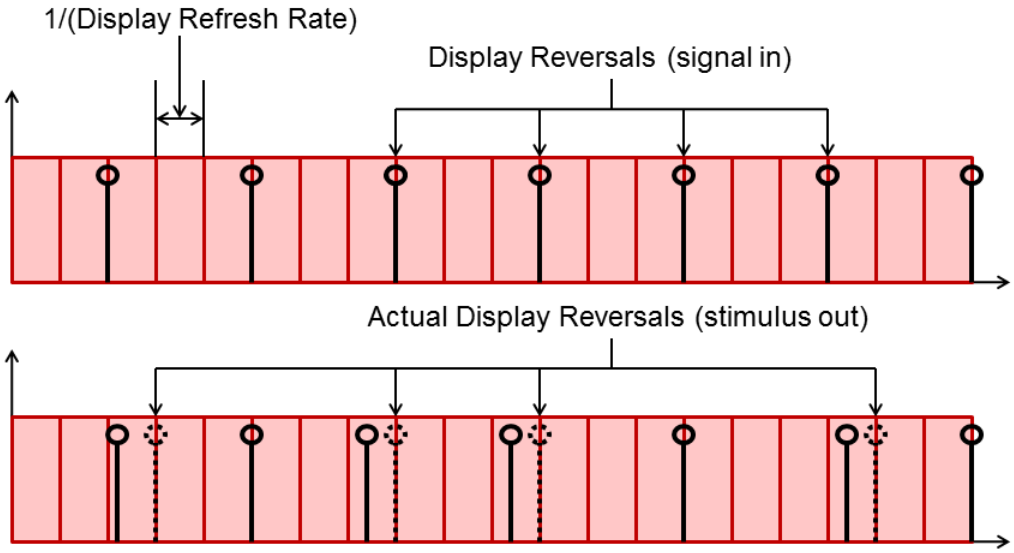

Figure 2.17 – Schematic diagram showing the refresh rate implications on CLAD sequence generation – The red bins in the above figure illustrate the refresh rate of a VDU. Any changes to stimulus output of the VDU can only occur as integer multiples of the refresh rate. In order to create CLAD sequences the stimulus onsets must be advanced and delayed individually. The solid stem plots represent the signal in to the VDU, the intended display reversal times. If a CLAD stimulation sequence requires a VDU to change stimulus between frames, the stimulus out (dashed stem plots) will not occur until the beginning of the next frame. With the stimulus onsets so crucial to the CLAD algorithm, the width of the frame intervals is a critical parameter of a CLAD compatible VDU.

Chapter 3 - Goals and Objectives

The primary goal of this dissertation is to acquire the unitary, or "per stimulus" PERG responses at rates which are of particular clinical significance, but currently are only able to be observed as steady-state responses. The aims to achieve that goal are as follows:

Specific Aims:

1) **The development of a PERG stimulator which will be compatible with our CLAD deconvolution algorithm.**

   Three potential, CLAD friendly displays were proposed and realized: An LED array design, a dual projector design, and a variable polarizer design. Each alternative implementation had its own strengths and unique design considerations that are described in detail in the next chapter.

2) **The development of CLAD sequences specifically tailored to acquire ERG responses at a number of rates.**

   For each stimulation rate, a unique CLAD sequence was created based on the sequence generation process described in the previous chapter.

3) **The acquisition of traditional PERG responses, both steady and transient, at traditional rates in a number of human subjects, using steady state stimuli.**

   In order to show that the CLAD technique does not alter the responses, traditional $PERG_{tr}$, $PERG_{ss}$ were acquired using the developed stimulator. These served as a control to compare with conventional PERG acquisition systems.

4) **Synthesis of the steady state response using extracted transient PERG responses.**

   In order to lend further credence to the deconvolution method we used and the test the superposition hypothesis describe in Chapter 2.4B, extracted transient responses were artificially reconvolved to generate synthetic steady state PERGS (synPERG$_{ss}$) and then compared with conventional steady state responses (PERG$_{ss}$).

5) **Study of the effects of rate on the PERG response.**

   The effect of rate on the PERG was investigated using both quasi steady state PERG (qPERG$_{ss}$) and extracted transient qPERG$_{tr}$ at all rates.

6) **Study of the dynamic aspects of the visual steady-state response using stimulation bursts.**

   One of the main assumptions of CLAD is that the response is not adapting during acquisition. To verify this, the dynamic aspects of the PERG$_{ss}$ response were investigated. This was achieved by using bursts of stimuli, so that the establishment of, and subsequent dying out of the PERG$_{ss}$ can be observed

Chapter 4 - Materials and Methods

4.1 Visual Displays for High Rate ERG testing.

Key to the aims of this dissertation was the realization of a CLAD compatible ERG display. As discussed earlier in this document, conventional methods for presenting ERG stimuli do not provide the temporal resolution necessary to be compatible with CLAD. As discussed in Chapter 2.6, in order to fully optimize CLAD sequences for ERG, a VDU would need to be able to reliably deliver stimuli with a temporal precision of *0.44 ms*. This corresponds to a VDU with a refresh rate over *2.2 kHz*. Chapter 2.7 describes the refresh rate of common CRT and LCD VDUs. These displays typically exhibit refresh rates between 60 and 75 Hz. Even specialty, 'high refresh rate' CRT monitors do not exceed 200 Hz (Elze, 2010). Unfortunately, these specifications fall far too short of what is required of a CLAD compatible VDU.

Three potential CLAD compatible VDUs, each using different methods for generating the stimulus were proposed, designed and implemented in the course of this research (Toft-Nielsen et al., 2011). The realized CLAD compatible VDUs are as follows: An LED array design, a dual projector design, and a variable polarizer design. Each alternative implementation had its own strengths and unique design considerations, the details of which will be elaborated on further later.

A. **Stimulus Parameters for Visual testing**

The various parameters for ERG stimuli were outlined in (Brigell et al., 2003; Holder et al., 2010). Where applicable, these standards were followed when designing the three custom displays. Some of the critical stimulus parameters are as follows:

- Luminance greater than 80 cd/m^2 for PERG (30 cd*s/m^2 for FERG)
- No transient changes in mean field luminance
- Contrast greater than 80%
- Field size between 10° and 30°
- Display patterns with even number of equally sized elements

B. **LED Array stimulator**

Light emitting diodes (LEDs) have been used in visual electrophysiological studies for many years (Evans et al., 1974; Krakau et al., 1977; Epstein, 1979; Mushin et al., 1983; Skuse et al., 1984; Kooijman and Dambof, 1986, Link et al., 2006). LEDs belong to family of epitaxial semiconductor junction diodes. These devices contain two layers of semi-conductive material containing different dopants; one primarily positive and the other primarily negative (see Figure 4.1). When a sufficient bias is placed across the junction, charge will move from one layer to another resulting in the emission of photons, i.e. light (In the case of white LEDs, the emitted photons are used to excite a phosphor, as in CRT monitors).

LEDs have many desirable characteristics as a light source. They are compact, inexpensive, efficient, and require low current, making them intrinsically safe for clinical use (Hogg, 2006). Additionally, they are simple to drive and have response times in the sub-millisecond range. This last factor is of utmost importance, as an LED based pattern

display would be capable of delivering both high rate stimuli, as well as the jittered CLAD stimuli.

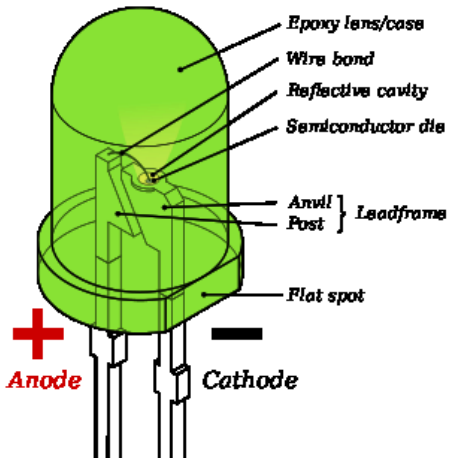

Figure 4.1 – Diagram for a typical LED: LEDs are an inexpensive yet efficient light source. Typically they are comprised of a junction of two semi-conductive materials. When the proper bias voltage is applied across the junction, current flows, and light is emitted.

Initially, the LED based display was structured with LEDs in an array, similar to the work done by Evans (Evans et al., 1974). 150 white LEDs were arranged in a 10 x 15 grid. LEDs were driven in two groups, with even rows being one group, and odd rows the other. In this way, the LED grid would approximate a pattern stimulus containing alternating black and white horizontal bars, with an ON group of rows serving as the white bars, and an OFF group of rows serving as the black bars. It is important to ensure an even number of pattern elements, with equal numbers of modulating pairs. This is in order to ensure that the overall net luminous intensity of the display remain constant, otherwise PERG waveforms will become contaminated by flash responses. At this point,

however, the LED array appears as 150 discrete points of light, rather than a continuous pattern. Ideally, the display should consist of bars of continuous and uniform intensity.

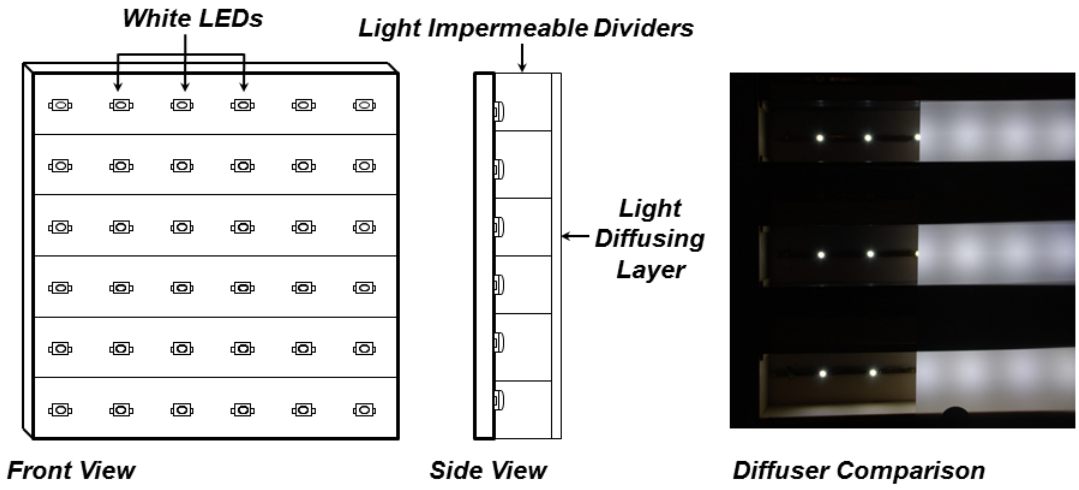

Figure 4.2 - Initial Design for LED array stimulator – An early prototype constructed from 36 white LEDs in a 6 x 6 grid and composed of 3 ON/OFF pairs. In order to illustrate the improved uniformity, the LED array stimulator is show above only half covered by the diffusing film. Notice the clear delineation between the lit (white) areas and the off (black) areas. This iteration of the stimulator was constructed prior to the development of the diffuser optimization program, and as such "hot spots" are still visible through the diffuser. (Toft-Nielsen et al., 2009)

In order to better approximate the uniform intensity of the pattern elements displayed on conventional stimulus displays optical diffusers were used in conjunction with the LED array. Using a layer of optical diffusing material, it is possible to eliminate the dark space between LEDs and create a continuous region of intensity. To determine the correct spacing between LEDs, and the appropriate height for the diffusing film, the LEDs were modeled and a program was developed. Traces showing the model versus the specifications of the LEDs can be seen in Figure 4.3. The desired diffuser height and LED spacing are entered into the program, and it, in turn, returns the total power distribution at the diffuser due to the array of LEDs, as shown in Figure 4.4. Additionally

the program returns the simulated uniformity based upon the parameters entered (see Figure 4.5).

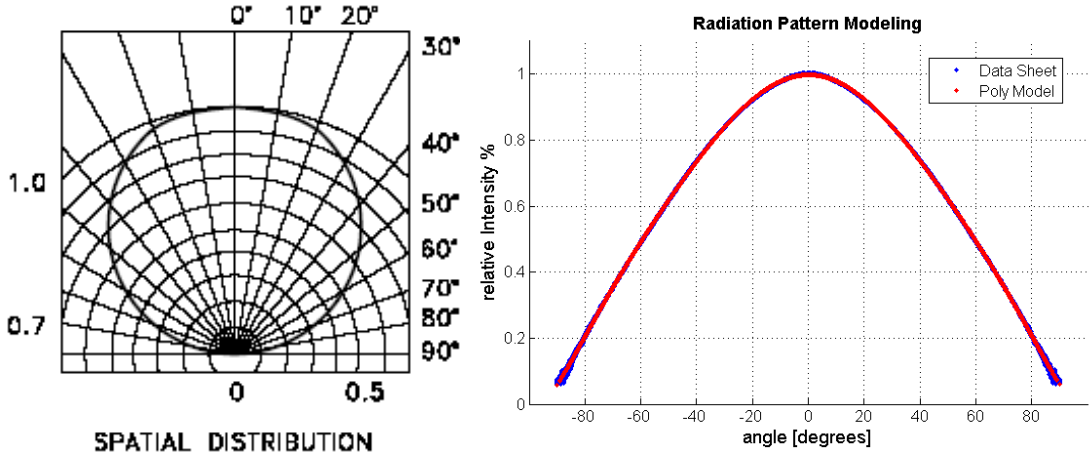

Figure 4.3 - Radiation Pattern Model – In order to determine the optimal LED spacing and diffuser height, the parameters of the LEDs were entered into the computer. The above graph shows the relative normalized intensity of one of the LEDs and a function of the viewing angle. The blue trace shows the data extracted from the LED datasheet, while the red trace shows the model designed which approximates the performance of the LED. (Toft-Nielsen et al., 2009)

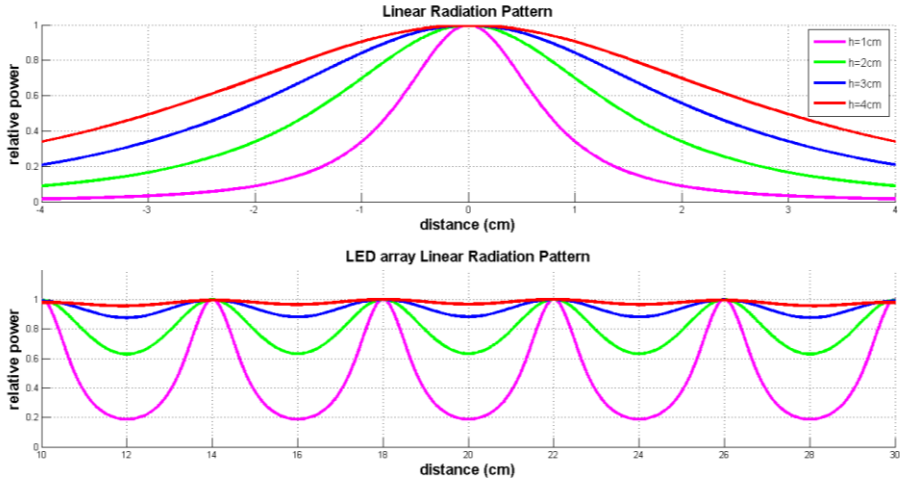

Figure 4.4 - Linear Radiation Patterns – Power distributions for a single LED (top) and for multiple LEDs spaced 4cm (Bottom) at diffuser heights ranging from 1 to 4 cm. In order to achieve uniform intensity across the pattern a relative power of 1 across the graph is desired. (Toft-Nielsen et al., 2009)

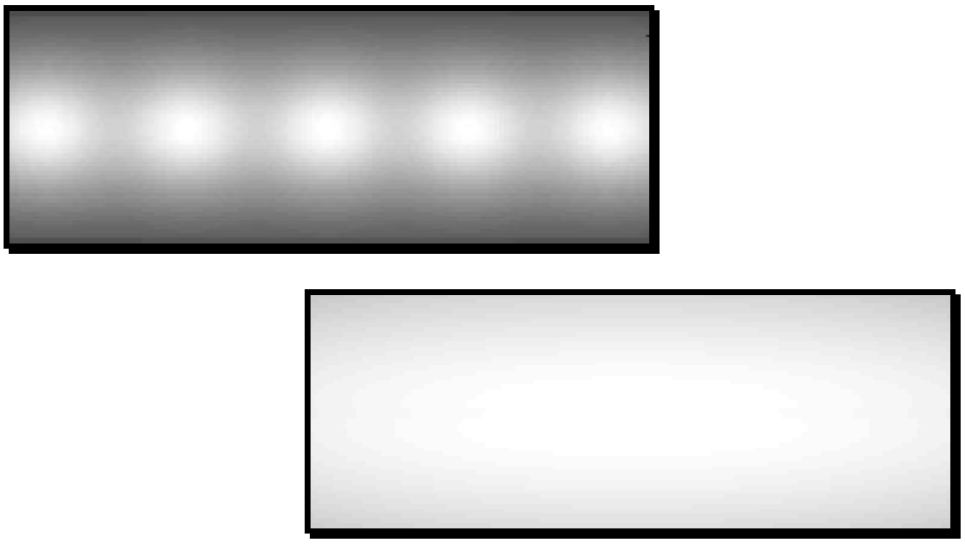

Figure 4.5 - Simulation of Uniformity at Diffuser –Two computer generated estimations of the uniformity of intensity for different diffuser heights and spaces using the developed program. The top image was produced for the diffuser height and LED spacing of the prototype shown in figure 4.2, and exhibits a similar pattern, complete with hot spots. The bottom image shows a more ideal intensity uniformity, which was used for later iterations.

An unwanted consequence of diffusion is the disruption of the structured nature of the stimulus granted by the arrangement of the LEDs and the loss of a well-defined pattern edge, as seen in Figure 4.6. In order to maintain a clear demarcation between pattern elements, light impermeable barriers must be used to separate pattern elements, similar to the work done by Link (Link et al., 2006). These barriers serve the purpose of preventing cross talk between adjacent bars, ensuring contrast ratio between black and white elements above 80% (Bach et al., 2000; Holder et al., 2010), as well as give a clean and well defined edge between black and white elements in the pattern stimulus.

Unfortunately, in this design, any thickness to the barriers between pattern elements will contribute to a pattern mismatch, where the black bars will actually appear thicker by two times the thickness of the boundaries, see Figure 4.6. It is imperative that white and black elements are equal in number and area for the pattern stimulus (Bach and Hoffman, 2006), and as such the thickness of the light impermeable boundaries must be minimized. In initial designs, boundaries were placed between rows of the LED grid with open air between them. However, as the boundary thickness was minimized it became difficult to find a material thin enough to maintain the structured stimulus and support the diffusing film in open air. As such, the final design employed clear acrylic as a sort of wave guide for the LEDs. The acrylic bars were coated with a reflective film which prevented cross talk between bars with negligible thickness. These waveguides were then affixed together and placed atop the LED grid. This structure formed continuous bars of light and darkness which were equal in area, prevented cross-talk between bars, and provided a continuous surface for the diffusing layer to rest upon.

Additionally, the LED array was also designed such that the ON/OFF pattern groups could be altered to turn on and off in phase, so that all pattern elements could be turned on and off in unison. This could be then be used to acquire FERG responses when used in conjunction with a diffusing eye piece to ensure complete retinal stimulation.

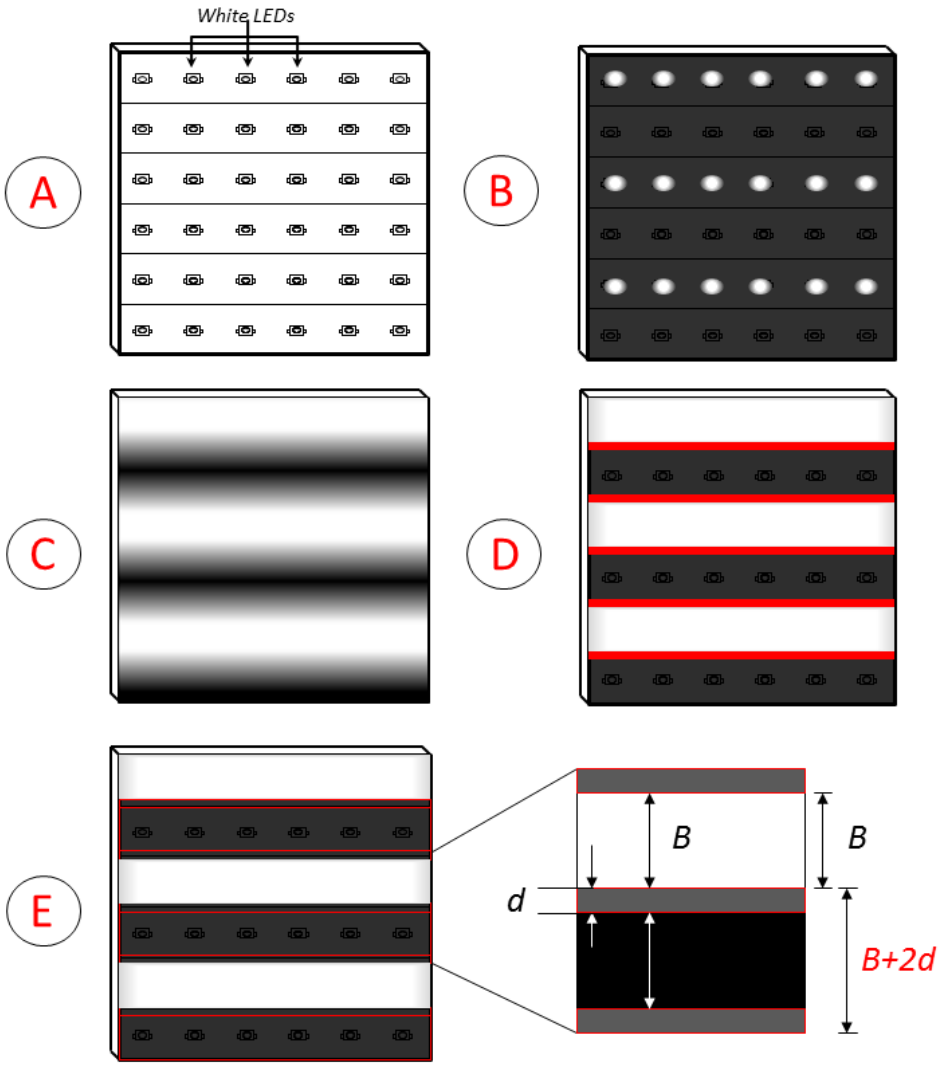

Figure 4.6 – Optimization of LED array – There were a number of hurdles in approximating the pattern stimulus field using discrete LEDs: A) Discrete white LEDs were arranged into the approximate pattern. B) Discrete LEDs along lines is not a good approximation of the pattern field. C) In order to eliminate gaps between discrete elements a diffuser was placed at a distance from the display. However, while horizontal diffusion is achieved, there is significant cross-talk into adjacent black bars and a poorly defined pattern edge. D) To eliminate cross-talk between ON and OFF pattern elements, light impermeable dividers were placed between pattern elements (shown in red). E) Utilizing a combination of diffusers and light impermeable dividers, the desired pattern of continuous black and white bars is achieved. However, the thickness of the barriers is a critical factor, as the thickness of the divider will contribute to the perceived thickness of the OFF elements. In the worst case scenario, white bars will appear to be the designed thickness, B, while black bars will be perceived as being B+2d (d being the thickness of the dividers) width. This results in an undesired pattern mismatch. To minimize this effect, dividers much be chosen to have minimum thickness, while still exhibiting the rigidity to maintain the pattern.

C. Projector VDU

Figure 4.7 – LCD Micro projector – Gigaware micro projector (Ignition L.P., 25-1198), a compact LCD projector. Two of these miniature projectors were used to alternate between pattern reversal stimuli.

The second proposed VDU is comprised of an enclosure and two micro projectors. The principle behind this VDU involves each of the projectors displaying one phase of the pattern stimulus. By aligning the two projections, and then alternating between the two, pattern reversals can be generated.

Two Gigaware Micro Projectors (Ignition L.P., 25-1198) were used to in this VDU (Figure 4.7). These projectors use LCD technology in creating images, have an LED based illumination system and are compact in size. Since the projectors utilize LCD technology to produce images, they possess all the limitations of the displays described in Chapter 3.1. However, the proposed VDU circumvents these limitations by using the projector only to display a static image. Each of the two projectors was configured to display one phase of the pattern stimulus (i.e. Black-White-Black on one projector, White-Black-White on the other). The projectors were then arranged in an enclosure

such that their projections overlap on a rear projection screen (Figure 4.8). Once the projectors are aligned, a subject viewing the screen from outside the enclosure would observe pattern reversals when the projectors alternate. A major hurdle of this implementation however is that the projectors have a significant start up lag, making it is impractical to power on and off the projectors to create reversals. To overcome this, the projectors were altered so that the illumination source (an LED) could be turned on and off independently of the other electronics of the projector. After this alteration, the projectors could effectively be turned on and off with an external trigger with the only factor limiting the reversal speed being the on/off time of the LED illumination source.

The projector design allows for flexibility in both the time and spatial resolution, as any patterns can be presented on the projectors. However, as alignment is crucial, it might prove a problem in this design.

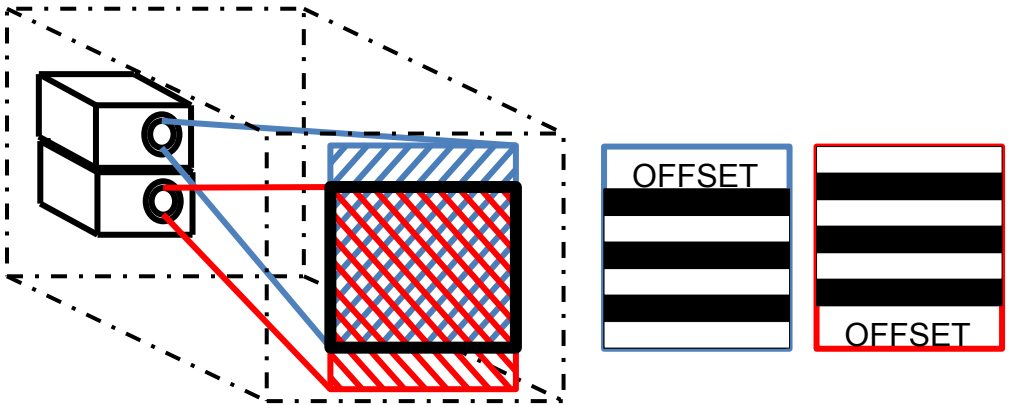

Figure 4.8 - Dual Projection stimulation –Two projectors placed in an enclosure are arranged so that their projections are overlapping on a rear projection screen. Each projection is then configured to display one state of the Pattern reversal stimulus (right). In order to compensate for misalignments, the patterns are offset to ensure the entirety of the stimulus falls on the rear projection screen.

D. **Variable Polarizer VDU**

The third proposed VDU, like the projector design, uses an overlay of two images. However, instead of the images coming from two different projectors, each image will consist of light of a different polarization. As described in Chapter 3.1, conventional LCD displays generate images by manipulating the polarization state of a white backlight (Husain et al., 2009; Elze, 2010). Images displayed on LCD VDUs are made up of groups of RGB pixels. Each LCD pixel is capable of altering the polarization state of the light passing through it, varying the polarization of red, blue and green light independently (Figure 4.9a). Depending on the intended color of the pixel, the RGB polarization state will be altered such that that color passes through the outer polarizing layer while the remaining portion of the white backlight is blocked by the outer polarizing layer. Because of the nature of the display, the blocked portion of the light happens to be the inverse of the intended image. Essentially, images on LCD displays are created by subtracting the inverse of the image from the white back light. If the outer polarizing layer of an LCD display was rotated by 90^{o}, the resulting image would invert (Figure 4.9b). Since white and black are inverses of each other, this principle of LCD displays can be exploited to create a pattern reversal VDU.

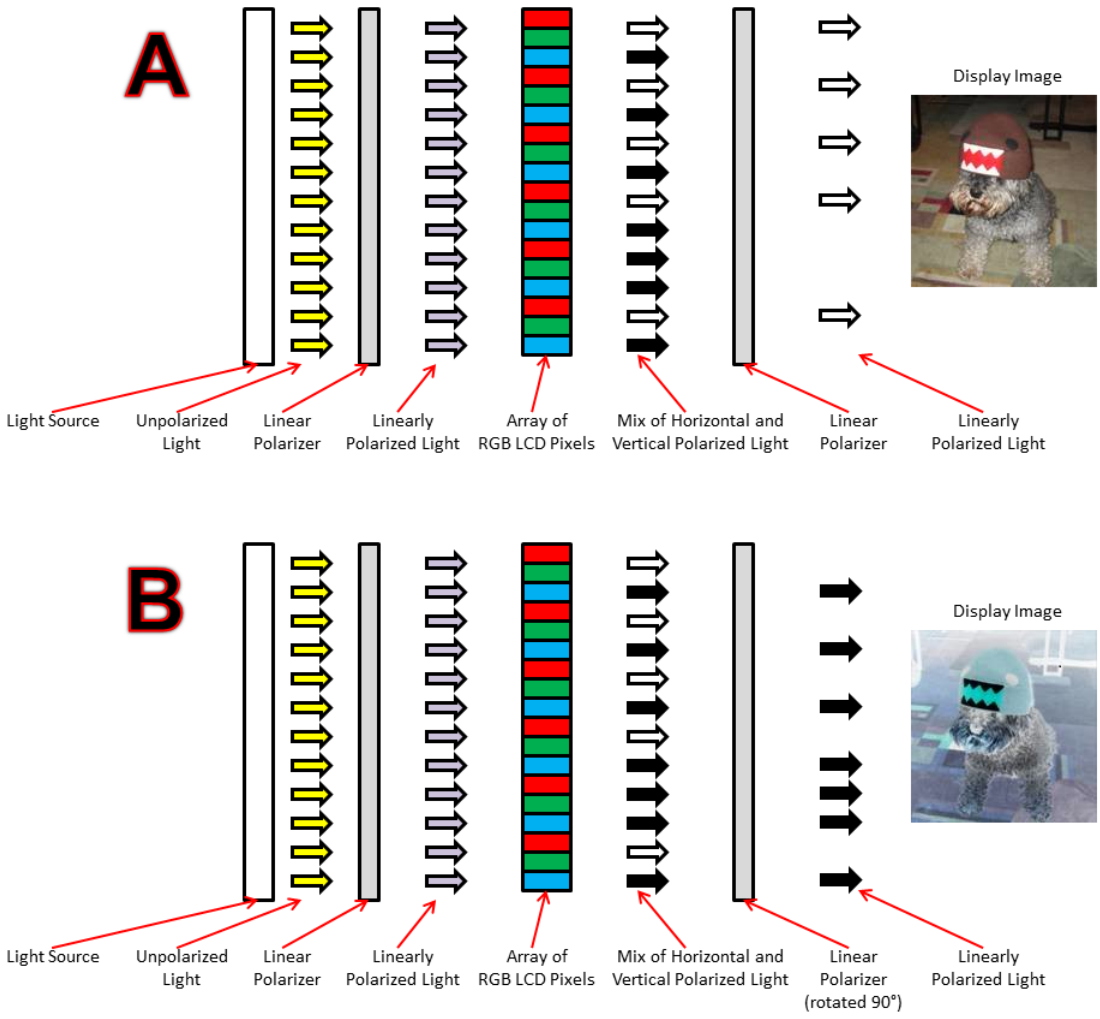

Figure 4.9 – Creating contrast reversals using an LCD display – (A) Conventional LCD displays alter the polarization of a back light in such a way that portions of the back light are blocked by an outer polarizing layer to create an image. (B) If the orientation of the polarizing layer is rotated by 90°, the components which are blocked and passed by the layer will exchange. This results in the inverse of the display image shown in (A)

Since human eyes cannot differentiate between polarization states of light directly, removing the outer polarizing layer of an LCD display results in a white field. The white light exiting the display has an image embedded in it by polarization. Physically rotating a linear polarizing filter 90° over the display will result in pattern reversals, however, mechanically rotating the polarizing layer is not practical. It is possible to introduce an element which will modulate the polarization of the entire field to achieve the desired

effect; such effects are often used in 3D display technologies (Pastoor and Wöping, 1997).

LCD shutters effectively behave like large scale LCD pixels. A single large LCD cell, placed over the entirety of the display, or alternatively, in front of the eye of an observer can be used to introduce an up to a 90° polarization shift depending on the state of the LCD cell. Typical LCD shutters have response times around 80 ms, which would impose the same restrictions on CLAD as CRT and conventional LCD technologies, however fast switching LCD shutters are available (Bos and Koehler, 1984). Pi-cells are fast switching LCD units which can reliably achieve switching rates of up to 1 kHz, making them suitable for a CLAD compatible VDU (Pastoor and Wöping, 1997).

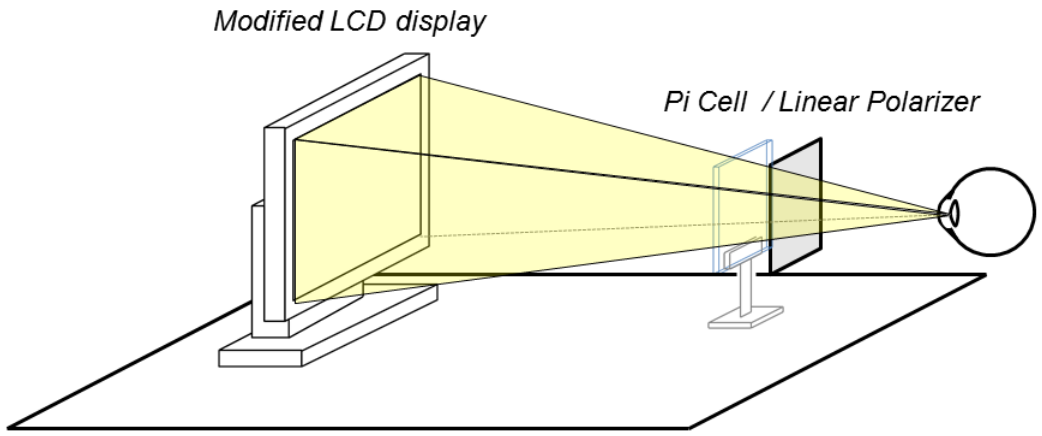

Figure 4.10 – VDU using modified LCD and Pi-cell –By creating a viewing system where a subject views a modified LCD through a linear polarizer and pi cell element it is possible to create pattern reversals by alternating the state of the pi-cell element, effectively acting as a variable polarizer. This VDU is capable of generating pattern reversals up to 1,000 rps.

E. **Microcontroller based Stimulator Driver**

In order to control the developed VDUs, a microcontroller interface was designed which could interpret the external trigger of the commercial acquisition system, and generate the different driving signals required for each unique stimulator, ensuring that data acquisition and stimulus presentation were synchronized. Depending on the type of experiment and the stimulator being used, different software sets, and daughter boards could be used with the microcontroller. For this purpose the Arduino Duemillanove was selected. The Arduino is desirable as it has an extensive library and a large community developing for it. The Arduino also supports in-line programming via USB, allowing the program on the microcontroller to be switched out or altered slightly at any time.

For each of the three CLAD compatible VDUs a daughter board was designed containing all the specific electronic components required for the operation of the specific VDUs (see Figure 4.11 and 4.12). Depending on which VDU was going to be utilized, the corresponding board could be attached to the microcontroller and allow the VDU to interface with the acquisition system. In this way, both the hardware and software necessary to drive the stimulator could be contained in a single, compact package.

The microcontroller shield designed for use with the LED VDU and Projector VDU, contains two LED drivers (VLD24-500, CUI inc). These drivers were chosen specifically for their output current stability. Additionally, these drivers allow for external brightness control, which was designed to be controlled by software via the microcontroller. Each driver controls every other bar in the LED array, in other words one driver controls the even bars, while the other controls the odd bars. By reprogramming the microcontroller,

it is possible to alternate between the two drivers and create a pattern-reversal stimulus, or to have the drivers activate and deactivate together, creating a flash stimulus. Additionally, by altering the software, the VDU could be configured to deliver square-wave reversals or sinusoidal reversals. The microcontroller can also be reprogramed to control the contrast of the LED VDU, or change the stimulus modality to pattern onset/offset or a number of other stimulus modes.

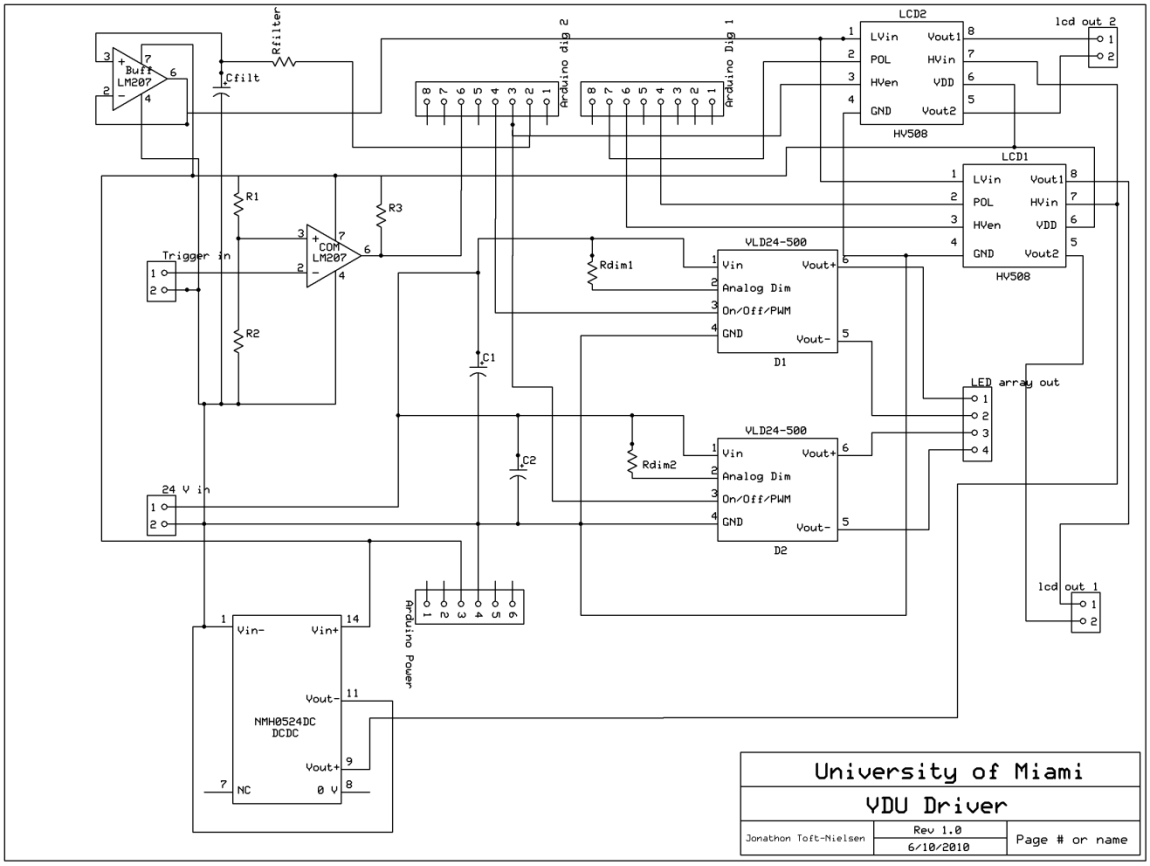

Figure 4.11 – Unified Arduino Shield Schematic –Schematic containing the driving electronics for all three developed VDUs. The LED drivers could be altered to handle the different loads of the LED array VDU or the dual projector VDU. For the variable polarizer VDU, high speed LCD shutter drivers for up to two variable polarizers were incorporated. Each of the hardware components was interfaced to the microcontroller to allow for software control of the hardware elements.

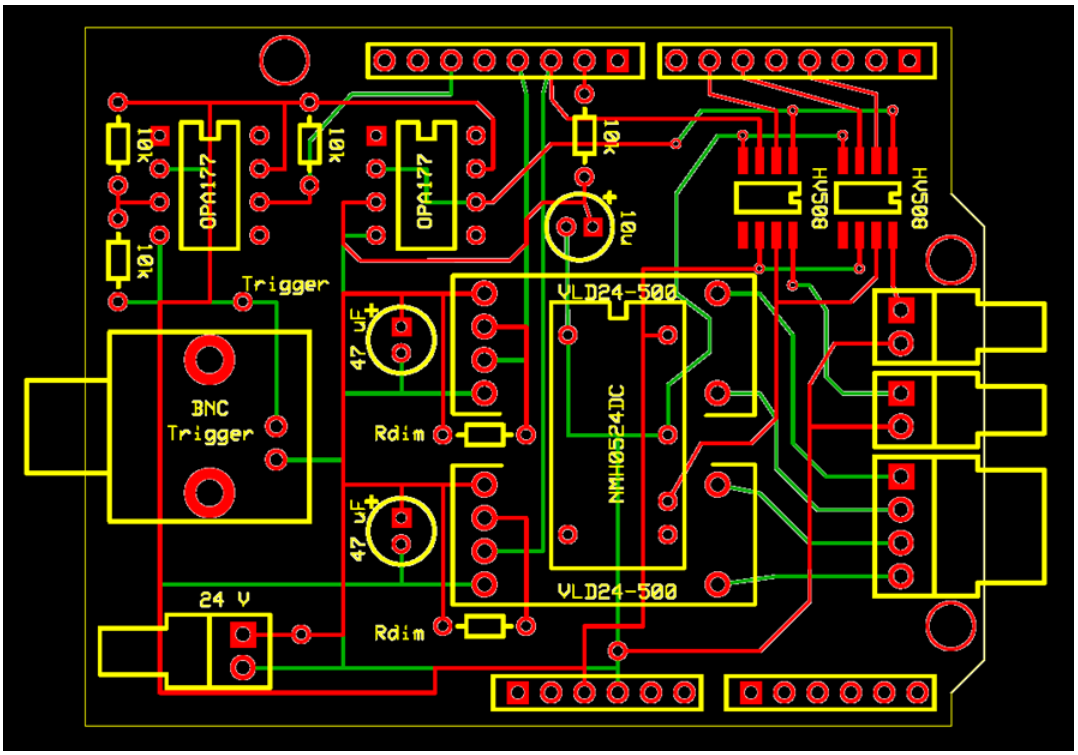

Figure 4.12 - Arduino Shield PCB – Printed circuit board design for the schematic in figure 4.11. The PCB was designed to rest atop the Arduino microcontroller board. A hybrid design was developed which could allow a single PCB design to be utilized for any of the three designed VDUs simply by soldering the corresponding hardware components for the desired VDU.

The pi cell driver board contains a DC/DC converter (NMH0524DC, Murata Power Solutions) to generate a 48 V signal required by the pi cell and a high voltage liquid crystal shutter driver (HV508, Supertex inc) to modulate the high voltage drive signal. The board was designed to accommodate two variable polarizers, for use with future experiments which will call for simultaneous stimulation of each eye at a different stimulation rate.

4.2 Subjects and Procedures

Subjects were recorded using an institutional review board (IRB) approved protocol. All subjects were normal with no history of retinal dysfunction. Subjects with corrected vision were tested with their corrective measures (lens/contacts) in place. Subjects were prepared for monocular recordings with gold skin electrodes placed on the lower eyelids and forehead (see Figure 4.12). The active electrode was placed below the subject‘s dominant eye, while the other eye was used as the reference. The reference eye was then occluded via a patch. The ground electrode was placed on the forehead (Tan et al., 1989 and Odom et al., 1987). Electrodes were then plugged into a commercial bio-amplifier which connected via fiber optics to the commercial acquisition system.

Gain settings for the bioamplifier were set with software to 100k, and analog filter settings were set to pass frequencies between 1-300Hz (Bach et al., 2012). The specially designed CLAD sequences were loaded into the corresponding acquisition software which sent a trigger signal to the microcontroller interface. Depending on the stimulator being used, the microcontroller would translate the trigger into the corresponding driving signal.

All responses were acquired using a commercial grade acquisition system (Universal Smart Box, M011110) developed by Intelligent Hearing Systems (IHS), Miami FL. The system includes an isolated bioamplifier, and a hardware acquisition box, along with associated acquisition software. All three stimulators were developed to utilize a trigger from the IHS system so that acquisition would be synchronized with the stimulus.

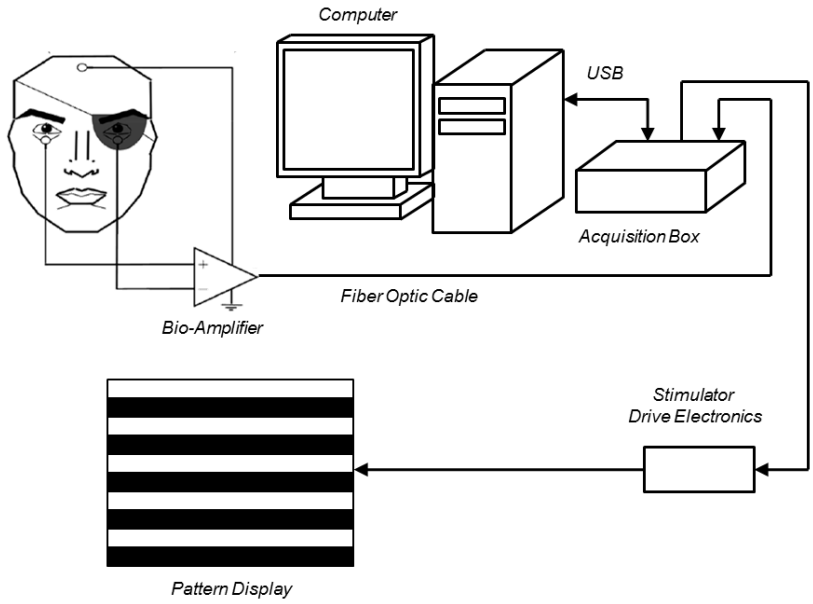

Figure 4.12 - Experimental Setup – Simplified block diagram of the experimental setup. An eye patch is used to occlude one of the subject's eyes for monocular recordings. Skin electrodes are placed beneath each of their eyes (active-unocculded eye, reference-occluded eye) and on the forehead (ground). The electrodes plug into a bioamplifier (Opti-Amp, Intelligent Hearing Systems) which is connected via a fiber optic cable to a commercial grade acquisition system (IHS USB Acquisition system, Miami, FL). The specially designed VDU drive electronics (section 4.1e) are connected to acquisition system. The VDU driver receives a trigger signal from the acquisition box which toggles the state of the connected VDU and is also used to synchronize the averaging. The associated acquisition software is run on an attached computer, allowing for real time monitoring and post recording processing of the signals.

4.3 Validation of Developed VDUs

A. VDU Strengths and Weaknesses

The primary motivation behind each of the developed VDUs was to provide enough temporal resolution to be able to utilize the CLAD algorithm on PERG responses. The secondary concern was that the VDUs met the requirements set out in the various standards for pattern electroretinography (outlined earlier in this chapter). While all three are capable of presenting pattern stimuli at a fast enough rate to utilize CLAD, each

implementation has additional strengths and weaknesses which influenced the decision for which VDU to use for the remainder of this study.

The LED VDU rise time and fall time were measured with a nanosecond photo detector (Model 1621, New Focus inc.). Plots showing the LED transitions from on to off are shown in Figure 4.13. The LEDs are capable of transitioning from ON to OFF in less than 0.5 ms, making them able to change states fast enough to be used with the CLAD algorithm. The LED display also generates a luminance of 150 cd/m^2, making it bright enough to be used for PERG (Bach et al., 2012). Luminance levels were validated using a Photometer (Gamma Scientific DS-2000-1).

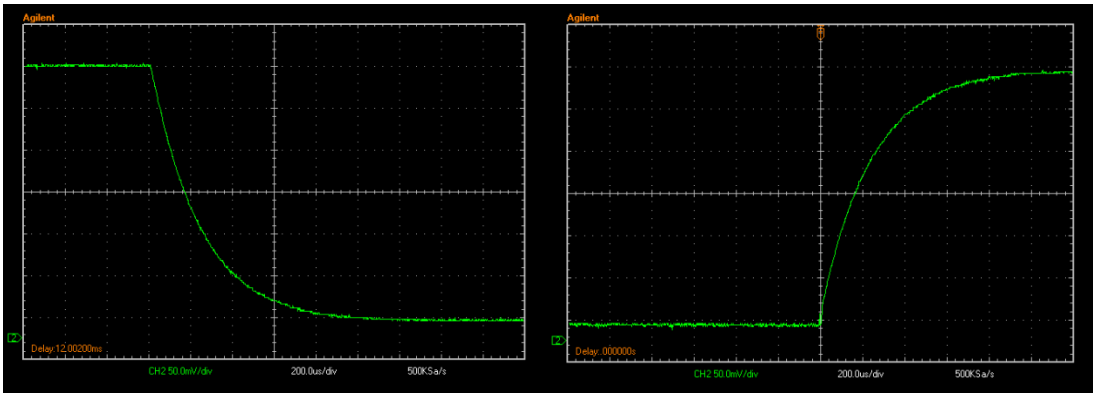

Figure 4.13 – LED VDU rise and fall time – LED on/off times were measured to have symmetric rise and fall times with a time constant of 200µs. This confirms that the LEDs are more than fast response enough to be used with CLAD for visual studies.

The primary limitation of the LED VDU is that the construction of the divisions and diffuser means that the VDU is built to a set spatial resolution. There is no simple way to vary the spatial resolution and this also limits the complexity of the patterns which can be displayed on it.

The Projector VDU has a luminance rating of approximately 100 cd/m^2, which is still above the 80 cd/m^2 required for PERG stimulation, but significantly lower than the LED VDU. The Projector VDU as has the flexibility of displaying any pattern and the spatial resolution can be altered just by changing the images displayed by the projectors. The limitations of the Projector VDU come from the enclosure which the projectors are housed in. The projectors need to be far from the subject so that they projection can reach sufficient size. This adversely affects the luminance and requires a large enclosure which makes the VDU large and difficult to handle. Additionally, the alignment of the projectors is crucial to generate pattern reversals. If the projectors shift any, the two projectors will be misaligned and the pattern reversals will be disrupted.

The Pi cell VDU utilizes a normal LCD monitor to display images. As such the luminance of the VDU is the same as the LCD being used. LCD luminance typically ranges from 150 to over 300 cd/m^2, so the Pi cell VDU meets the luminance requirements of a Pattern VDU. Additionally, since it uses a LCD monitor to display images, it is just as flexible as the projector VDU. The Pi cell VDU does not suffer from the misalignment problems of the Projector VDU. The reversals arise from toggling the polarization state of the LCD image, and as such, the pattern is always perfectly aligned. Unfortunately, the pi cell's maximum switching speed is 1 kHz, and while that is much better than conventional displays it is significantly slower than the LED or Projector VDUs, and generating CLAD sequences for it might become problematic when getting to higher reversal rates. Additionally, since the Pi cell requires a high voltage modulated signal to operate, it creates a significant stimulus artifact in the recording.

Figure 4.14 shows the various VDU set ups and a set of pilot data from each of the VDUs. Pilot data was acquired from three subjects, as described in Chapter 4.2. Responses were acquired at three different rates to validate each of the displays. Conventional $PERG_{tr}$ were acquired at 2.2 rps. Then $PERG_{ss}$ and jittered $qPERG_{ss}$ were acquired at 17.4 rps, a rate which is suggested in the literature for steady state recordings (Holder, 2010; Bach et al., 2012) and is used clinically (Porciatti & Ventura, 2004). Finally, $PERG_{ss}$ and $qPERG_{ss}$ were obtained at a rate which was beyond the capability of conventional displays, 78.1 rps. For each rate, three 128 sweep recordings were obtained and averaged. The 384 sweep subject averages were used to construct an 1152 sweep grand average of the three subjects. Grand averages are shown in Figure 4.14. CLAD was used to deconvolve the $qPERG_{ss}$ responses, obtaining a 'per stimulus' $qPERG_{tr}$ response at 17.4 and 78.1 rps for each of the three stimulators. At 2.2 rps, responses obtained from all three VDUs exhibit the conventional waveform morphology, with N35, P50 and N95 components easily identifiable. Additionally, CLAD was successful in deconvolving a 'per stimulus', high rate transient with each of the VDUs.

While all three displays were capable of acquiring PERG responses, the LED display produced the cleanest and most reproducible signal. Coupled with the fast response times of the LEDs, and the ease of using the VDU, it was decided that the LED based display will be the VDU utilized for the remainder of this study.

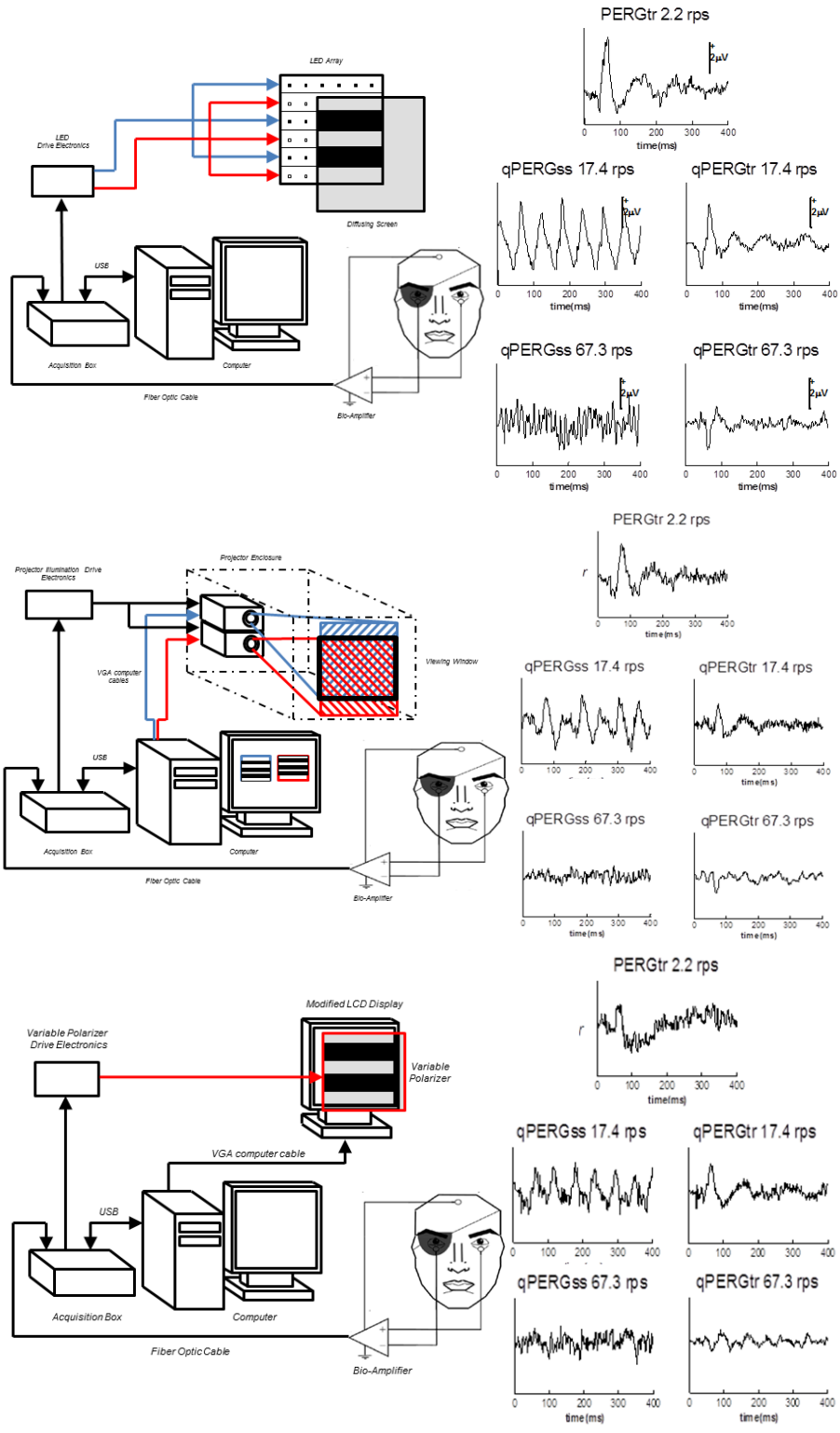

Figure 4.14 – VDU pilot data – Pilot data was gathered from each display at 3 rates, 2.2 rps, 17.4 rps and 67.3 rps.

4.4 Experimental Procedures

A. Acquisition of conventional $PERG_{tr}$ with LED display

Initially, conventional $PERG_{tr}$ responses were acquired from all subjects participating in the experiments. $PERG_{tr}$ were acquired at 2.2 rps monocularly from nine subjects using the criteria outlined in Chapter 4.2. These responses served as a control for all other experiments. Subject preparations were the same as described in Chapter 4.2. Each recording was composed of 128 sweeps, and each sweep was 450 ms long. Bandpass analog filters for the records were set between 1 and 300 Hz. Three separate $PERG_{tr}$ responses were acquired and averaged to a subject average consisting of 384 sweeps. Subject averages will be digitally low pass filtered after acquisition from 1-45Hz (Bach et al., 2012). After offline filtering, individual waveform component amplitudes and latencies were measured as described in Holder et al., 2010. Acquired $PERG_{tr}$ were then compared with standard $PERG_{tr}$ morphology and component values to verify the responses obtained with the LED display system.

B. Effects of Stimulus Reversal Rate on PERGs

In order to observe the effects of increased stimulation rate on the PERG, responses were acquired at seven reversal rates: 17.4 rps, 28.2 rps, 36.7 rps, 41.2 rps, 56.4 rps, 67.3 rps and 78.1 rps. Stimulation sequences were jittered CLAD sequences, so that after acquisition, deconvolution could be performed. Subject preparation and selection criteria were the same as described in Chapter 4.2. Recordings were obtained monocularly from nine subjects. Each recording was composed of 128 sweeps with a sweep length of 450 ms. Three separate recordings were acquired at each rate from each subject. After

acquiring the $qPERG_{ss}$ response at each rate, CLAD was used to extract the $qPERG_{tr}$ response at each rate. For each subject at each rate, deconvolved $qPERG_{tr}$ responses were averaged, creating responses consisting of 384 sweeps. Averaged responses were off line filtered between 1-45 Hz. Analysis of the deconvolved $qPERG_{tr}$ responses was performed in the time domain (measuring peak amplitudes and latencies).

C. Steady State PERGs and their Synthesis from Transient Responses

In order to test the superposition theorem of steady state responses (Capilla et al., 2011; Toft-Nielsen et al., 2012) and validate the $qPERG_{tr}$ responses acquired in the previous experiment, deconvolved $qPERG_{tr}$ responses were synthetically convolved to create synthetic steady state responses. Conventional $PERG_{ss}$ and jittered $qPERG_{ss}$ responses were obtained at five reversal rates: 6.5 rps, 10.9 rps, 15.2 rps, 17.4 rps, and 26.0 rps. Additionally, conventional $PERG_{tr}$ were also obtained. Recordings were obtained monocularly from eight subjects. Subject preparation and selection criteria were as described in section 4.2. Each recording was composed of 128 sweeps with a sweep length of 450 ms. Three separate recordings were acquired at each rate from each subject. After obtaining $qPERG_{ss}$ responses, CLAD was used to extract the $qPERG_{tr}$ response at each rate. Once $qPERG_{tr}$ responses were extracted, synthetic $PERG_{ss}$ responses were computed by mathematically convolving each $qPERG_{tr}$ response with a steady stimulation sequence of the same mean reversal rate. Additionally, another set of synthetic responses was computed using the conventional 2.2 rps $PERG_{tr}$ responses. The two sets of synthetic responses: $synPERG_{ss}$ and $synPERG_{ss(2rps)}$ were compared with conventional $PERG_{ss}$ at each rate. Responses were compared using correlation coefficient in the time domain and using phasor analysis in the frequency domain.

D. **Dynamic PERG averaging**

As discussed previously in section 2.8, one of the essential assumptions made when using the CLAD algorithm is that there is no temporal adaptation in the response during the acquisition of the qSS response. There is, in fact, evidence that the $PERG_{ss}$ response adapts during prolonged periods of stimulation (Porciatti and Ventura, 2009). The PERG recordings previously obtained throughout this study have been comprised of 128, 450 ms long sweeps. This results in a period of continuous stimulation of slightly longer than a minute. This experiment will explore the dynamics of PERG over the course of one minute of continuous stimulation to confirm one of the essential assumptions of CLAD.

For this experiment jittered $qPERG_{ss}$ were acquired monocularly from five subjects following the same selection criteria and subject preparation described in Chapter 4.2. After preparing the subjects, the LED VDU was used to continuously deliver pattern stimuli at a rate of 17.4 rps for a period of one minute. Immediately following the minute of stimulation, the VDU reverted to a grey field equal in luminance to the pattern stimulus, remaining in the state for 30 seconds. This pattern of reversals for one minute followed by a gray field for 30 seconds was repeated 5 times for each recording, comprising one recording trial. For the duration of each trial, acquisition was continuous. Additionally, artifact rejection was completely disabled, in order to assure that no dynamic effects of the response were missed due to rejected sweeps. Subjects were encouraged to limit blinks or other movements which might result in artifact contamination of the signal to periods when the stimulus was a grey field.

Each recording trial consisted of 960 raw sweeps, made up of five uninterrupted periods of stimulation separated by five periods of the isoluminant grey field. Since there was no averaging or artifact rejection performed, any dynamic effects of the response should be preserved by this paradigm. Recordings were processed and averaged offline using a specially designed Graphic User Interface (GUI) which could dynamically average the signals, choose particular segments of the response to process and deconvolve responses from any segment. Additionally, deconvolution of particular segments of the response could be performed. The dynamics of the response were examined in both the time and frequency domains.

Chapter 5 - Results

In the following chapter the results from the four experiments performed in this study will be presented.

5.1 Acquisition of conventional $PERG_{tr}$ with LED display

$PERG_{tr}$ are PERG responses which have settled entirely before the delivery of the next pattern reversal. With $PERG_{tr}$ individual waveform components (N35, P50, and N95) are fully distinguishable and quantifiable. Since the VDUs used in this study were developed specifically for the acquisition of high rate PERG, it was important to first verify the instrumentation by acquiring the most rudimentary PERG responses, the transient response. Different display modalities can introduce various peak time shifts, and or broadening of waveform components (Husain et al., 2009; Link et al., 2006b; Nagy et al., 2011). It was important to quantify any discrepancies between $PERG_{tr}$ acquired with the developed LED system and conventional VDUs.

Additionally, it was important to have a large population of $PERG_{tr}$ data to utilize as a baseline for comparison with the responses acquired in the other studies herein. One of the primary benefits of the CLAD technique is to acquire temporal information which is lost in convolution. This is primarily in the form of waveform components which are normally obscured by convolution at higher reversal rates. The deconvolved $qPERG_{tr}$ responses extracted in this study exhibit clearly distinguishable components and it was necessary to have conventional $PERG_{tr}$ responses to compare with $qPERG_{tr}$.

Conventional $PERG_{tr}$ were acquired at 2.2 rps from the right eye of nine subjects. Subject selection criteria and preparation were as described in Chapter 4.2. Individual subject recordings, consisting of 384 averaged sweeps, are overlaid on one another in order to show reproducibility of responses across subjects (shown in Figure 5.1). The population average, comprised of 3456 sweeps from all eyes, is shown in Figure 5.1 in red. Individual waveform components, N35, P50 and N95, are labeled.

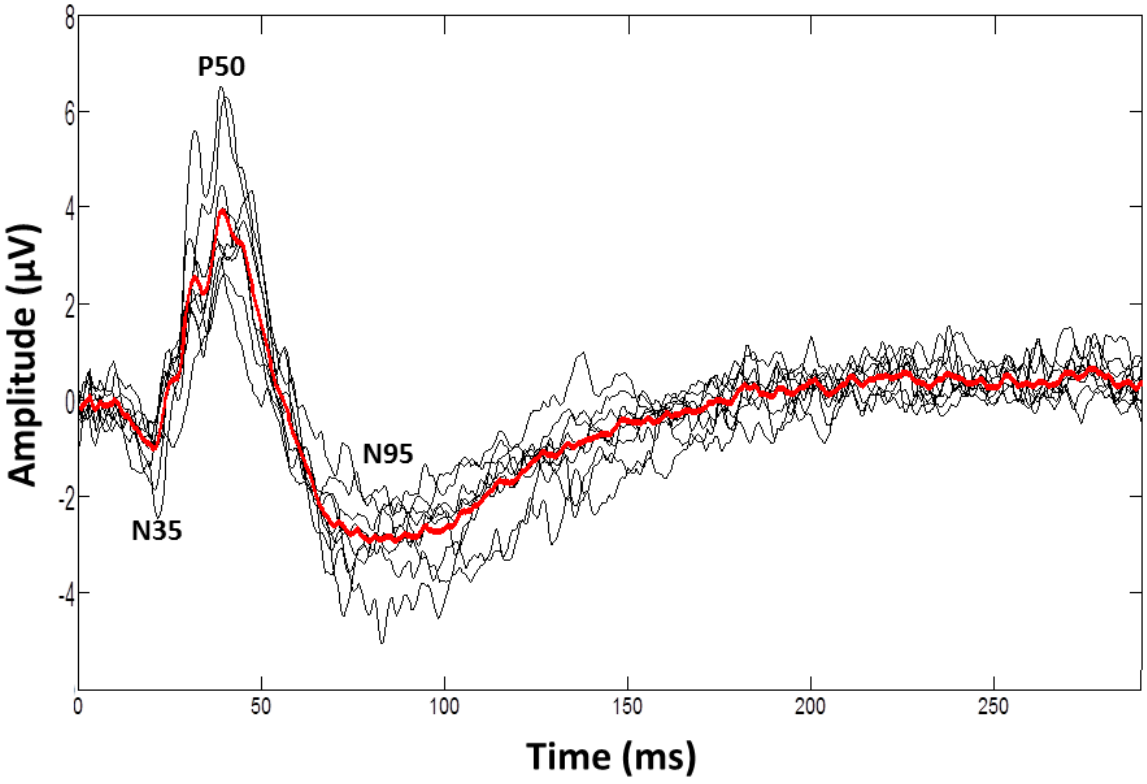

Figure 5.1- Acquired $PERG_{tr}$ – Conventional $PERG_{tr}$ was acquired using a stimulation rate of 2.2 rps. Individual recordings from nine subjects are overlaid on each other and shown in black, while the population average is shown in red. Individual waveform components (N35, P50 and N95) are labeled.

Component amplitudes are consistent with expected values from standards (Holder et. al, 2012) although somewhat smaller. Component latencies however, are consistently earlier than standards indicate. Reasons for the discrepancies between the LED display and conventional displays will be addressed in the discussion chapter. Figure 5.2 shows a typical normal PERG, obtained from ISCEV standards (Holder et al., 2012), which has been lowpass filtered from 1-45 Hz. In order to compare latencies, amplitudes and waveform morphology, acquired $PERG_{tr}$ population average was filtered from 1-45 Hz and displayed on the same scale (trace shown in blue). Notice that while the baseline of the responses shown in Figure 5.1 is at zero, the acquired trace in Figure 5.2 exhibits a non-zero baseline. The response obtained from the standard (Bach et al., 2012) defined the lowest potential (trough of N95) as zero, rather than the baseline as zero. In order to have both traces at the same baseline for comparison purposes, an offset was added to the acquired $PERG_{tr}$ population average so that the responses would have the same baseline. Again, it is evident in Figure 5.2 that the acquired $PERG_{tr}$ and the PERG from the standard exhibit the same morphology and the intervals between peaks are consistent for both. However, the acquired $PERG_{tr}$ differs from the standard response by having smaller amplitude and a shorter latency from the stimulus onset. Reasons for the discrepancies between latencies and amplitudes of the acquired $PERG_{tr}$ and the standard response will be presented and discussed in Chapter 6.1 of the next section.

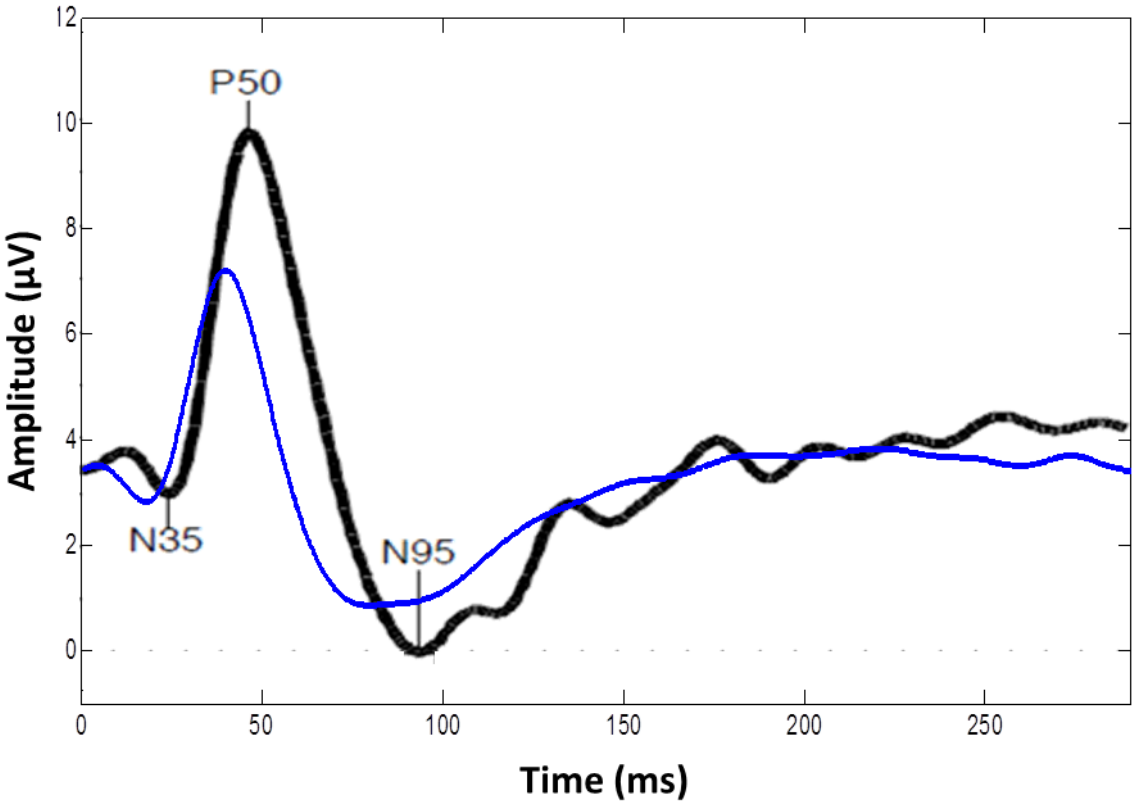

Figure 5.2 - Standard $PERG_{tr}$ versus Acquired $PERG_{tr}$ – The black trace above shows a $PERG_{tr}$ taken from ISCEV standards. The blue trace shows the acquired $PERG_{tr}$ population average (nine subjects). Both traces were offline lowpass filtered from 1-45 Hz. The waveform morphology of the acquired $PERG_{tr}$ is consistent with the standard, but individual waveform components latencies are earlier than those of the standard and amplitudes of the acquired response are smaller.

5.2 Effects of Stimulus Reversal Rate on PERGs

As reversal rate increases and the ISI of the stimulus becomes shorter than the PERG response length, subsequent PERG responses begin to overlap with each other and steady-state responses are generated. As described previously steady-state responses gathered around 17 rps (8.5 Hz) are extensively studied and used clinically (Bach et al., 2012; Porciatti & Ventura, 2004). For this study we explored further rate increases using the specially designed VDUs.

In Chapter 2.8, the CLAD algorithm was introduced. Using CLAD it is possible to deconvolve high rate EPs, revealing the temporal information obscured by overlapping responses. CLAD implementation requires the creation and optimization of a jittered stimulation sequence for each desired stimulation rate, as discussed in Chapter 2.8 and illustrated in Figure 2.15. This requires precise control of the onset and offset of the stimuli presented. Applying CLAD to visual responses is complicated by the periodic refresh rates of most available VDUs. Ideally, a CLAD compatible VDU would need to be able to reliably update every 0.44 ms, a parameter far beyond what is capable with most displays. The LED VDU proposed and developed in this study is capable of meeting this stimulus onset constraints and has been shown to be able to elicit reproducible $PERG_{tr}$ that are consistent with standards. In this study it was further tested by acquiring jittered $qPERG_{ss}$ responses at a number of reversal rates ranging from 17.4 to 78.1 rps.

Responses were collected from nine eyes, at seven stimulation rates. The nine subjects who participated in this study were the same nine who participated in the $PERG_{tr}$ acquisition as described in Chapter 5.1. Jittered CLAD stimulation sequences were used to elicit responses at seven jittered stimulation rates with mean reversal rates of: 17.4 rps, 28.2 rps, 36.7 rps, 41.2 rps, 56.4 rps, 67.3 rps and 78.1 rps. Responses were acquired monocularly with the same setup described in Section 4.2. Responses were analog bandpass filtered from 1 to 300 Hz as specified in ISCEV standards (Bach et al., 2012). Each recording consisted of 128 sweeps, 450 ms in length. Three recordings were acquired from each of the nine subjects at each reversal rate. Acquired $qPERG_{ss}$ and CLAD deconvolved $qPERG_{tr}$ are shown in Figure 5.3.

Figure 5.3 is split into two columns. Column A shows the acquired $qPERG_{ss}$ responses from all subjects. Column B shows the CLAD deconvolved $qPERG_{tr}$ responses extracted from the responses in Column A. Individual subject recordings are shown in black to show the reproducibility of the responses across subjects. Population averages comprised of 3456 sweeps are overlaid in red. The responses due to different reversal rates are offset vertically, increasing in rate from 2.2 rps to 78.1 rps traveling down the column. Observing Column A, the amplitude of the $qPERG_{ss}$ response decreases as reversal rate increases beyond 17.4 rps, gradually decreasing from 28.2 rps to 41.2 rps. Additionally, individual responses (black traces) become less consistent. However, as reversal rate increases beyond 56.4 rps, $qPERG_{ss}$ amplitudes begin to increase again from 67.3 rps to 78.1 rps. Also, individual responses begin to become more consistent again at 67.3 rps and 78.1 rps.

In the transient responses acquired at 2.2 rps, individual waveform components (N35, P50, and N95) are clearly visible and while peak latencies are consistently earlier, latencies and amplitudes are within acceptable ranges defined in standards (Holder et al., 2012). However, as reversal rates increase, component latencies and amplitudes start to change. Between 17.4 rps and 36.7 rps the gradual reduction of the P50 component can be observed, as well as the narrowing of the N95 component. Between 41.2 rps and 56.4 rps, the individual waveform components become difficult to distinguish. However, as reversal rate is increased beyond 56.4 rps, a new and consistent morphology arises, one which is very different from conventional PERG morphology, and conventional peak names are no longer applicable.

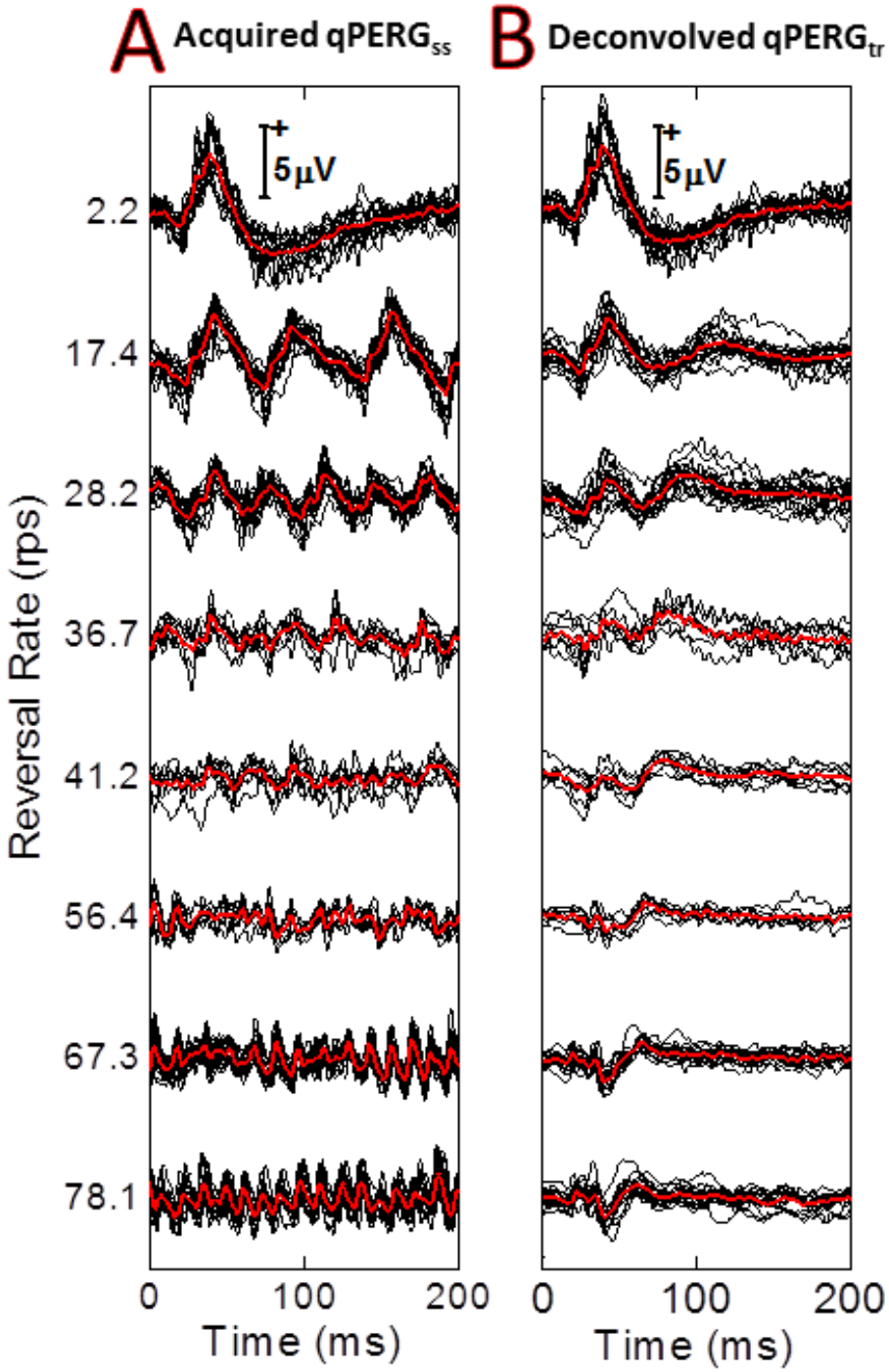

Figure 5.3 - Acquired qPERG$_{ss}$ and Deconvolved qPERG$_{tr}$ – Column A (left) shows qPERG$_{ss}$, acquired using jittered CLAD sequences. Column B (right) shows the corresponding deconvolved responses acquired using CLAD. At the top of each column, conventional PERG$_{tr}$ is displayed for reference. PERG$_{tr}$ was acquired at a reversal rate of 2.2 rps for all subjects. Individual subject recordings for each rate are overlaid to show consistency in responses across subjects. Population averages (9 eyes from 9 subjects) are overlaid in red.

In order to refer and quantify the PERG peaks observed at higher rates new peak names have been assigned for this study. Peak reporting conventions are illustrated in Figure 5.4. For rates below, 41.2 rps conventional waveform components are still distinguishable and peak naming and quantifying will follow standards as shown in Figure 5.4A. For rates above 41.2 rps, deconvolved responses exhibit a very different morphology. In order to quantify these peaks a new convention was established. The three major components which are consistent at rates above 41.2 rps were named P_{α}, N_{α}, and P_{β}. Figure 5.4B shows the 78.1 rps responses and the new peaks names and conventions which have been established in this study. Latency and amplitude measurements were kept consistent with PERG conventions, with latencies measured from the onset of the stimulus to the tip of the peak and amplitude measured in regards to the peak of the previous component. Both responses in Figure 5.4 have been digitally filtered from 1-45 Hz in order to facilitate the quantifying of peaks.

In order to better visualize the rate based morphology changes of the $qPERG_{tr}$ peaks, we used 3D techniques as shown in Figure 5.5. Figure 5.5 compiles the deconvolved $qPERG_{tr}$ population averages from column B of Figure 5.3 and displays them in three dimensions to show how waveform morphology transitions as reversal rate increases.

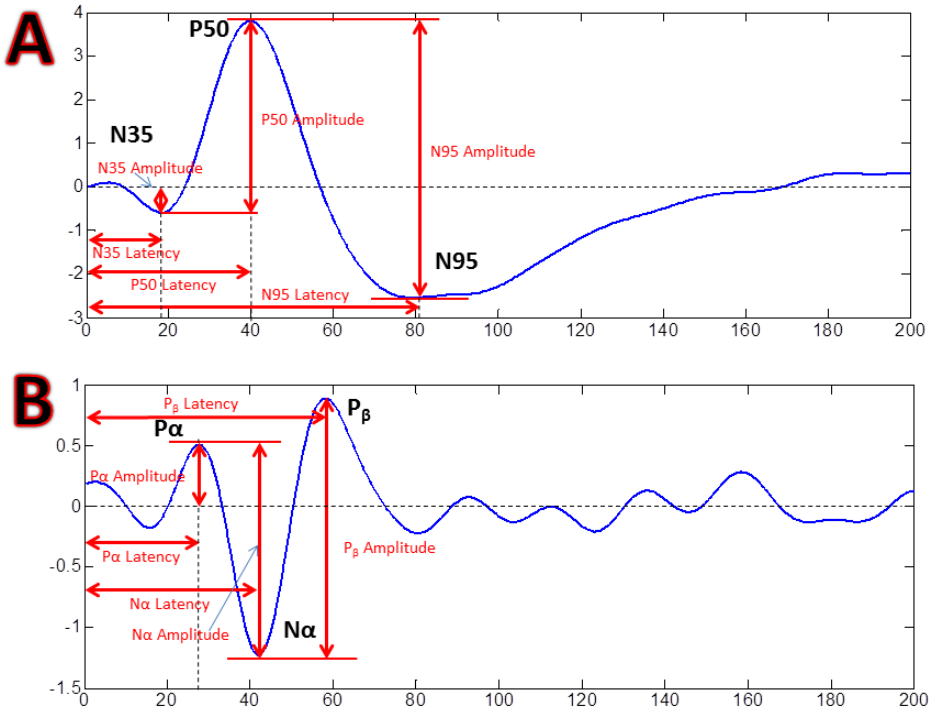

Figure 5.4 - Peak Names, Latencies and Amplitudes – (A) Low rate Transient PERG components (N35, P50, and N95) and how the component latencies and amplitudes are defined. (B) For reversal rates higher than 41.2 rps, the CLAD extracted qPERG$_{tr}$ responses exhibit a different morphology. There are three consistent waveform components at high reversal rates, an initial positive peak, Pα, followed by a negative peak at approximately the same latency as the P50 component, Nα, and second positive component labeled P$_{\beta}$. These components have not been observed before, so aforementioned names have been given to them and the amplitude and latency measurements have been defined as shown in (B). Baseline is shown as a dashed horizontal line.

In Figure 5.5 the x-axis shows time from the stimulus onset, the y-axis show reversal rate and the z-axis shows amplitude which is also denoted by the color of the plot (negative components are rendered in blue, while positive components are rendered in red. Baseline values are green). This information is also displayed in a 2D surface plot on the following page, where component amplitudes illustrated using a color scale alone are shown versus stimulation rate and time from stimulus onset.

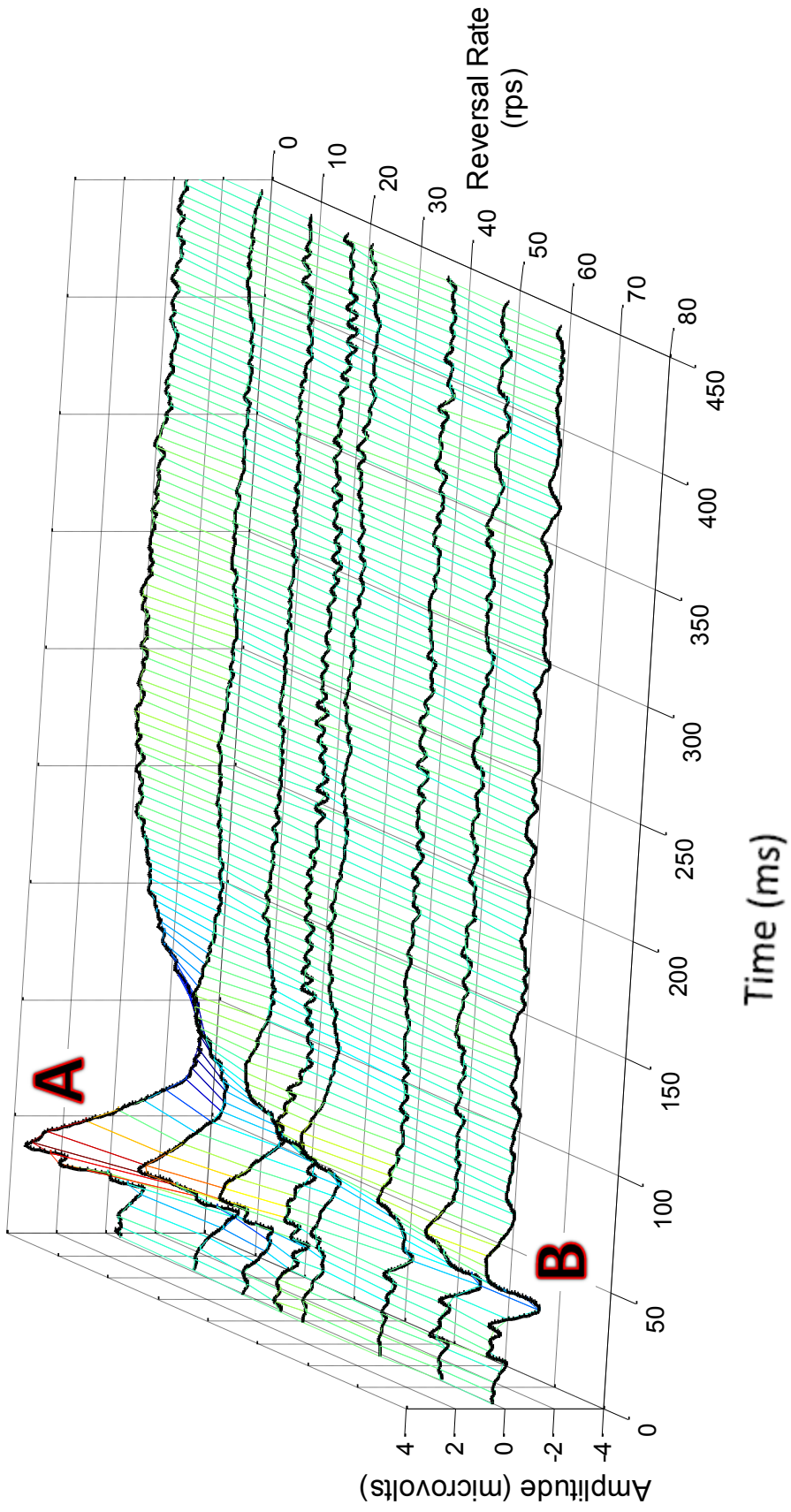
A
B
Amplitude (microvolts)
4
2
0
-2
-4
0
50
100
150
200
250
300
350
400
450
Time (ms)
Reversal Rate (rps)
0
10
20
30
40
50
60
70
80

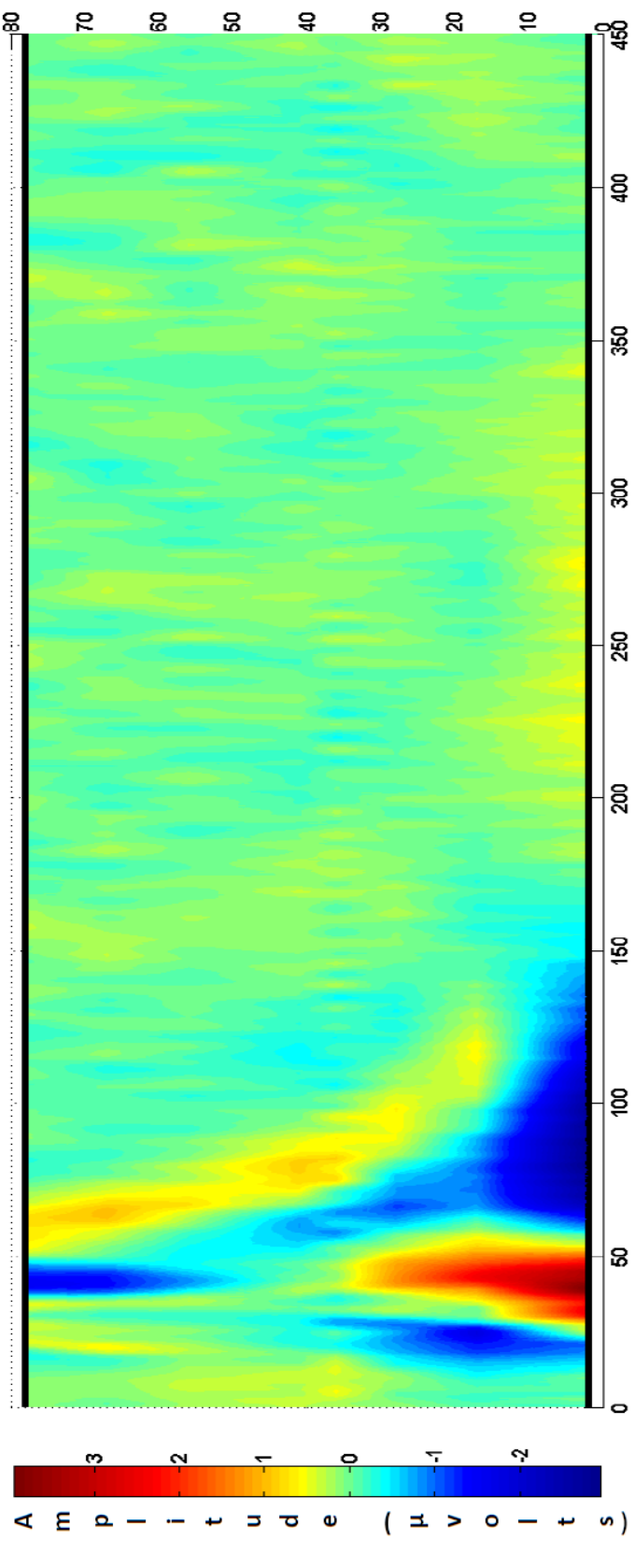

Figure 5.5 - Rate based morphology changes – The three dimensional plots above illustrate the peak transitions as reversal rate increases. (Previous page) Waveform A (rendered in black) shows the population average (9 eyes) of the 2.2 rps transient response. Waveform B (rendered in black) shows the population average deconvolved 78.1 rps response. The two waveforms differ greatly in their morphology, but by constructing the plot showing time, amplitude and rate information, we can see how the morphology transitions gradually as reversal rate increases. (Above) In the above plot, color has been mapped to amplitude of the response to illustrate how peaks of the PERG response adapt with increasing reversal rate.

The surface created in Figure 5.5 illustrates how the individual waveform components transition and change as reversal rate is increased. The familiar $PERG_{tr}$ has been labeled with an 'A'. There is an initial negativity (N35 in blue), followed by a large positivity (P50 in red) and then a broad negativity (N95 in blue). The first observable rate based effect is the rapid narrowing and reduction of the N95 component. This is followed by gradual reductions in amplitude and slight increased latencies of the P50 and N35 components. Additionally, there is an additional positive component which appears to crest as N95 recedes. At 41.2 rps and 56.4 rps waveform components seem to almost vanish from the surface plot. However as reversal rates are increased beyond this, there is the emergence of the new components outlined in Figure 5.4, the most prominent of which is a large negative component with occurs as roughly the same latency as P50. The 78.1 rps response is labeled 'B'.

Before quantifying waveform components, responses were lowpass filtered from 1-45 Hz (Bach et al., 2012). Mean and standard deviations of latency and amplitude measurements for each rate are listed in Table 5.1. In Figure 5.6 the amplitude and standard deviations for the peak amplitude and latency measurements are plotted as a function of reversal rate. From Figure 5.6a the increase in N35 and P50 latencies as rate increases can be observed while the N95 components gets earlier as rate increases. The high rate components Pα, Nα, and Pβ all tend to move earlier in latency as reversal rate increases. Figure 5.6b illustrates how the P50 and N95 components both reduce in amplitude significantly are reversal rate increases. Nα, and Pβ both increase in amplitude as rate increases from 56.4 rps to 78.1 rps.

Table 5.1 - Population averages and standard deviations for individual waveform component amplitudes and latencies obtained at conventional and 4 low rates (top table) and three high rates (bottom table) See text for more details on peak labels:

		N35		P50		N95	
		Latency (ms)	Amplitude (μv)	Latency (ms)	Amplitude (μv)	Latency (ms)	Amplitude (μv)
2.2 rps	AVG	18.70	0.64	39.70	4.62	85.35	6.60
	STD	2.11	0.51	2.21	1.83	5.07	1.81
17.4 rps	AVG	23.53	1.28	43.45	3.44	75.55	3.42
	STD	2.21	0.54	2.46	1.03	2.42	0.90
28.2 rps	AVG	23.75	0.93	44.05	2.22	67.05	2.36
	STD	2.29	0.51	1.99	0.92	2.76	0.69
36.7 rps	AVG	29.25	0.65	44.48	1.16	60.98	1.28
	STD	4.71	0.37	4.73	0.59	1.82	0.53
41.2 rps	AVG	28.20	0.53	41.48	0.85	58.05	1.11
	STD	4.43	0.57	2.89	0.92	1.63	0.58

		Pα		Nα		Pβ	
		Latency (ms)	Amplitude (μv)	Latency (ms)	Amplitude (μv)	Latency (ms)	Amplitude (μv)
56.4 rps	AVG	28.28	0.26	47.70	1.00	67.05	1.36
	STD	7.12	0.26	4.48	0.30	3.73	0.37
67.3 rps	AVG	24.75	0.42	43.05	1.62	63.55	2.19
	STD	3.83	0.18	2.29	0.28	2.02	0.27
78.1 rps	AVG	27.60	0.52	42.55	1.81	58.30	2.36
	STD	1.62	0.33	2.05	0.63	3.24	0.49

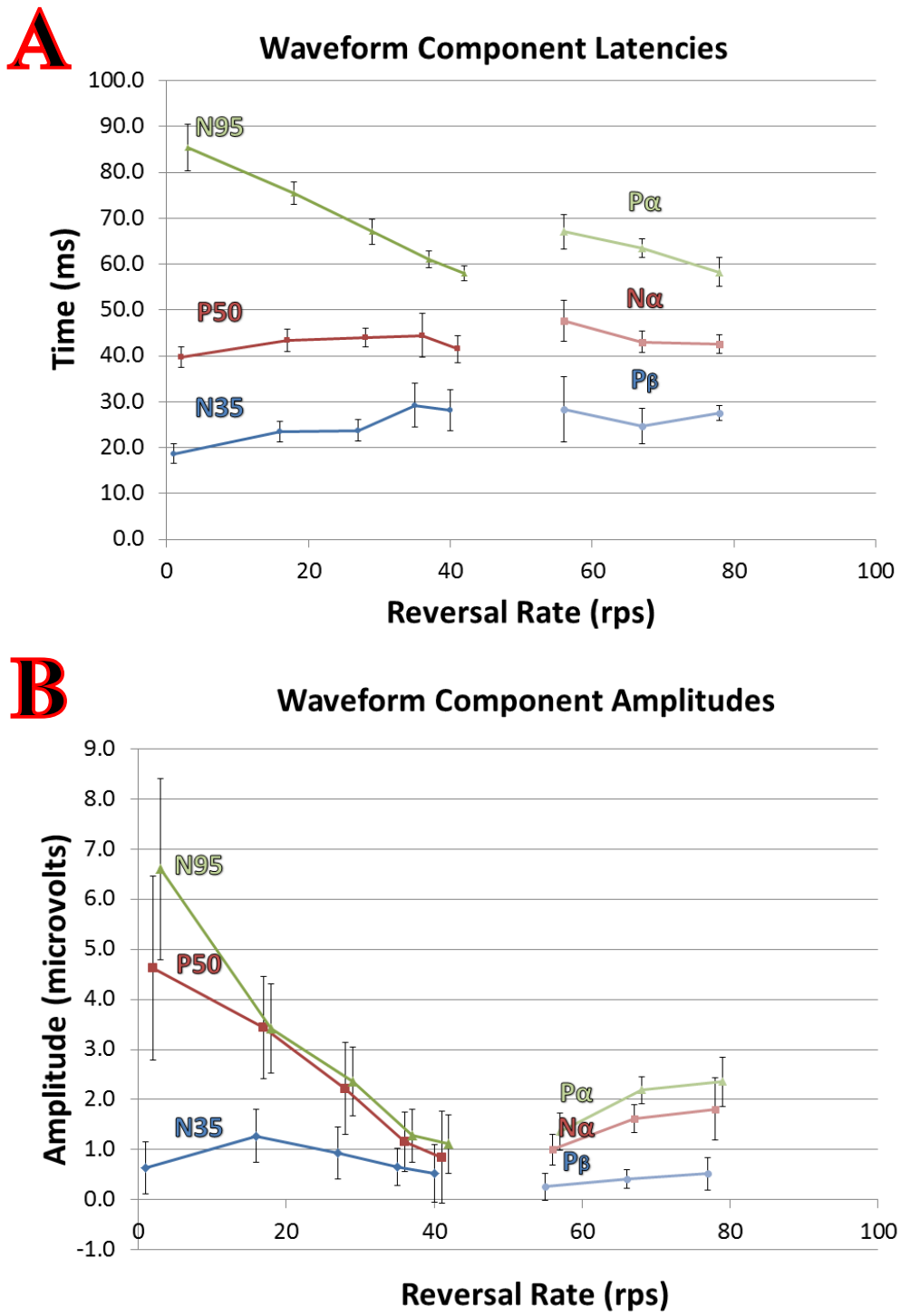

Figure 5.6 - Peak Latencies and Amplitudes – Population averages (9 eyes) and standard deviations for waveform component latencies (A) and amplitudes (B) versus stimulus reversal rate. Components have been separated into conventional peak names (N35, P50, N95) for rates below 50 rps and high rate peak names (Pα, Nα, Pβ) for rates above 50 rps.

5.3 Steady State PERGs and their Synthesis from Transient Responses

As discussed in the previous section, by utilizing the LED VDU and CLAD, it was possible to extract $qPERG_{tr}$ from acquired $qPERG_{ss}$ responses. The $qPERG_{tr}$ response is a transient response which exhibits individual waveform components that can be quantified with peak based measurements. By increasing reversal rate, we observed some interesting rate based adaptation effects in the extracted $qPERG_{tr}$ responses. The extracted $qPERG_{tr}$ can be regarded as the contribution of a single pattern reversal to the establishment of the $PERG_{ss}$ response. If this is in fact the case, then true $PERG_{ss}$ responses can be reconstructed by convolving $qPERG_{tr}$ responses.

For this study we tested the validity of the superposition theorem (Capilla et al. 2011; Toft-Nielsen et al., 2012) and the rate based adaptation observed in Chapter 5.2 by investigating the ability of the deconvolved $qPERG_{tr}$ to predict a conventional, isochronic $PERG_{ss}$ response of the same reversal rate. A population of eight subjects was recorded for this study. Of the eight subjects, three were participants in the previous experiments and five were new subjects. Responses were recorded monocularly as described in Chapter 4.2. Initially, conventional $PERG_{tr}$ was acquired from each of the subjects. Additionally, conventional isochronic $PERG_{ss}$ were acquired at five rates ranging from 6.5 rps to 26 rps as well as jittered $qPERG_{ss}$ responses at the same mean reversal rates. Recordings consisted of 128 sweeps, 450 ms in length. Each recording was repeated three times for each subject. Analog band pass filters were set between 1 and 300 Hz (Bach et al., 2012).

In addition to low rates used to test the steady state response generation, we explore the validity of the superposition hypothesis at high rates. They will be described separately.

A. Steady State PERGs at Low Rate

Acquired $PERG_{ss}$ and $qPERG_{ss}$ recording for 5 rates are shown in columns A and B of Figure 5.7 respectively. CLAD deconvolved $qPERG_{tr}$, (extracted from the $qPERG_{ss}$ from column B) are shown in Figure 5.7 column C. At the top of each column, conventional transient PERGs, acquired at 2.2 rps from each subject, are shown for reference purposes. Isochronic stimulation sequences and CLAD jittered sequences were used to elicit conventional $PERG_{ss}$ and $qPERG_{ss}$ at five additional reversal rates: 6.5 rps, 10.9 rps, 15.2 rps, 17.4 rps and 26.0 rps.

Conventional $PERG_{tr}$ responses were consistent in terms of waveform morphology and individual component latencies and amplitudes, with standards. As reversal rate is increased, adaptation can be observed in the deconvolved $qPERG_{tr}$ both in the narrowing and reduction of the N95 component and the gradual reduction of the P50 component similar to the adaptation observed in section 5.2.

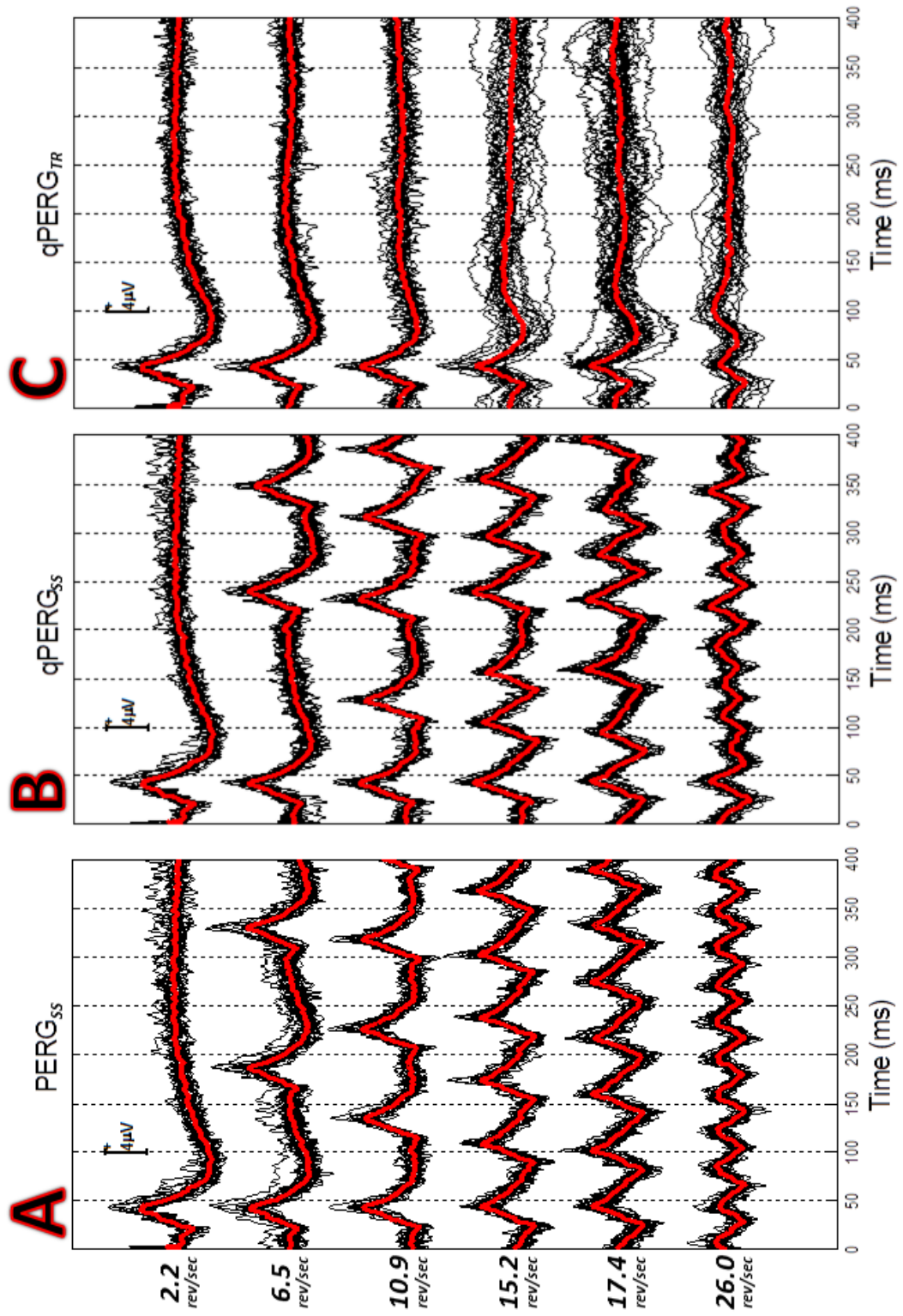
A
B
C
PERG$_{SS}$
qPERG$_{SS}$
qPERG$_{TR}$
4µV
2.2 rev/sec
6.5 rev/sec
10.9 rev/sec
15.2 rev/sec
17.4 rev/sec
26.0 rev/sec
0 50 100 150 200 250 300 350 400
Time (ms)

Figure 5.7 (Previous page) - Steady State, Quasi-Steady State and Deconvolved Transient PERG – Individual subject recordings are rendered in black and overlapped in order to show reproducibility of the responses across subjects. Population averages (8 eyes) are overlaid in red. At the head of each of the three columns are conventional transient PERG, acquired at 2.2 rps. (A) Conventional steady state PERG, acquired at the 5 reversal rates shown (6.5, 10.9, 15.2, 17.4, 26.0). (B) Quasi Steady State PERG, acquired at the same mean reversal rates as column A, but using jittered CLAD stimulation sequences. (C) Deconvolved Transient PERG, extracted from the responses shown in column B using CLAD deconvolution. Responses in column C represent the contribution to the response due to a single pattern reversal.

After extracting the deconvolved $qPERG_{tr}$ using CLAD (shown in column C of Figure 5.7), $qPERG_{tr}$ were mathematically convolved with the ischronic stimulation sequences used to generate the $PERG_{ss}$ (column A responses), resulting in a synthetic steady state response ($synPERG_{ss}$). Additionally, conventional $PERG_{tr}$ was also used to create second set of synthetic responses $synPERG_{ss(2rps)}$. The rationale behind this experiment is illustrated in Figure 5.8. After acquiring conventional $PERG_{tr}$, two additional responses were acquired from each subject at each reversal rate, one using a steady stimulation sequence and one using a jittered CLAD sequence. This results in a steady $PERG_{ss}$ response and a jittered $qPERG_{ss}$ response. The $qPERG_{ss}$ response is deconvolved using CLAD to acquire the first computed response, the extracted $qPERG_{tr}$. As stated earlier the $qPERG_{tr}$ for each rate is the contribution of a single pattern reversal to the establishment of the steady state response at that rate. At this point in the analysis there are two transient responses, one conventional $PERG_{tr}$ acquired at 2.2 rps and one extracted $qPERG_{tr}$ at the reversal rate. Each of these transients is convolved with the steady sequence used to acquire the $PERG_{ss}$ response at each rate, resulting in two synthetic $PERG_{ss}$ responses ($synPERG_{ss}$). The $synPERG_{ss}$ computed using the

conventional $PERG_{tr}$ ignores any rate based adaptation effects and will be referred to as $synPERG_{ss(2rps)}$. The $synPERG_{ss}$ computed using the deconvolved $qPERG_{tr}$ incorporates any rate based adaptation in the $qPERG_{tr}$. For each reversal rate, the $synPERG_{ss}$ and $synPERG_{ss(2rps)}$ are compared with the acquired isochronic $PERG_{ss}$.

Figure 5.9 shows the two sets of synthetic responses and compares them to real $PERG_{ss}$. Synthetic responses and real steady state responses are shown with analog filtering only, in column A, and filtered to include 5 harmonics of the stimulation frequency in column B.

In order to quantify the ability of the transients, both conventional and deconvolved, to predict steady state responses the correlation coefficient was used. The correlation coefficient can be used to quantify the temporal alignment of two signals (Cohen, 1988). Correlation coefficient values measured between the two $synPERG_{ss}$ sets and real $PERG_{ss}$ can be found in Table 5.2.

Synthetic responses were also compared to real $PERG_{ss}$ in the frequency domain. Phasor plots were constructed at the fundamental frequency of each reversal rate. Figure 5.10 shows the phasor plots for each rate. Red phasors represent the population average (8 eyes) for the real $PERG_{ss}$ with individual subject data points shown as red markers. Black phasors show the population average of the $synPERG_{ss}$ constructed with the deconvolved transient at each rate, with black markers showing the individual subject data points. Blue phasors show the population average of the $synPERG_{ss}$ constructed with conventional 2.2 rps $PERG_{tr}$. Just as $synPERG_{ss(2rps)}$ loses alignment in the time domain with $PERG_{ss}$ in Figure 5.9, in the frequency domain, $synPERG_{ss(2rps)}$ phasor

deviates in magnitude and phase as reversal rate is increased. The black synPERGss phasor, on the other hand, remains consistent in both magnitude and phase with PERGss regardless of the reversal rate.

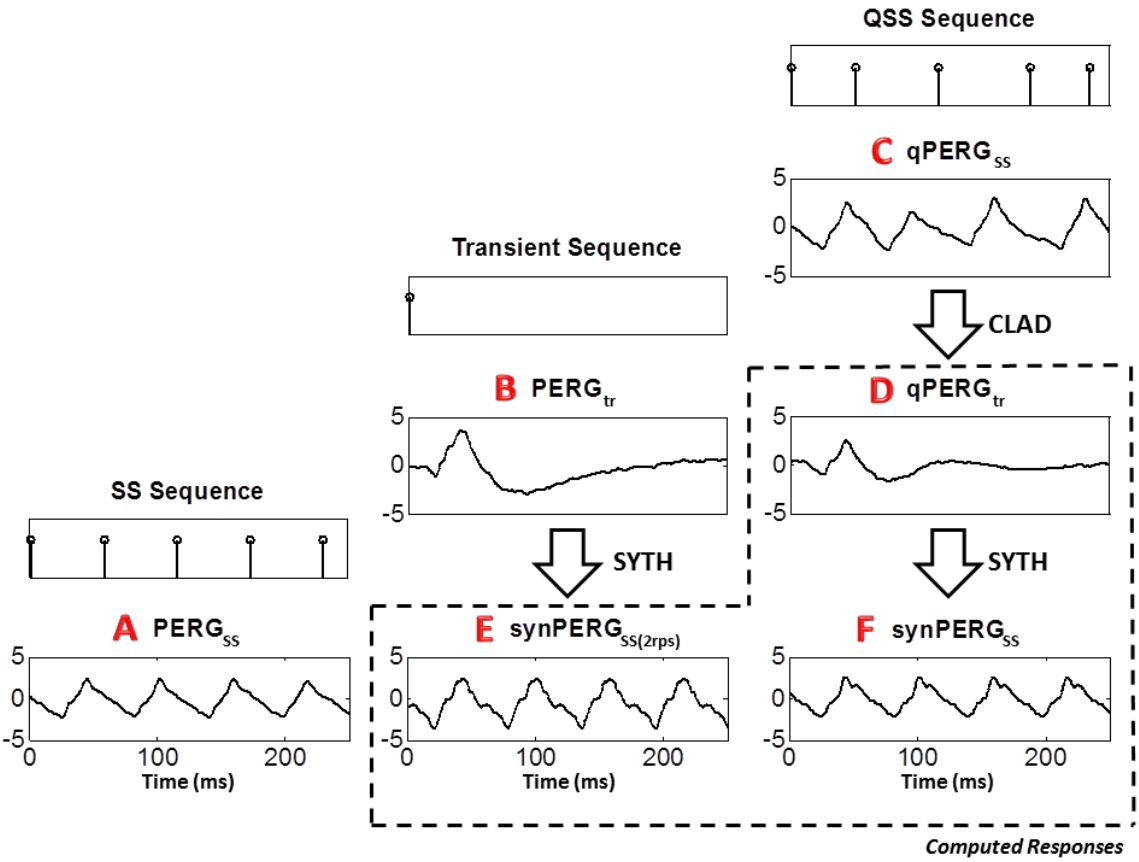

Figure 5.8 - Acquired and Computed PERG responses – Traces A, B, and C show the population average of the acquired responses. Above responses show the 17.4 rps data. (A) Conventional $PERG_{ss}$ elicited with an isochronic stimulation sequence. (B) Conventional $PERG_{tr}$ acquired at 2.2 rps. (C) $qPERG_{ss}$ elicited with a jittered sequence. Traces D, E and F show responses computed from the acquired responses. (D) Deconvolved $qPERG_{tr}$, the response contribution from a single reversal. (E) $synPERG_{ss(2rps)}$ the synthetic $PERG_{ss}$ generated using a conventional 2.2 rps $PERG_{tr}$. (F) $synPERG_{ss}$, the synthetic $PERG_{ss}$ generated using the deconvolved $qPERG_{tr}$ shown in (D).

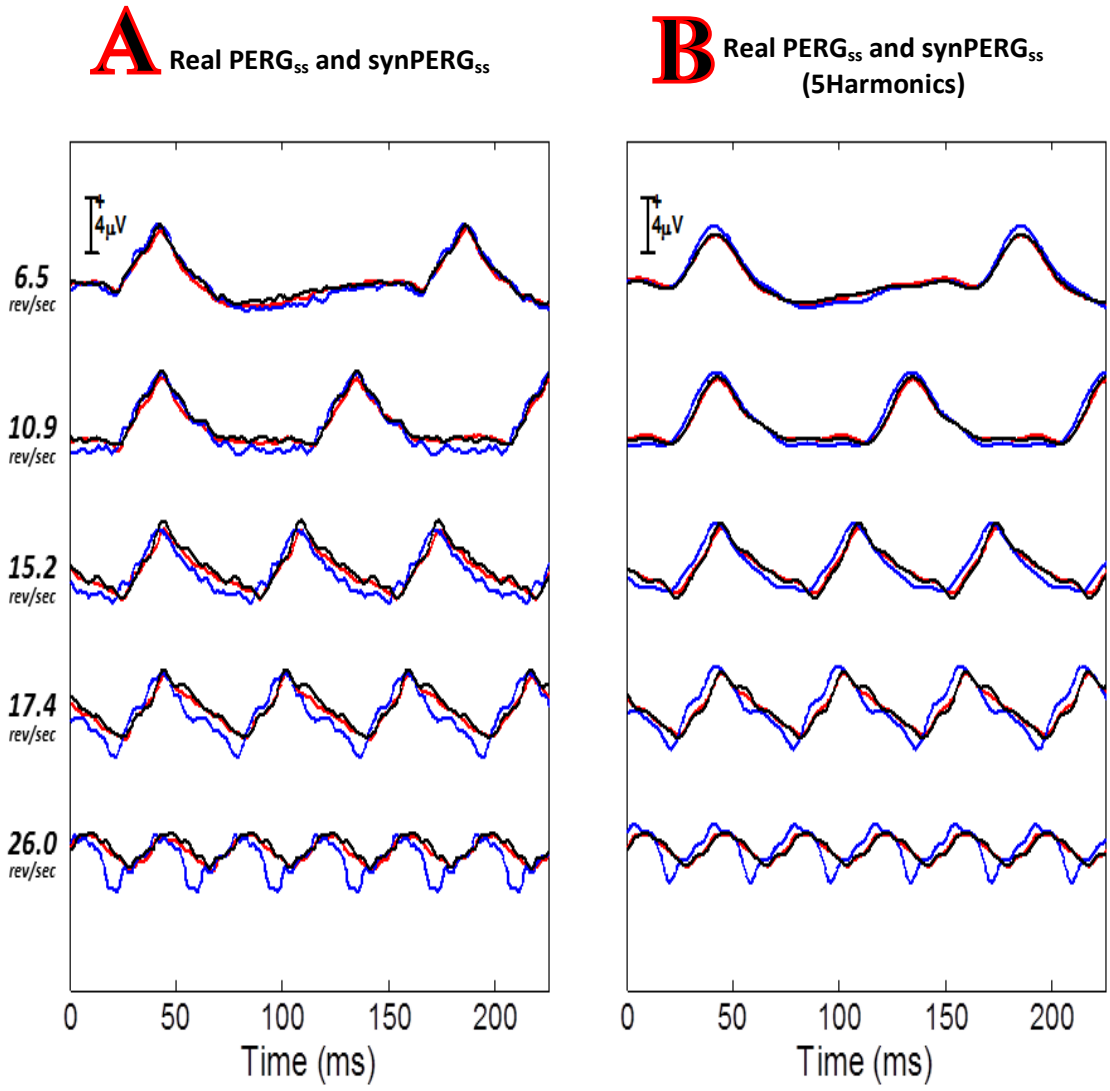

Figure 5.9 - Synthetic PERG and real Steady State PERG – Real ischronic $PERG_{ss}$ traces are rendered in red. Blue traces show $synPERG_{ss(2rps)}$ generated from the 2.2 $PERG_{tr}$ responses. Black traces show $synPERG_{ss}$ generated from the deconvolved $qPERG_{tr}$ from each rate. Column A shows responses filtered only by analog filters used in acquisition. Column B shows the same responses digitally filtered to include 5 harmonics of the reversal rate of each response. Responses at each reversal rate are overlaid to show the ability of the synthetic responses to predict the real $PERG_{ss}$. At lower reversal rates (6.5 and 10.9 rev/sec) both synthetic responses (blue and black) align well temporally. However, as reversal rates increase, deconvolved $qPERG_{tr}$ (black traces) maintain their prediction ability while conventional transients (blue traces) become a progressively worse predictor.

Table 5.2 - Correlation coefficients between real $PERG_{ss}$ and $synPERG_{ss}$:

Rps	*Correlation Coefficient*	
	Real $PERG_{ss}$ –$synPERG_{ss(2rps)}$ (5 HARM)	*Real $PERG_{ss}$ – Deconvolved $synPERG_{ss}$ (5 HARM)*
6.5	*0.98 (0.99)*	*0.99 (0.99)*
10.9	*0.97 (0.98)*	*0.99 (0.99)*
15.2	*0.90 (0.911)*	*0.99 (0.99)*
17.4	*0.86 (0.87)*	*0.98 (0.99)*
26.0	*0.65 (0.66)*	*0.96 (0.98)*

Figure Table 5.3 shows quantitative waveform measurements from 2.2 rps $PERG_{tr}$ and $qPERG_{tr}$ from all other rates. It lists N35, P50, and N95 latency and amplitude population averages and standard deviations. Similar to the quantitative data collected in Table 5.1, N95 latency decreases as rate is increased while N35 and P50 latencies increase. Additionally, amplitude reductions of the P50 and N95 component are also consistent with the data from Table 5.1. This study included several intermediate rates not acquired in the study covered in section 5.2. Examining the quantitative data collected in Table 5.3 alongside the data in Table 5.1 provides a clearer picture of how $qPERG_{tr}$ adapt with increasing reversal rate. The component means and standard deviations from Table 5.3 are graphed in Figure 5.11.

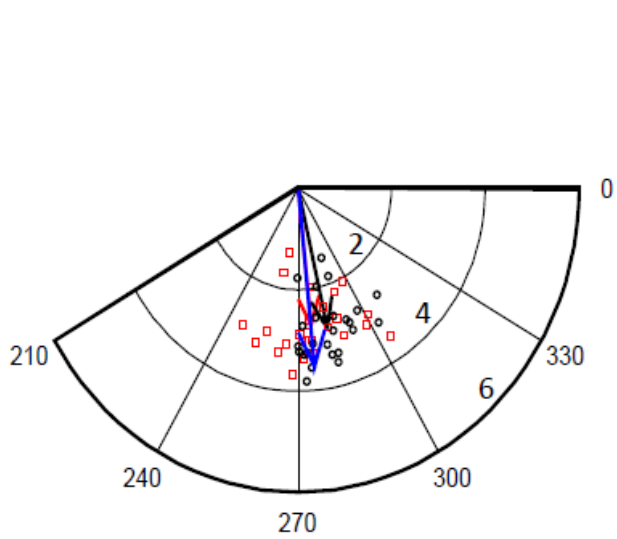

Rate: 6.9 rps

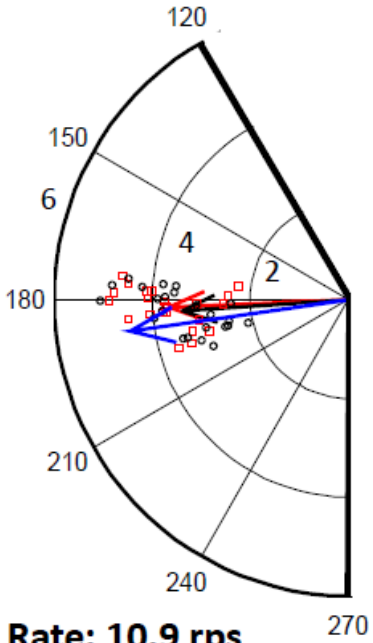

Rate: 10.9 rps

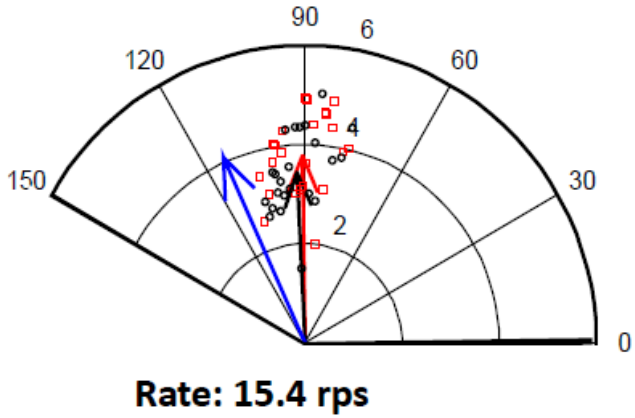

Rate: 15.4 rps

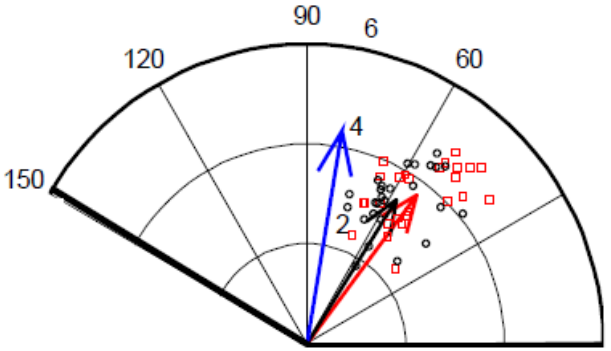

Rate: 17.4 rps

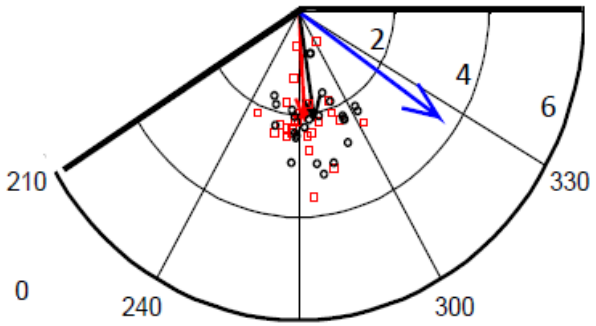

Rate: 26.0 rps

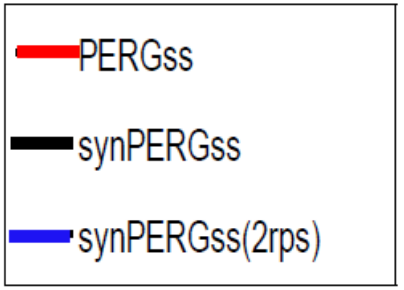

Figure 5.10 (Previous page) - Synthetic PERG and real Steady State PERG Phasor diagrams – Phasor diagrams are shown for reversal rates of 6.5, 10.9, 15.2, 17.4, and 26.0. Red markers represent individual recording magnitude and phase of $PERG_{ss}$. Red phasors represent the population average (8 eyes) of $PERG_{ss}$ for each rate. Black markers represent individual recording magnitude and phase of $synPERG_{ss}$ generated with $qPERG_{tr}$. Black phasors represent population average (8 eyes) of $synPERG_{ss}$. Blue phasors represent population average of $synPERG_{ss(2rps)}$ generated with conventional $PERG_{tr}$. At low rates, magnitude and phase values of both synthetic responses are closely grouped with real $PERG_{ss}$. However, as reversal rate increases, the blue phasor moves further and further from the real response, while the black phasor remains closely grouped.

Table 5.3 - Population averages and standard deviations for individual waveform component amplitudes and latencies obtained at 6 rates:

		N35		*P50*		*N95*	
		Latency (ms)	*Amplitude (μv)*	*Latency (ms)*	*Amplitude (μv)*	*Latency (ms)*	*Amplitude (μv)*
2.2 rps	*AVG*	*18.45*	*0.63*	*41.40*	*4.33*	*86.63*	*6.15*
	STD	*1.68*	*0.32*	*1.40*	*1.18*	*6.97*	*0.86*
6.5 rps	*AVG*	*19.58*	*0.56*	*41.57*	*3.92*	*82.58*	*5.33*
	STD	*1.91*	*0.24*	*1.13*	*0.97*	*5.10*	*0.98*
10.9 rps	*AVG*	*22.33*	*0.87*	*42.47*	*4.00*	*83.03*	*4.63*
	STD	*1.82*	*0.42*	*1.23*	*0.80*	*4.91*	*0.63*
15.2 rps	*AVG*	*23.74*	*0.97*	*43.71*	*3.51*	*80.78*	*3.87*
	STD	*1.55*	*0.42*	*1.43*	*0.82*	*4.10*	*0.72*
17.4 rps	*AVG*	*24.64*	*0.86*	*44.89*	*3.06*	*80.05*	*3.77*
	STD	*1.92*	*0.34*	*3.02*	*0.61*	*9.69*	*0.99*
26.0 rps	*AVG*	*25.99*	*1.23*	*46.41*	*2.05*	*71.49*	*1.78*
	STD	*1.31*	*0.29*	*3.27*	*0.50*	*4.26*	*0.42*

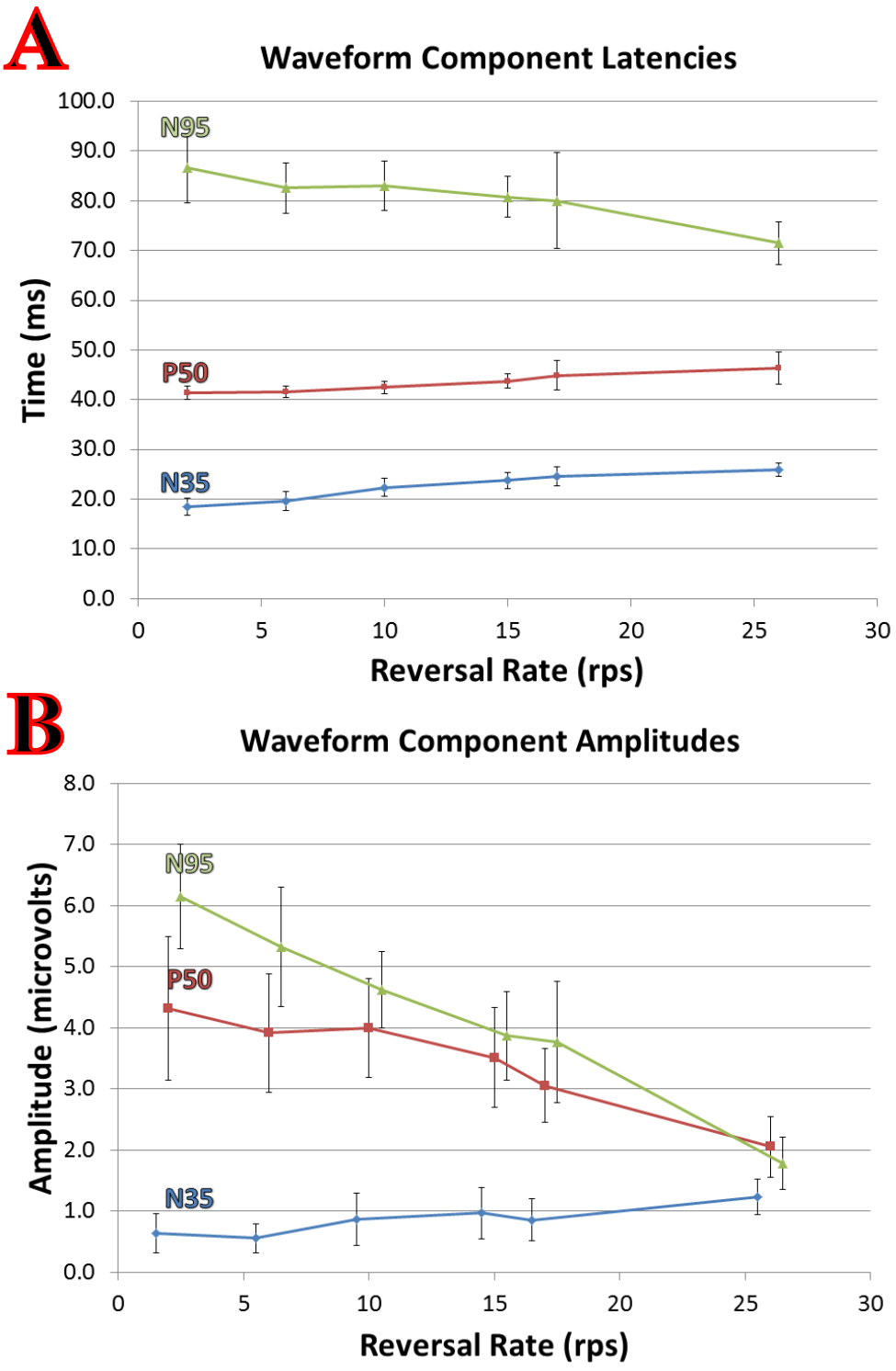

Figure 5.11 - Low rate PERG peak latencies and amplitudes – Population (8 eyes) averages and standard deviations for waveform component latencies (A) and amplitudes (B) are plotted as a function of stimulus reversal rate.

B. Synthesis of Steady State PERG using high rate Transients

The reversal rates tested in the synthesis study covered in section 5.3A ranged from 2.2 to 26.0 rps. These rates were chosen in order to observe the early rate based adaptation effects. The study did not include any reversal rates which resulted in the high rate morphology shown in Figure 5.4B, $qPERG_{tr}$ responses extracted at reversal rates exceeding 56.4 rps. As previously stated and shown in the results of section 5.3, $qPERG_{tr}$ when convolved with a steady stimulation sequence will generate a close approximate of the $PERG_{ss}$ response at the corresponding reversal rate. If the high rate response shown in Figure 5.4b can predict the $PERG_{ss}$ response at that reversal rate, it confirms the high rate adaptation observed in section 5.2.

In order to validate the morphology changes observed at higher reversal rates, an additional rate was added to the synthesis study described in Chapter 5.3. Four of the subjects who were recorded during this study were asked back in order to acquire $PERG_{ss}$ and $qPERG_{ss}$ at 78.1 rps. Three recordings were acquired of each from each subject. As described previously in Figure 5.8, $qPERG_{tr}$ was extracted from the $qPERG_{ss}$ recordings at 78.1 rps. The $qPERG_{tr}$ was then synthetically convolved using the steady stimulation sequence used to acquire $PERG_{ss}$ at 78.1 rps. The resulting $synPERG_{ss}$ is plotted along with the $PERG_{ss}$ in Figure 5.12, filtered for three harmonics of the reversal rate. The correlation coefficient was calculated to quantify the alignment between the synthetic and real responses. Correlation between $PERG_{ss}$ at 78.1 and $synPERG_{ss(2rps)}$ was only 0.22, while correlation between $PERG_{ss}$ and the $synPERG_{ss}$ generated from $qPERG_{tr}$ at 78.1 rps was 0.93.

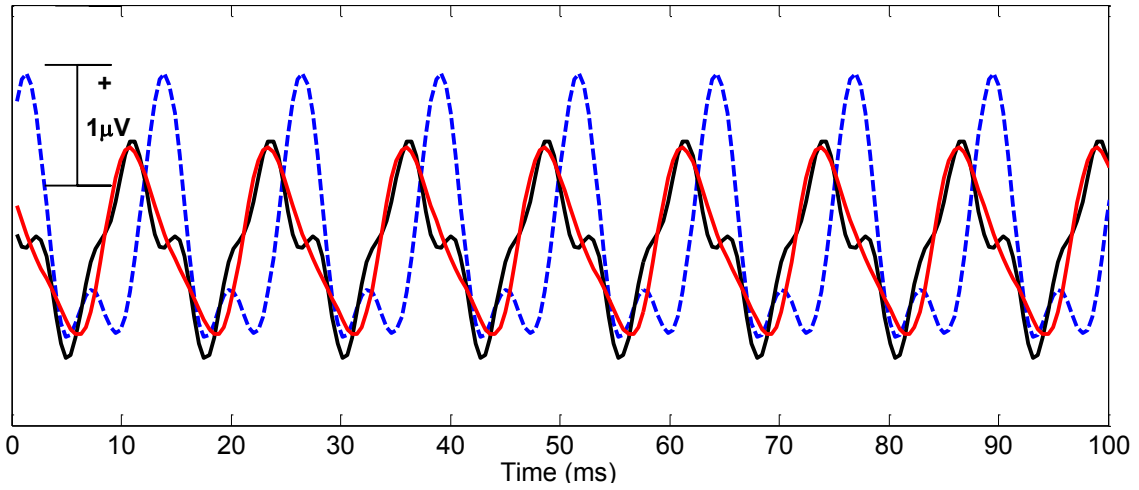

Figure 5.12 - $PERG_{ss}$ and $synPERG_{ss}$ at 78.1 rps (3 Harmonics) – In order to test the prediction ability of the high rate $qPERG_{tr}$, synthetic responses were computed for 78.1 rps. The red trace shows isochronic $PERG_{ss}$ acquired at 78.1 rps. The black trace shows the $synPERG_{ss}$ response computed using deconvolved $qPERG_{tr}$ at 78.1 rps. The blue trace shows $synPERG_{ss(2rps)}$, the prediction of the 78.1 rps $PERG_{ss}$ using a conventional 2.2 rps $PERG_{tr}$. The correlation coefficient between the blue trace and the red trace was 0.22, while the correlation coefficient between the black trace and red trace was 0.93.

The synthetic responses were also compared in the frequency domain. Figure 5.13 shows the phasors of the fundamental frequency of the reversal rate (78.1 rps). The red phasor represents the population average (4 eyes) for the real $PERG_{ss}$ with individual subject data points shown as red markers. The black phasor shows the population average of the $synPERG_{ss}$ constructed with the deconvolved 78.1 rps $qPERG_{tr}$, with black markers showing the individual subject data points. Blue phasors show the population average of the $synPERG_{ss}$ constructed with conventional 2.2 rps $PERG_{tr}$. As observed at lower rates black ($synPERG_{ss}$) and red ($PERG_{ss}$) phasors overlap very closely while the blue phasor representing 2.2 rps $PERG_{tr}$ construction is very different from the others.

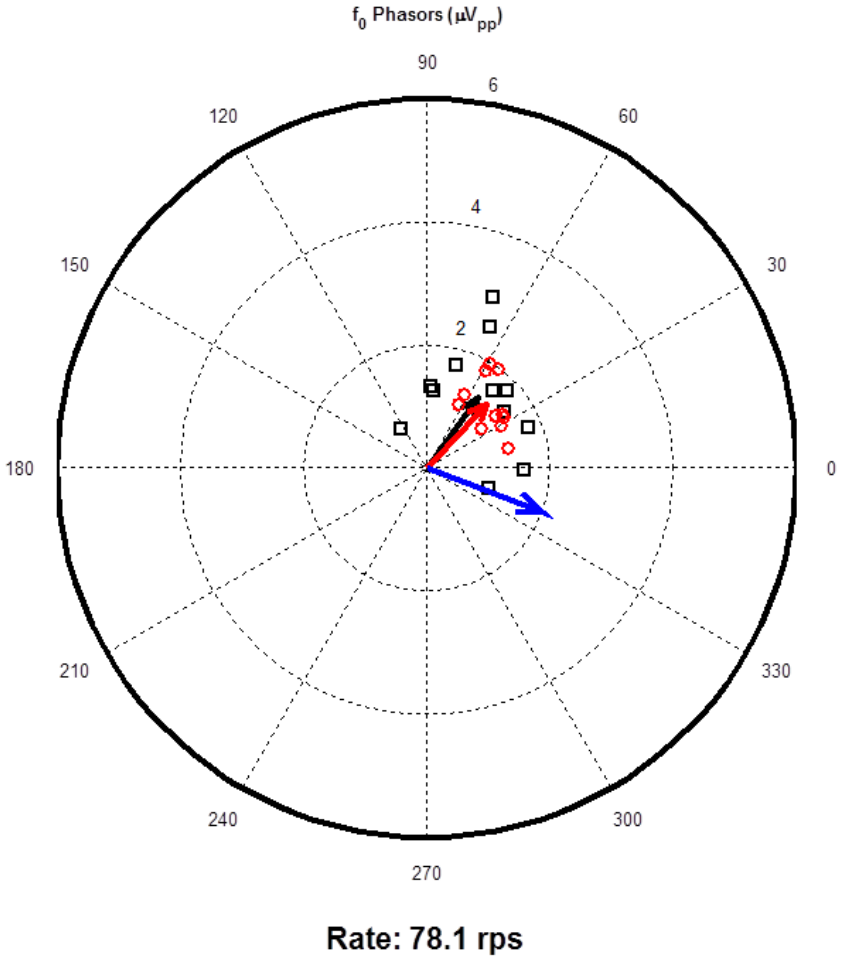

Figure 5.13 - $PERG_{ss}$ and $synPERG_{ss}$ phasors at 78.1 rps – Red markers represent individual recording magnitude and phase of $PERG_{ss}$. Red phasor represent the population average (4 eyes) of $PERG_{ss}$ at 78.1 rps. Black markers represent individual recording magnitude and phase of $synPERG_{ss}$ generated with $qPERG_{tr}$ at 78.1 rps. Black phasor represent population average (4 eyes) of $synPERG_{ss}$ generated with $qPERG_{tr}$ at 78.1 rps. Blue phasor represent population average of $synPERG_{ss(2rps)}$ generated with conventional $PERG_{tr}$. For this reversal rate, the black individual markers have a wider spread due to the jitter of the 78.1 rps sequence. Despite this, the population average phasor corresponding to the black markers is a good predictor of the real $PERG_{ss}$, while the blue phasor does not predict the real $PERG_{ss}$.

5.4 Dynamic PERG averaging

As discussed previously in section 2.8, one of the essential assumptions made when using the CLAD algorithm is that there is no temporal adaptation in the response during the acquisition of the qSS response. There is, in fact, evidence that the $PERG_{ss}$ response adapts during prolonged periods of stimulation (Porciatti and Ventura, 2009). The responses acquired during this study all consisted of 128, 450 ms long sweeps. This corresponds a duration of sustained stimulation of approximately 57.6 seconds assuming no sweeps were rejected for containing artifacts. A more realistic approximation is 60-80 seconds per recording depending on artifact rejection.

The commercial acquisition system used during this study (Universal Smart Box, M011110, Intelligent Hearing Systems) normally only returns an average of the specified sweeps after acquisition has completed. The raw un-averaged data is not normally saved. In order to observe any adaptation effects that might be present during the acquisition of PERG a new procedure was developed which would allow for averaging to be performed off line and dynamically.

For this experiment jittered qPERGss were acquired using the LED VDU to deliver a continuous stimulus train at a reversal rate of 17.4 rps for a period of one minute. At the end of one minute of continuous stimulation, the VDU reverted to a grey field equal in luminance to the pattern stimulus. The VDU remained on the grey stimulus field for a period of 30 seconds, after which the stimulus would begin again. This pattern of reversals for one minute followed by a gray field for 30 seconds was repeated 5 times. During the period, acquisition was continuous. Additionally, artifact rejection was

completely disabled, in order to assure that no dynamic effects of the response were missed due to rejected sweeps. Subjects were encouraged to limit blinks or other movements which might result in artifact contamination of the signal to periods when the stimulus was a grey field.

Each recording consisted of 960 raw sweeps, made up of five uninterrupted periods of stimulation (each 128 sweeps long) separated by five periods of the isoluminant grey field (each 64 sweeps long). Since there no averaging or artifact rejection was performed, any dynamic effects of the response should be preserved by this paradigm. Recordings were performed using the same conditions described in section 4.2. Five subjects participated in this experiment and four recordings were obtained from each subject.

Initially, raw files were manipulated in such a way as to preserve any dynamic effects of the response. Raw files were broken up by the regions of stimulus state (segments of 128 sweeps during pattern stimulation and 64 sweeps during isoluminant field) and averaged. Each recording consisted of 5 separate trials of stimulus and grey field. In each trial, any adaptation occurring over the minute of continuation should be identical in subsequent trials. Averaging of the raw data in this fashion preserves any temporal adaptation as the relative location from the beginning and end of the stimulation train (pattern to grey and grey to pattern) is the same in each of these raw segments (see Figure 5.14). In this way, the SNR of the responses can be improved enough to see the PERGss without averaging out any adaptation effects. Once enough trials have been averaged, comparisons are made between different segments of the response from the stimulus train (see Figure 5.15).

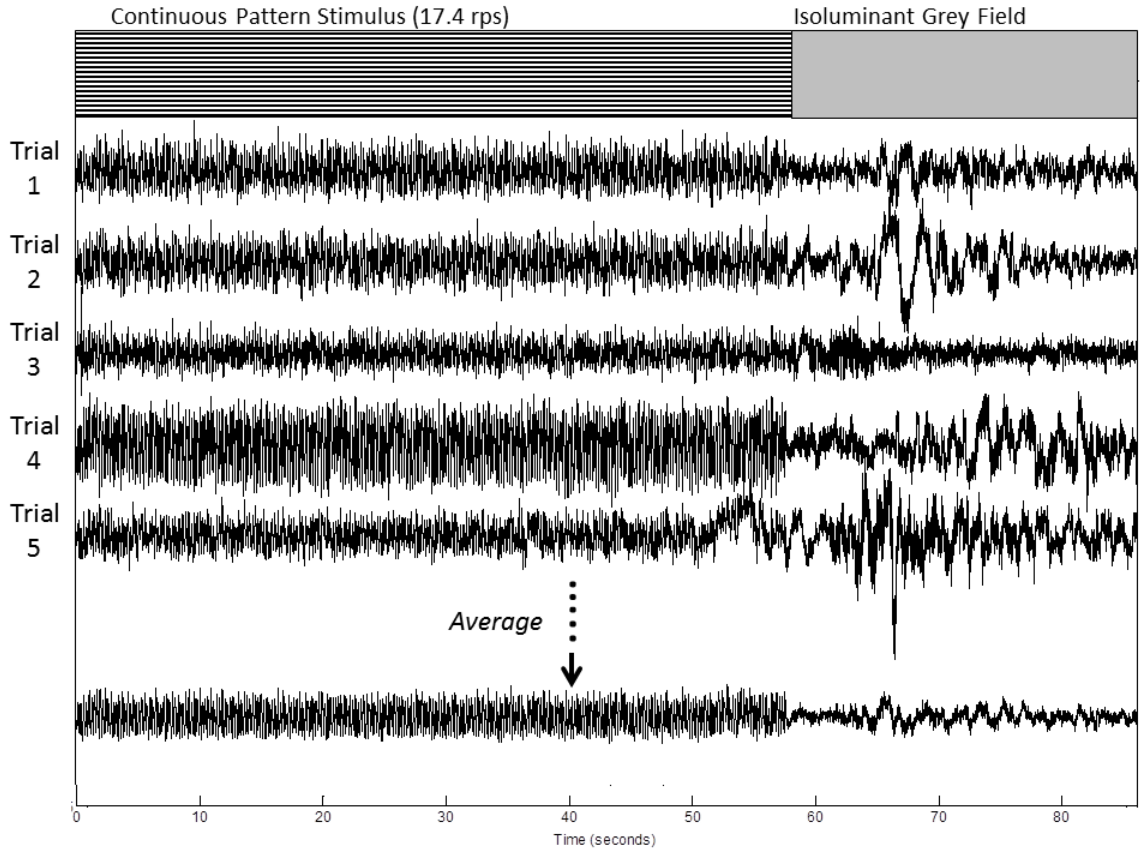

Figure 5.14 - Averaging trials to preserving any dynamics of the response – Each recording consisted of 5 one minute long stimulus trains. Each stimulus train was followed by a 30 second period where no stimulus was delivered and the LED VDU displayed an isoluminant grey field. In conventional sweep averaging, successive sweeps are averaged together. This can obscure temporal adaptation or other effects dependent on time from the initial stimulus. Each recording was separated into the five 90 second trials (1 minute of continuous stimulation, 30 seconds of grey). Averaging the complete trials together should preserve any adaptation that takes place over the minute of stimulation as it should be identical in each of the trials.

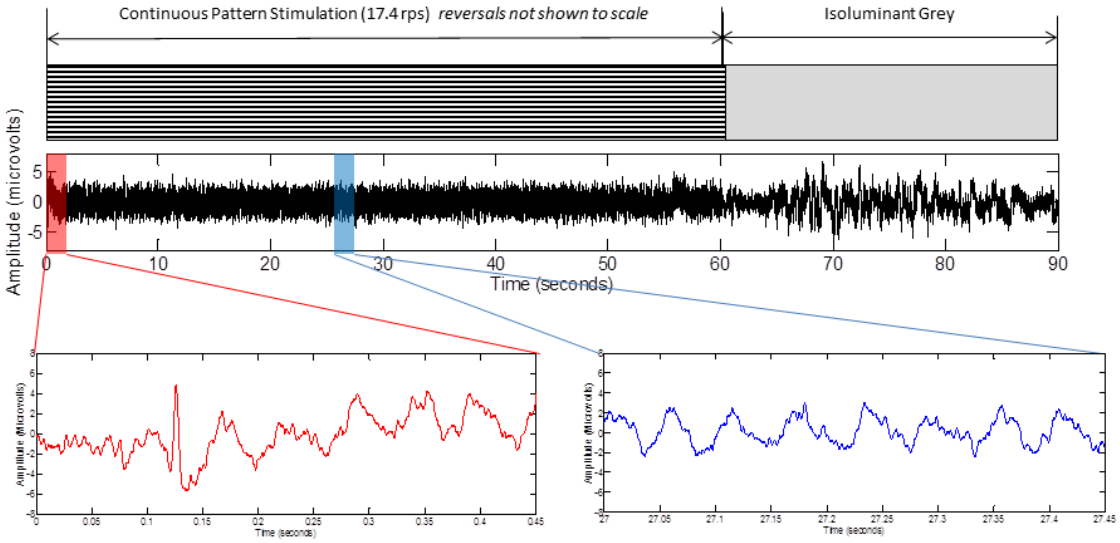

Figure 5.15 - Responses along the stimulus train – No successive sweeps have been averaged but 75 separate trials have been averaged as described in Figure 5.14. The red trace shows response from the initial 0.45s of the stimulus train. The blue trace shows the response between 27 and 27.45 seconds from the onset of the stimulus train. In order to further improve the SNR, some successive sweeps will have to be averaged.

Figure 5.15 shows the response with no successive sweep averaging. While the $PERG_{ss}$ is visible, the signal is still noisy and there are artifacts present. To improve the response further, some degree of successive sweep averaging had to be performed. In order to dynamically average and process the files a GUI was developed (see Figure 5.16). The GUI allows the user to specify how many successive sweeps to average together. The GUI then constructs a plot of the response from the onset of the pattern reversals to the end of the isoluminant grey period. Depending on how many successive sweeps are averaged, samples of the signal are created. These samples are referred to in terms of the time bins the samples represent (Porciatti and Ventura, 2009). Depending on the number of successive sweeps averaged the time bins increase. The GUI can display the data from 0.45 sec/sample ('raw', no successive sampling) to 30 sec/sample (which

averages the pattern stimulation train into 2 bins). The GUI can be used to select two time bins to display and compare. The GUI displays the response from each bin overlaid in the time domain (see Figure 5.16B) and also shows the fundamental frequency domain component of each bin at the reversal rate (see Figure 5.16C).

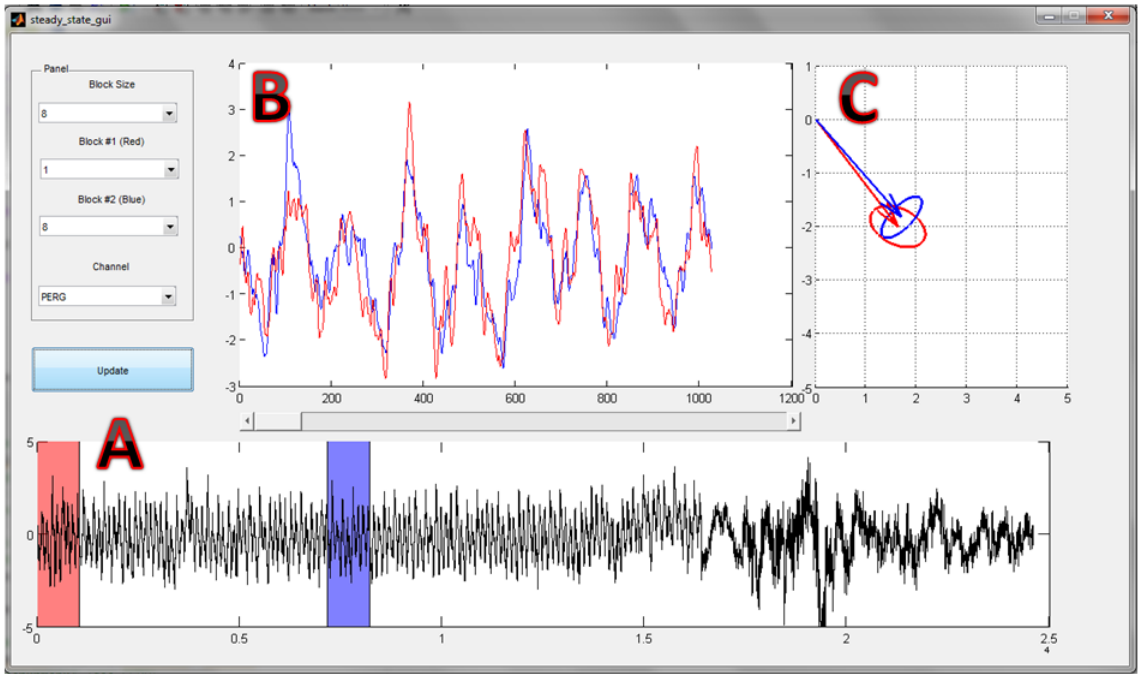

Figure 5.16 - Dynamic $PERG_{ss}$ GUI – GUI developed to examine the adaptation of the PERG response over time. The GUI processes files of raw $PERG_{ss}$ data acquired from continuous trains of stimulus. The GUI allows for dynamic re-averaging of the raw waveform. The user can select how many successive sweeps to average. The averaged waveform is displayed in (A). Additionally, the user can select which of the resultant time bins to visualize from the successive sweep averaged response. The two bins selected are highlighted in (A) in red and blue. (B) Display of the two samples from the selected bins. (C) Display of the primary frequency component of the response in each bin at the reversal rate (17.4 rps). In the above figure, 8 successive sweeps were averaged, resulting in bins which represent 15 sec of real time (15 seconds/sample).

Since a qSS sequence was used in this study, each bin can be deconvolved using CLAD (see Figure 5.17). In Figure 5.17, 16 successive samples were averaged resulting in 8 bins representing 7.5 seconds of the original data. The 8 segments were labeled A-

H. The responses were then deconvolved using CLAD. Traces in Figure 5.17 are colored the same as their bins. The importance of combining CLAD with adaptation studies will be discussed later.

Frequency domain analysis was also used to investigate any adaptation effects of the $qPERG_{ss}$ response. In Figure 5.18, the magnitude of the fundamental component of the reversal rate is shown for each successive sample. Figure 5.18A shows the data with 2 successive samples averages (0.9 sec/sample), while Figure 5.18B shows the same data but with 16 successive samples averaged (7.5 sec/sample). Blue data points are qPERGss magnitude during the stimulus train, while red data points are magnitudes during the isoluminant grey stimulus field. A linear regression was performed on the data points during the stimulus train. The result from the linear regression for the 0.9s/sample data was $y = -8.7 * 10^{-6}x + 3.1$ and for the 7.5 s/sample data it was $y = -6.2 * 10^{-4}x + 3.1$.

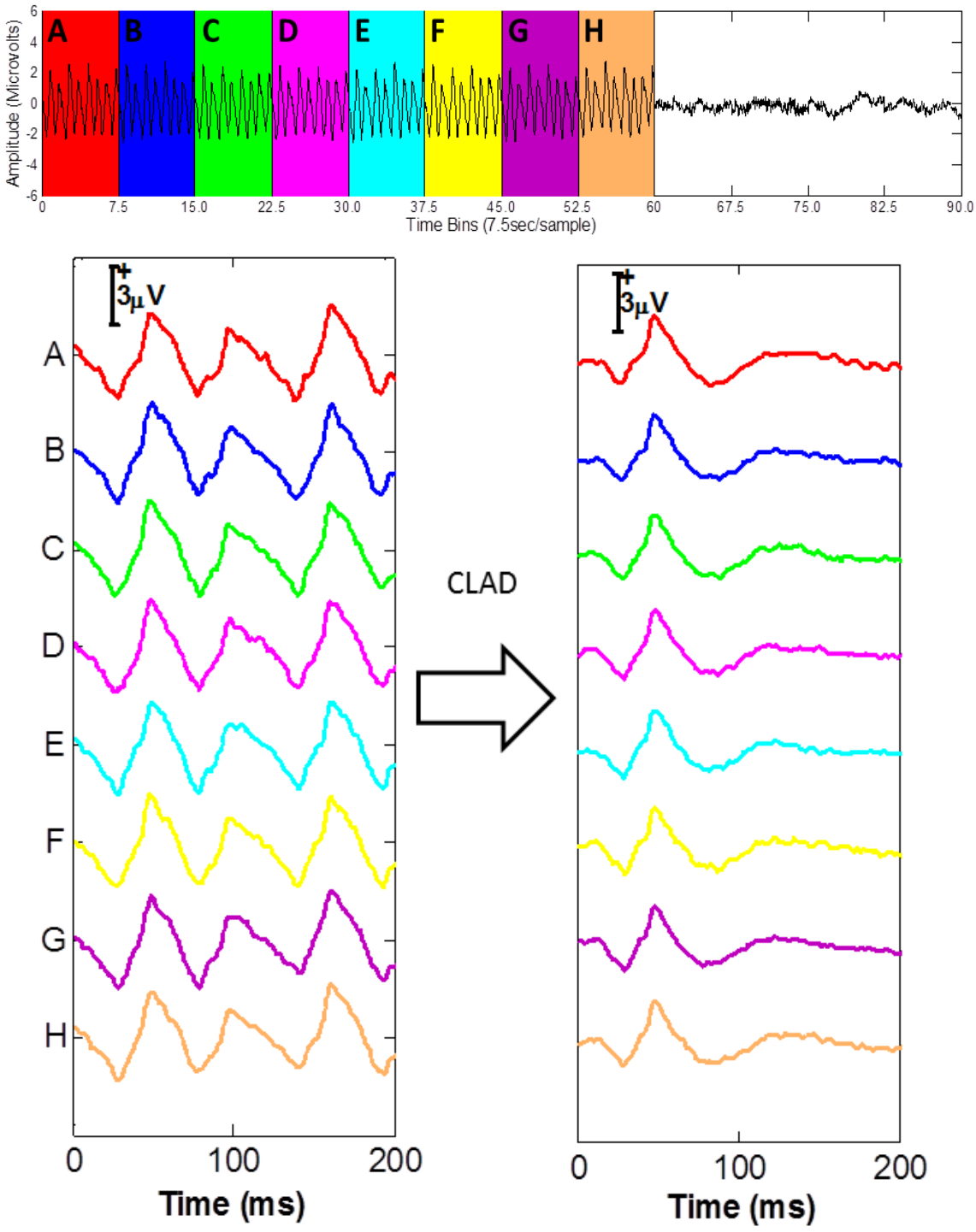

Figure 5.17 - Deconvolution of different samples – For the above data, successive sweeps were averaged in groups of 16. This results in 8 samples with 7.5 sec/sample. The successive samples have been labeled A-H. Using CLAD, each sample can be deconvolved individually. To the left, the $PERG_{ss}$ at each sample, colored according to the top figure. To the right, the corresponding deconvolved $qPERG_{tr}$ are shown, showing the extracted transient every 7.5 seconds over the 60 seconds of stimulation.

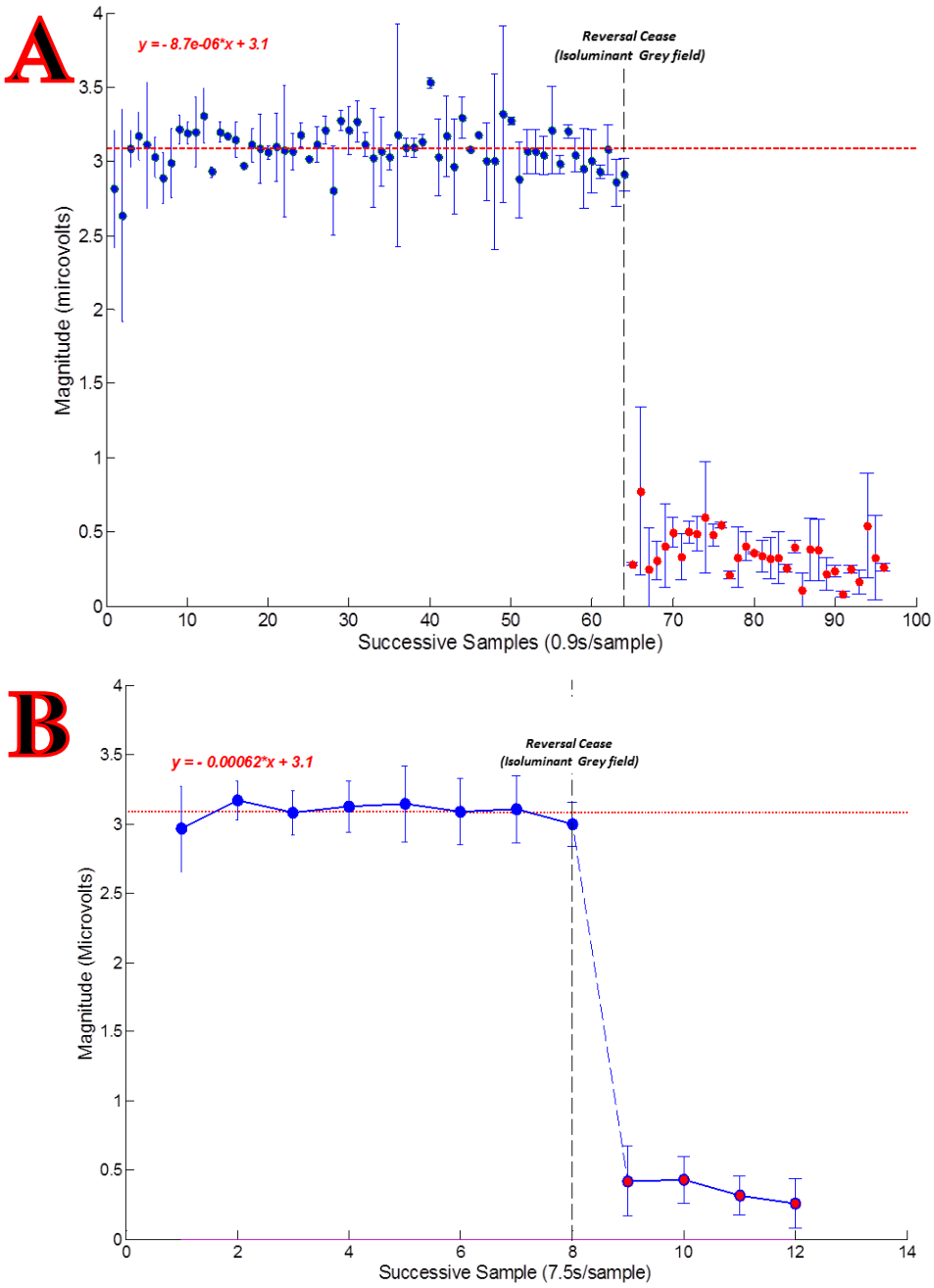

Figure 5.18 - Magnitude of the fundamental reversal rate component – (A) Every two sweeps of the raw data was successively averaged (0.9 sec/sample). Linear regression was performed on the magnitudes during the stimulus train. The slope of the regression was $-8.7*10^{-6}$. At the moment the stimulus train finishes and the stimulus field goes to grey, the magnitude drops off quickly. (B) In the lower plot 16 successive sweeps were averaged (7.5 sec/sample) The standard deviations improved greatly by increasing the number of successive averages. The slope of the linear regression was $-6.2*10^{-4}$. There did not appear to be significant magnitude adaptation regardless of the number of successive sweeps averaged.

Chapter 6 - Discussion

6.1 Acquisition of conventional $PERG_{tr}$ with LED display

Before beginning the more elaborate experiments within this study it was important to build a baseline of conventional $PERG_{tr}$ responses. This was multifold; $PERG_{tr}$ was used as an initial validation of the LED VDU, it was used as a baseline against rate based adaptation observed in deconvolved $qPERG_{ss}$, and it was used as a control in generating synthetic $PERG_{ss}$.

$PERG_{tr}$ were acquired at 2.2 rps from nine subjects as described in Chapter 4.4. Figure 5.1 shows that the acquired $PERG_{tr}$ were reproducible, not only when acquired from one subject, but across subjects as well. Waveform morphology was consistent with standards and individual waveform components N35, P50 and N95 can be easily identified. Amplitudes are also consistent with standards with P50 amplitudes between 2 and 6 μV (Holder et al., 2012).

Figure 5.2 shows the population average of the acquired responses alongside a $PERG_{tr}$ taken from the standards. While the waveform morphology is consistent between both traces, there are some differences which must be addressed. First of all, amplitudes of the acquired responses were lower than the standard response. This discrepancy can be explained by the electrodes used. Responses shown in the ISCEV standard were acquired using electrodes which contact the cornea or bulbar conjunctiva. The paradigm adopted for these experiments utilized skin electrodes on the lower eyelids. It is commonly known that the use of skin electrodes in PERG studies results in lower

amplitudes than electrodes which make contact with the eye itself (McCulloch et al., 1998; Hidajat et al., 2003; Coupland, 2006; Holder et al., 2012). Despite this, the skin electrode paradigm is desirable in many clinical applications due to being less invasive than other electrode setups, and the added comfort skin electrodes afford subjects can greatly improve the quality of responses. As such, it is a viable alternative which is used in a number of clinical and research settings (Kikasu et al., 1986, Porciatti and Ventura, 2004). Despite the reduced amplitude when compared to the standard waveform, the acquired $PERG_{tr}$ responses are still well within the normal range (2-6 μV) established in the standards.

Another discrepancy that needs to be addressed is the difference in latencies, between the acquired responses and the standard. In Figure 5.1, individual subject recordings are displayed in black, and from this figure, it is clear that the waveform component peak times are very consistent among subjects. This can also be observed in the Table 5.1 and Figure 5.6 which display component amplitudes and peak times. Typically, a leeway of 10-15 ms is given for component peak times (Bach et al., 2012), and the acquired data is much more consistent than that, even considering N95, which because of the broadness of the component is typically not reported (Holder et al., 2010). The standard deviation for the N35, P50 and N95 waveforms components were 2.1, 2.2 and 5.1 ms respectively. Given the consistency of the peak times amongst the subjects, it is likely that the latency difference observed in Figure 5.2 is systemic difference between the VDUs used in acquiring the responses. Latencies for the components of acquired responses were consistently earlier than component latencies found in standards. In Figure 5.2, it can be seen that the discrepancy is consistent for all the components, and

that the component intervals (i.e. N35 to P50 interval) are the same in the acquired $PERG_{tr}$ and the $PERG_{tr}$ standard. Figure 6.1 shows the acquired $PERG_{tr}$ from Figure 5.2 and a shifted $PERG_{tr}$ in red. The discrepancy between the acquired $PERG_{tr}$ and the standard $PERG_{tr}$ was measured to be 7.2 ms.

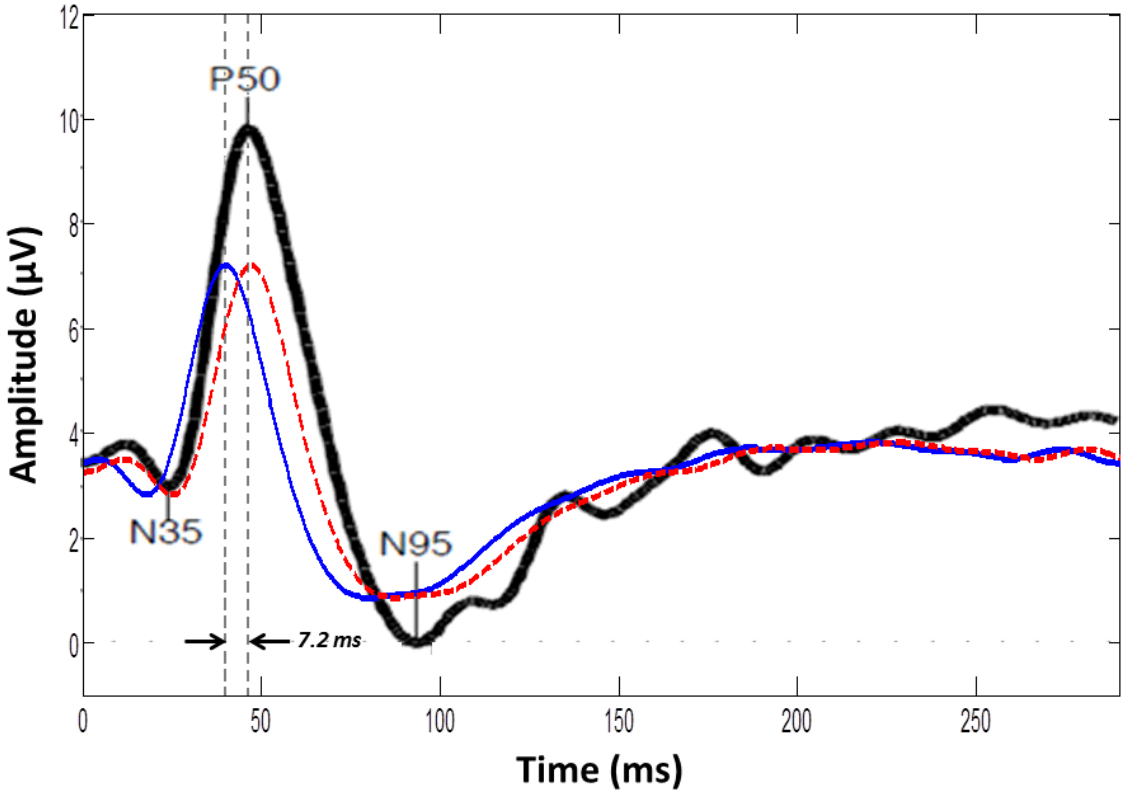

Figure 6.1 - Standard $PERG_{tr}$ versus Acquired $PERG_{tr}$ and latency adjusted $PERG_{tr}$ – The black trace above shows a $PERG_{tr}$ taken from ISCEV standards. The blue trace shows the acquired $PERG_{tr}$ population average (nine subjects). Both traces were offline lowpass filtered from 1-45 Hz. The waveform morphology of the acquired $PERG_{tr}$ is consistent with the standard, but individual waveform components latencies are earlier than those of the standard. A latency corrected population average is shown in red. It has been shifted 7.2 ms so that components between acquired response and the standard align.

From Figure 6.1 it is clear that intervals between waveform components are consistent between standards and acquired $PERG_{tr}$, and once an artificial delay was added

to the acquired $PERG_{tr}$, waveform components aligned well. The fact that the earlier latencies were consistent for different subjects and that intervals between components were the same as those in the standards again points to the difference coming from the display. Many studies have been performed on different display technologies used in PERG studies (Zele & Vingrys, 2005; Hogg, 2006; Husain et al., 2009; Elze, 2010; Nagy et al., 2011). Different visual display units (VDUs) used can alter stimulus definition and timing. As discussed in Chapter 2.6, the frame rate of CRT monitors can affect the delay between signal input and stimulus output. This delay can alter the effective time zero of the PERG response. This is supported by the fact that the discrepancy between the two responses was 7.2 ms. When using CRT VDUs there is the potential for a jitter of plus or minus 50% the frame period to be introduced into the implicit time of the response (Hogg, 2006). Assume a CRT with a minimum refresh rate of 75 Hz (the minimum suggest refresh rate given in the standard (Bach et al., 2012)), the uncertainty of the implicit time of the response would be ±6.7ms. Assuming a refresh rate of 70 Hz (another common CRT refresh rate) gives an uncertainty of 7.1 ms. One of the motivating factors in designing the LED display developed for this project was as a VDU with a high temporal resolution, so that the display would be CLAD compatible, and able to accurately convey a wide number of CLAD sequences. Because of the fast acting nature of the LED display, it makes sense that latencies would skew earlier than conventional VDUs, as the LED display was designed to minimize the delay between signal in and stimulus out. Given that the discrepancy is consistent with standard refresh rates for CRT VDUs it is plausible that the difference in the display technologies accounts for the latency shift.

The $PERG_{tr}$ responses acquired with the LED based VDU resulted in responses which were similar in morphology, component amplitudes and component latencies to collected standards for $PERG_{tr}$. Any slight discrepancies in latency and amplitude can be explained by the custom designed, fast acting LED VDU, and the skin electrode recording paradigm.

6.2 Effects of Stimulus Reversal Rate on PERGs

The motivation behind this experiment was to verify that CLAD could be used to deconvolve $PERG_{ss}$ responses at a number of stimulation rates. Secondary to this was the observation of rate based adaptation, if indeed there was any, in the deconvolved $qPERG_{tr}$ response. After confirming that the LED based VDU was capable of eliciting PERG responses within established standards, the study was expanded to acquire PERG at a number of higher stimulation rates. $qPERG_{ss}$ responses were acquired at the following rates: 17.4, 28.2, 36.7, 41.2, 56.4, 67.3 and 78.1 rps. Using CLAD, it was possible to extract $qPERG_{tr}$ for each of these rates. Extracted $qPERG_{tr}$ responses are shown in Figure 5.3. Typically, at higher reversal rates, analyses of PERG responses have to be performed in the frequency domain, measuring magnitude and phase (Bach et al., 2012). Having access to $qPERG_{tr}$ responses means that individual waveform components can be observed and quantified regardless of the stimulation rate, and a more specific analysis of rate based adaptation can be performed. Typically, as stimulation rate increases, adaptation of evoked responses results in reduction in waveform component amplitudes and increases in component latencies (Ozdamar et al., 2007).

In this study, some interesting and unexpected rate effects were observed. Initially, observed PERG appeared to adapt normally, with the P50 waveform component gradually reducing in amplitude and increasing in latency. N95 amplitude also decreased in amplitude, but appeared to *decrease* in latency, see Figure 5.6, becoming earlier. It is believed that this decrease in latency is a least partially due to the narrowing of the N95 component. N95 is a very broad component and determining the exact latency is difficult (Holder et al., 2010). As N95 amplitude decreases with rate, and becomes narrower, the peak latency might merely appear to be moving earlier. As reversal rates approached 41.2 rps, component amplitudes had decreased to the point that it became difficult to discern the individual waveform components. Normally, in adaptation studies this would eventually lead to the dying out of the response, as the demand of the increasing stimulus becomes too much for the cellular generators of the response to keep up, and the event related potentials become indistinguishable from the noise floor. As reversal rate was increased beyond 41.2 rps, there was an observed increase in the amplitude of the response, but the waveform morphology was no longer similar to the response at the lower reversal rates. The new morphology had its own distinct individual waveform components which are consistent amongst many subjects. While the conventional $PERG_{tr}$ morphology starts with an initial negativity, N35, the high rate morphology begins with a positive peak, which we have labeled P_{α}. P_{α} is followed by a negative peak at roughly the same latency as the P50 component, which was named N_{α}. Finally, there is another positive component call P_{β}. Population averages for component amplitudes and standard deviations were compiled in Table 5.1. Figure 6.2 shows the deconvolved $qPERG_{tr}$ responses for each of the reversal rates. Responses are separated into two

groups, based upon the observed waveform morphology. Blue responses exhibit the conventional N35→ P50→ N95 morphology, while red responses exhibit Pα→Nα→Pβ morphology. Corresponding components in subsequent responses have been connected with black traces to illustrate component shifts as reversal rate is increased.

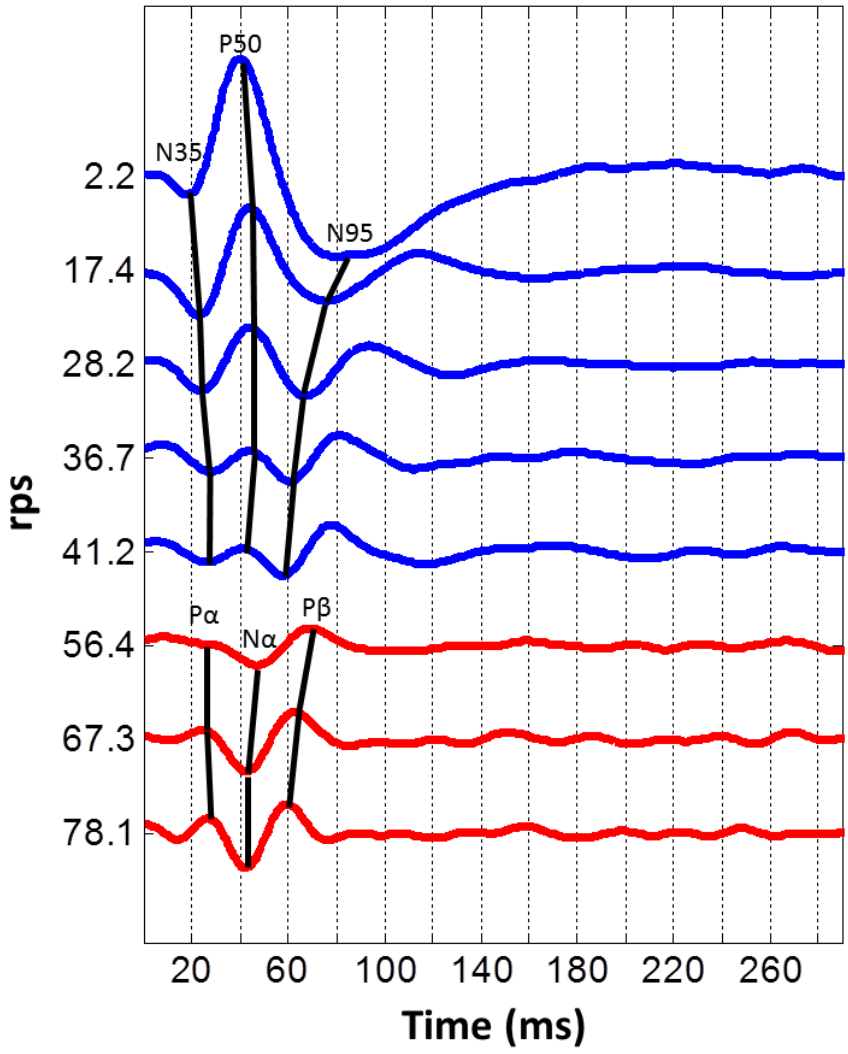

Figure 6.2 - qPERG$_{tr}$ waveform adaptation with increasing reversal rate – Above are the deconvolved qPERG$_{tr}$ responses at each reversal rate. Responses have been lowpass filtered from 1-45 Hz. The blue traces denote responses of 41.2 rps and below, where conventional waveform components (N35, P50, and N95) can be distinguished. Red traces show rates higher than 41.2 rps. In these responses there is a new morphology, (P_α, N_α, and Pβ). Black traces have been overlaid on the plot connecting the individual waveform components of each waveform to the corresponding components of the waveform below it.

While the high rate morphology was reproducible across subjects, at this time it is unclear as to the exact origin of the new waveform components. Origins of the high rate components might be explained by the response of a different cell population that exhibit higher temporal sensitivity, or alternatively the components might be the responses of intermediate cells normally obscured by conventional PERG, but revealed at high rates. The exact origin of the high rate components Pα, Nα, and Pβ will be the subject of future research.

6.3 Steady State PERGs and their Synthesis from Transient Responses

Deconvolved $qPERG_{tr}$ responses have been claimed in the studies herein to be the contribution of a single pattern reversal to the establishment of the $PERG_{ss}$ response. If this is indeed the case, then the extracted $qPERG_{tr}$ should be able to recreate the $PERG_{ss}$ response when synthetically convolved. The motivation of this experiment was to test the generation theory of the $PERG_{ss}$ response (Capilla et al., 2011) by creating synthetic $PERG_{ss}$ responses, $synPERG_{ss}$, and comparing the synthetic responses with real acquired $PERG_{ss}$ and also to add validity to the adaptation effects observed in Chapter 5.2.

Figure 5.7 shows the $qPERG_{ss}$ and $PERG_{ss}$ responses acquired from the eight subjects. The responses can be differentiated visually by inspecting the time between the peaks of the response. For the $PERG_{ss}$ responses, stimulation was isochronic, with constant ISI, and it is apparent in the responses that the peaks have constant spacing as well. In the $qPERG_{ss}$ responses, there is an apparent variation in the spacing between response peaks, which corresponds to the jittered ISIs. The individual subject responses (overlaid black traces) show that whether jitter is present or absent in the stimulus the

reproducibility of the responses across subjects remains. Applying the CLAD algorithm to the $qPERG_{ss}$ responses in column B of Figure 5.7 results in the $qPERG_{tr}$ responses shown in column C of Figure 5.7. Again, $qPERG_{tr}$ responses represent the contribution of a single stimulus, in this case a pattern reversal, to the overall establishment of the steady state response. Taking the $qPERG_{tr}$ responses for the five reversal rates (6.5 rps, 10.9 rps, 15.2 rps, 17.4 rps, and 26.0 rps) and convolving them with an isochronic stimulation sequence of the same mean reversal rate, as shown in Figure 5.9 results in a $synPERG_{ss}$ response for each reversal rate. Additionally, a conventional 2.2 rps $PERG_{tr}$ population average was computed from responses acquired from each of the eight subjects. This conventional $PERG_{tr}$ response was also convolved with each of the isochronic steady stimulation sequences to create a second set of synthetic responses referred to as $synPERG_{ss(2rps)}$ responses. The $synPERG_{ss(2rps)}$ responses, synthesized from conventional $PERG_{tr}$, represent $PERG_{ss}$ if there was no rate based adaptation of the "per stimulus" response. Figure 5.9 overlays the real $PERG_{ss}$ response with both the $synPERG_{ss}$ and $synPERG_{ss(2rps)}$ responses. A correlation coefficient was also calculated between the real $PERG_{ss}$ and each of the $synPERG_{ss}$ responses and can be found in Table 5.2. Observing the alignment of the responses in Figure 5.9 and the correlation coefficients in Table 5.2, it can be seen that for lower rates (6.5 rps and 10.9 rps) both synthetic responses align well with the real $PERG_{ss}$ and both have correlation coefficients greater than 0.98. However, as reversal rate was increased, the $synPERG_{ss(2rps)}$ which did not account for adaptation, became a progressively worse predictor of the real $PERG_{ss}$, losing alignment in Figure 5.9 and dropping in correlation gradually to 0.65 at 26.0 rps. The $synPERG_{ss}$ constructed with the $qPERG_{tr}$ at each rate however, maintained its

prediction ability, regardless of the reversal rate (maintaining good alignment and a correlation greater than 0.95 for all rates). This trend continued for higher rates as well, as shown for 78.1 rps responses in Figure 5.12. When synthetic responses were generated at 78.1 rps, the $synPERG_{ss(2rps)}$ was even poorer at predicting the steady state response, with a correlation coefficient of only 0.22. The synthetic response generated with the rate specific transient however, continued to predict well, with a correlation coefficient of 0.93.

In addition to the temporal comparisons between real and synthetic PERG, frequency domain analysis was also performed. Phasor diagrams were constructed for the fundamental frequencies of the reversal rate for each of the 5 stimulation rates. These diagrams are found in Figure 5.10 and 5.13. For all tested stimulation rates, $synPERG_{ss}$ remained an excellent predictor of the real $PERG_{ss}$ response keeping similar values for both phase and amplitude. The $synPERG_{ss(2rps)}$ on the other hand, was a decent predictor for lower rates, but as reversal rate increased, However, as reversal rate was increased $synPERG_{ss(2rps)}$ began to lag more and more from real $PERG_{ss}$ response, and amplitude changed as well. Quantitative measurement of individual waveform component latencies and amplitudes was performed and is gathered in Table 5.3. Despite a different subject population and different sequences recorded, latency and amplitude was consistent with quantitative waveform information now. These findings not only suggest that there is the presence of rate based adaptation in PERG, but also support the superposition theorem of transient and steady state responses (Capilla et al., 2011; Toft-Nielsen et al., 2012).

6.4 Dynamic PERG averaging

One of the assumptions made with the CLAD algorithm is that the response to be deconvolved is not adapting over time. If there is any adaptation, the deconvolved qPERGtr will not be an accurate representation of the response. While the findings in section 5.3 suggest that there is no adaptation going on, (an inaccurate $qPERG_{tr}$ would not predict $PERG_{ss}$ as well as the results show in that study) a more deliberate examination of the dynamic behavior of the $PERG_{ss}$ was carried out in this study.

The data shown in Figure 5.17 and 5.18 didn't appear to show any adaptation over the minute long stimulation trains. In Figure 5.18, frequency domain analysis was used to construct a two magnitude plots, one with average magnitude values every 0.9 seconds, the other showing average magnitude values for every 7.5 seconds. Linear regressions were performed on each of the magnitude plots. The resulting slopes of the regression were $-8.7*10^{-6}$ and $-6.2*10^{-4}$ respectively. These findings show very little change to the magnitude over the minute long intervals of continuous stimulation. These findings validate one of the central assumptions of CLAD, and add more evidence to the accuracy of the $qPERG_{tr}$ responses presented in this study.

However, the findings appear to contradict evidence found in the literature (Porciatti & Ventura, 2009). A possible explanation for the lack of adaptation lies in the jitter of the qSS sequence used. It is possible the variation in times between stimuli due to the jitter of the CLAD sequence disrupted the temporal adaptation. Another explanation of the lack of adaptation could be the length of the grey periods between the minute long stimulation trains. It is possible the time between stimulation trials was not

long enough for the cellular generators in the retina to recover and thus, adapted and non-adapted responses were being averaged together, obscuring adaptation effects. Yet another possibility lies in the length of the stimulation trains. It is possible that temporal adaptation is occurring much earlier in the stimulation train (within the first seconds), and the length of the stimulation trains need to be shortened to observe the adaptation. These possibilities will be carefully addressed and investigated in future research.

While no significant adaptation effects were observed in this study, it was shown that CLAD could be used with sustained stimulation trains, and that a 'per-stimulus' response could be extracted from any point during the prolonged stimulation. In electrophysiological responses were significant adaptation occurs, either due to exhaustion of cellular mechanism or some other reason, CLAD could be used to get a more detailed view of how the response is changing. Being able to distinguish the individual waveform components of an adapting response might expand the understanding of what is causing the dynamic changes in the response.

Chapter 7 - Conclusions

The primary motivation behind this study was the acquisition of the high rate transient PERG response through the CLAD decovolution method. Applying CLAD to visual responses however, required a display technology which could reliable deliver stimuli with sub-millisecond precision. Unfortunately, conventional VDUs fell far below these requirements. As such, it was necessary to develop custom, fast responding pattern VDUs in order to accomplish this task.

Three VDUs were developed which were capable of delivering pattern stimuli within the parameters outlined in standards (Brigell et al., 2003; Holder et el., 2010; Bach et al., 2012), and satisfactory pilot data was successfully obtained from the three. While the LED VDU was the primary display used for the majority of this study, the projector VDU and variable polarizer VDU, both exhibit unique strengths which might make them the preferable high rate visual display for future lines of research (for instance, the projector VDU can potentially be used for chromatic reversals).

Since the study employed unproven technologies, efforts were made to validate the responses acquired with the developed displays. Using the LED VDU, $PERG_{tr}$ were acquired which were comparable to standards in morphology and peak amplitudes. Peak times were consistently earlier using the LED VDU, but this was expected due to the fast response of the LEDs (LED onset/offset time constant was 0.2 ms) and as conventional CRT and LCD displays are known to introduce delays in peak times due to timing issues inherent to the respective technologies (Hogg, 2006; Elze, 2010). Additionally, isochronic $PERG_{ss}$ responses acquired followed standards when analyzed in the

frequency domain. Once conventional responses were acquired and validated, the VDU was used to deliver jittered CLAD sequences for the first time.

A number of temporal rates were investigated beyond the range on conventional displays in order to investigate the effects of increasing reversal rate on the PERG response. These $qPERG_{ss}$ responses were then deconvolved using CLAD to acquire $qPERG_{tr}$, the high rate transient response. $qPERG_{tr}$ were shown to have individual waveform components which normally are lost in convolution of successive responses. The extraction of these components show that CLAD can be used to regain temporal information normally lost at higher reversal rates potentially providing a new perspective of these responses to researchers and clinicians. Another finding in this study was the consistent morphology changes in the $qPERG_{tr}$ response as reversal rate is increased. While ascertaining the generation source behind the high rate morphology was beyond the scope of this study, the changes were very reproducible and consistent across subjects.

Another contribution of this study was the validation of the superposition hypothesis of steady state EPs (Capilla et al., 2011; Toft-Nielsen et al., 2012). Using the CLAD extracted high rate transient responses, synthetic steady state responses were computed mathematically. If the superposition hypothesis is valid and if the extract $qPERG_{tr}$ responses were indicative of the 'per reversal' contribution to the establishment of the $PERG_{ss}$ response, then the synthetic responses generated from the extracted high rate transients should predict the conventions $PERG_{ss}$ responses at the same mean reversal rate. Using the correlation coefficient as a test of the prediction ability it was shown that synthetic responses predicted the real $PERG_{ss}$ with correlation values above

0.9 for all reversal rates (with many rates higher than 0.95 correlation). These transient recordings were validated by the responses' ability to predict the $PERG_{ss}$ at the corresponding rate.

Additional future lines of research include studies of the contrast response of the retina, as well as response to pattern onset/offset responses. The microcontroller based VDU driver developed during this study allows for users to reprogram how the driver interprets a trigger from the acquisition system. This allows the VDUs to alter their modalities via software, and varying contrast levels of the stimulus or switching to a onset/offset paradigm already possible, and might give additional insight into understanding the PERG response and its generators.

It is the hope of the researchers involved in this study that deconvolution of PERG responses will become another tool in the analysis of the complex electrophysiology of the human retina. Historically, our understanding of the retina has been expanded by combining and altering various stimulus parameters, be it spatial and temporal characteristics, subject adaptation level, temporal rate of the stimulus, intensity level of the stimulus, pattern contrast, chromaticity of pattern or other factors. Deconvolution can be used to get a more specific view of the temporal dynamics of the PERG response and using it conjunction with other stimulus paradigms may provide a unique perspective into understanding the human visual system.

REFERENCES

Bach, M., Hawlina, M., Holder, G.E., Marmor, M.F., Meigen, T., Vaegan, & Miyake, Y. (2000). "Standard for pattern electroretinography." *Doc Ophthalmol*. 101(1), 11–18.

Bach, M., Brigell, M.G., Hawlina, M., Holder, G.E., Johnson, M., McCulloch, D. Meigen, T. Viswanathan, S. (2012). "ISCEV standard for clinical pattern electroretinography (PERG) – 2012 update". Manuscript submitted for publication.

Bach, M., Unsoeld, A.,Philippin, H., Staubach, F., Maier, P., Walter, H., Bomer, T., & Funk, J. (2006). "Pattern ERG as an early glaucoma indicator in ocular hypertension: a long-term, prospective study". *Invest Ophthalmol Vis Sci*. 47(11), 4881-7.

Bach, M. & Hoffman, M.B. (2006). "The origin of the pattern electroretinogram In JR Heckenlively and GB Arden (Eds.), *Principles and Practice of Clinical Electrophysiology of Vision* (pp. 185-96). Cambridge, The MIT press.

Baker, C. L., Jr & Hess, R. F. (1984). "Linear and nonlinear components of the pattern electroretinogram". *J Neurophysiol*. 51(5), 952-67.

Ben-Shlomo, G., Bach, M., Ofri, R. (2007). "Temporal and spatial frequencies interact in the contrast transfer function of the pattern electroretinogram." *Vision Res*. 47(15), 1992-9.

Bohórquez, J., & Ozdamar, O. (2006). "Signal to noise ratio analysis of maximum length sequence deconvolution of overlapping evoked potentials." *J Acoust Soc Am*. 119(5), 2881-8.

Bos, P.J., & Koehler/Beran, R. (1984). "The pi-Cell: A fast liquid-crystal optical switching device." *Mol Cryst Liq Crsyt*. 113. 329-39.

Brannan, J., Bodis Wollner, I., & Storch, J. (1992). "Evidence for two distinct non-linear components in human pattern ERG." *Vision Res*. 32 (1), 11-7.

Brigell, M., Bach, M., Barber, C., Moskowitz, A., Robson, J. (2003). "Guidelines for calibration of stimulus and recording parameters used in clinical electrophysiology of vision." *Doc Ophthalmol*. 107: 185-93.

Capilla, A., Pazo-Alvarez, P., Darriba, A., Campo, P., and Gross, J. (2011). "Steady-state visual evoked potentials can be explained by temporal superposition of transient event-related responses." *PLoS One*. 6(1), e14543.

Coupland, S.G. (2006). "Electrodes for Visual Testing." In JR Heckenlively and GB Arden (Eds.), *Principles and Practice of Clinical Electrophysiology of Vision* (pp. 265-83). Cambridge, The MIT press.

Curcio, C. A., & Allen, K. A. (1990). "Topography of ganglion cells in human retina." *J Comp Neurol*. 300 (1), 5–25.

De Rouck, A.F. (2006). "History of the Electroretinogram." In JR Heckenlively and GB Arden (Eds.), *Principles and Practice of Clinical Electrophysiology of Vision* (pp. 3-10). Cambridge, The MIT press.

Drasdo, N. (1989). "Receptive field densities of the ganglion cells of the human retina." *Vision Res*. 29(8), 985-8.

Elze, T. (2010). "Achieving precise display timing in visual neuroscience experiments." *J Neurosci Methods*. 191. 171-9.

Epstein, C.M. (1979). "True checkerboard pattern reversals with light emitting diodes". *Electroencephalogr Clin Neurophysiol*. 47(5), 611-3.

Evans, B.T., Binnie, C.D. & Lloyd D.S. (1974). "A simple visual pattern stimulator." *Electroencephalogr Clin Neurophysiol*. 37(4), 403-6.

Ferraro, J.A. (2000). "Electrocochleography." In RJ Roeser, M Valente and H Hosfort-Dunn (Eds.). *Audiology Diagnosis (*pp. 425-50). New York/Stuttgart: Thieme.

Fiorentini, A., Maffei, L., Pirchio, M., Spinelli, D., and Porciatti, V. (1981). "The ERG in response to alternating gratings in patients with diseases of the peripheral visual pathway." *Invest Ophthalmol Vis Sci*. 21(3), 490-3.

Frishman, L.J. (2006). "Origins of the Electroretinogram." In JR Heckenlively and GB Arden (Eds.), *Principles and Practice of Clinical Electrophysiology of Vision* (pp. 139-84). Cambridge, The MIT press.

Goodale, M.A., Milner, A.D. (1992). "Separate visual pathways for perception and action." *Trends Neurosci*. 15(1), 20-25.

Gunkel, R.D., Bergsma, D.R., Gouras, P. (1976). "A Ganzfeld stimulator for electroretinography." Arch Ophthalmol. 94(4), 669-70.

Hess, R. F. & Baker. C. L., Jr (1984). "Human pattern-evoked electroretinogram." *J Neurophysiol*. 51(5), 939-51.

Hidajat, R., McLay, J.L., Elder, M.J., Goode, D.H., Morton, J.P. & Burley C D. (2003). "A comparison of two patient friendly ERG electrodes." *Australas Phys Eng Sci Med*. 26 (1), 30-4.

Hogg, C. (2006). "Stimulus Devices, Calibration, and Measurement of Light." In JR Heckenlively and GB Arden (Eds.), *Principles and Practice of Clinical Electrophysiology of Vision* (pp. 265-83). Cambridge, The MIT press.

Holder, G.E. (2001). "Pattern electroretinography (PERG) and an integrated approach to visual pathway diagnosis." *Prog Retin Eye Res*. 20(4), 531-561.

Holder, G.E., Celesia, G.C., Miyake, Y., Tobimatsu, S., & Weleber, R.G. (2010). "International Federation of Clinical Neurophysiology: Recommendations for visual system testing." *Clin Neurophysiol*. 121(9), 1393-409.

Holder, G.E., Brigell, M.G., Hawlina, M., Meigen, T. (2007). "ISCEV standard for clinical pattern electroretinography—2007 update." *Doc Ophthalmol*. 114(3), 111–6.

Husain, A.M., Hayes, S., Young, M., Shah, D. (2009). "Visual evoked potentials with CRT and LCD monitors: When newer is not better." *Neurology*. 72. 162-4.

Kikasu, Y., Mizota, A., Adachi, E. (1986). "Clinical application of the pattern electroretinogram with lid skin electrodes." *Doc Ophthalmol*. 63(2), 187-94.

Kolb, H. (2006). "Functional Organization of the Retina." In JR Heckenlively and GB Arden (Eds.), *Principles and Practice of Clinical Electrophysiology of Vision* (pp. 47-64). Cambridge, The MIT press.

Kooijman, A.C. & Damhof, A. (1986). "A tricolor light source for stimulation and adaptation in electroretinography." *Doc Ophthalmol*. 63(2), 195-203.

Krakau, C.E., Nordenfelt, L., Ohman, R. (1977). "Routine ERG recording with LED light stimulus." *Ophthalmologica*. 175(4), 199-205.

Larsson, J. & Andreasson, S. (2001). "Photopic 30 Hz flicker ERG as a predictor for rubeosis in central retinal vein occlusion". *J Ophthalmol*. 85(6), 683-5.

Link, B., Junemann, A., Horn, F.K. (2006). "Pattern reversal ERG with LED stimulation using cyclic summation technique." *Doc Ophthalmol*. 112(1), 53-60.

Link, B., Ruhl, S., Peters, A., Junemann, A., Horn, F.K. (2006). "Pattern reversal ERG and VEP – comparison of stimulation by LED, monitor and a Maxwellian-view system." *Doc Ophthalmol*. 112(1), 1–11.

Maffei, L. & Fiorentini, A. (1990). "The pattern electroretinogram in animals and humans: Physiological and clinical applications". *Res Publ Assoc Res Nerv Ment Dis*. 67, 289-96.

Marmor, M.F., Holder, G.E., Porciatti, V., Trick, G.L., Zrenner, E. (1996). "Guidelines for basic pattern electroretinography. Recommendations by the International society for clinical electrophysiology of vision." *Doc Ophthalmol*. 91(4), 291–8.

Marmor, M.F., Fulton, A.B., Holder, G.E., Miyake, Y., Brigell, M., & Bach, M. (2009). "ISCEV Standard for full-field clinical electroretinography (2008 update)." *Doc Ophthalmol*. 118(1), 69-77.

Masland, R.H. (2001). "The fundamental plan of the retina." *Nat Neurosci*. 4(9), 877-86.

McCulloch, D.L., Van Boemel, G.B., Borchert, M.S. (1998). Comparison of contact lens, foil, fiber and skin electrodes for pattern electroretinograms. *Doc Ophthalmol*. 94, 327-40.

Mushin, J. Hogg, C.R., Dubowitz, L.M., Skouteli, H., & Arden G.B. (1984). "Visual evoked responses to light emitting diode (LED) photostimulation in newborn infants." *Electroencephalogr Clin Neurophysiol*. 58(4), 317-20.

Nagy, B.V., Gemesi, S., Heller, D., Magyar, A., Farkas, A. Abraham, G., Varsanyi, B. (2011). "Comparison of pattern VEP results acquired using CRT and TFT stimulators in the clinical practice." *Doc Ophthalmol*. 122(3), 157-62.

Neves, G., Lagnado, L. (1999). "The retina." *Curr Biol*. 9 (18), 674-677.

Odom, J.V., Maida, T.M., Dawson, W.W., Hobson, R. (1987). "Pattern Electroretinogram: Effects of reference electrode position." *Doc Ophthalmol*. 65(3), 297-306.

Ozdamar, O. & Bohórquez, J. (2006). "Signal to noise ratio and frequency analysis of continuous loop averaging deconvolution (CLAD) of overlapping evoked potentials." *J Acoust Soc Am*. 119(1), 429-38.

Ozdamar, O, Bohórquez, J, Ray, S.S. (2007). "P(b) (P(1)) resonance at 40 Hz: effects of high stimulus rate on auditory middle latency responses (MLRs) explored using deconvolution" *Clin Neurophysiol*. 118(6), 1261-73.

Pastoor, S. & Wopking, M. (1997). "3-D displays: A review of current technologies." *Displays*. 17, 100-10.

Popovic, Z. & Sjöstrand, J. (2001). "Resolution, separation of retinal ganglion cells, and cortical magnification in humans." *Vision Res*. 41(10-11), 1313-9.

Porciatti, V. & Ventura, L.M. (2004). "Normative data for a user-friendly paradigm for pattern electroretinogram recording." *Ophthalmology*. 111(1), 161- 8.

Porciatti, V. (2007). "The mouse pattern electroretinogram." *Doc Ophthalmol*. 115(3), 145-53.

Porciatti, V. & Ventura L. (2009). "Adaptive changes of inner retina function in response to sustained pattern stimulation." *Vision Res*. 49. 505-13.

Porciatti, V., Burr, D.C., Morrone, M.C., & Fiorentini, A. (1992). "The effects of ageing on the pattern electroretinogram and visual evoked potential." *Vision Res*. 32(7), 1199-209.

Regan. D. (1968). "Evoked potentials and sensation." *Percept Psychophys*. 4, 347-50.

Sjostrand, J., Olsson, V., Popovic, Z., & Conradi, N. (1999). "Quantitative estimations of foveal and extra-foveal retinal circuitry in humans." *Vision Res*. 39 (18), 2987–98.

Skuse, N.F., Burke, D. & McKeon, B. (1984). "Reproducibility of the visual evoked potential using a light-emitting diode stimulator." *J Neurol Neurosurg Psychiatry*. 47(6), 623-9.

Tan, C.B., King, P.J., & Chiappa, K.H. (1989). "Pattern ERG: effects of reference electrode site, stimulus mode and check size." *Electroencephalogr Clin Neurophysiol*.74(1), 11-8.

Toft-Nielsen, J.A., Bohorquez, J., Ozdamar, O. (2009, May). *Visual Display for the Acquisition of High Rate Pattern Electroretinograms*. Presentation at the 25th annual Southern Biomedical Engineering Conference, Miami FL.

Toft-Nielsen, J.A., Bohorquez, J., Ozdamar, O. (2011, Aug). *Innovative Pattern Reversal Displays for Visual Electrophysiological Studies*. Poster presentation at the 2011 Annual International Conference for the IEEE EMBC. Boston, MA.

Toft-Nielsen, J.A., Bohorquez, J., Porciatti, V., Ozdamar, O. (2012). "Generation of steady state pattern electroretinograms explained by convolution of transient responses." *ARVO Meeting Abstracts*. 53:5708.

Ventura, L.M., Porciatti, V., Ishida, K., Feuer, W.J. & Parrish, R.K. (2005). "Pattern electrorentinogram abnormality and glaucoma." *Ophthalmology*. 112(1), 10-9.

Wu, S. & Burns, S.A. (1996). "Analysis of retinal light adaptation with the flicker electroretinogram." *J Opt Soc Am*. 13(3), 649-57.

Zele, A.J. & Vingrys A.J. (2005). "Cathode-ray-tube monitor artefacts in neurophysiology." *J Neurosci Methods*. 141(1), 1-7.